

DEVELOPMENT OF INSTRUMENTATION AND SIMULATION OF
REGENERATIVE MOTOR-PUMP SYSTEM FOR HYDRAULIC
HYBRID VEHICLE

MOHAMAD HILMAN BIN NORDIN

DISSERTATION SUBMITTED IN FULFILMENT OF THE
REQUIREMENTS FOR THE DEGREE OF MASTER OF
ENGINEERING SCIENCE

FACULTY OF ENGINEERING
UNIVERSITY OF MALAYA
KUALA LUMPUR

2012

UNIVERSITI MALAYA

ORIGINAL LITERARY WORK DECLARATION

Name of Candidate: MOHAMAD HILMAN BIN NORDIN

Registration/Matric No: KGA090089

Name of Degree: Master of Engineering Science

Title of Project Paper/Research Report/Dissertation/Thesis ("this Work"):
DEVELOPMENT OF INSTRUMENTATION AND SIMULATION OF
REGENERATIVE MOTOR-PUMP SYSTEM FOR THE APPLICATION OF
HYDRAULIC HYBRID VEHICLE

Field of Study: Advance Manufacturing Technology

I do solemnly and sincerely declare that:

- (1) I am the sole author/writer of this Work;
- (2) This Work is original;
- (3) Any use of any work in which copyright exists was done by way of fair dealing and for permitted purposes and any excerpt or extract from, or reference to or reproduction of any copyright work has been disclosed expressly and sufficiently and the title of the Work and its authorship have been acknowledged in this Work;
- (4) I do not have any actual knowledge nor do I ought reasonably to know that the making of this work constitutes an infringement of any copyright work;
- (5) I hereby assign all and every rights in the copyright to this Work to the University of Malaya ("UM"), who henceforth shall be owner of the copyright in this Work and that any reproduction or use in any form or by any means whatsoever is prohibited without the written consent of UM having been first had and obtained;
- (6) I am fully aware that if in the course of making this Work I have infringed any copyright whether intentionally or otherwise, I may be subject to legal action or any other action as may be determined by UM.

Candidate's Signature

Date

Subscribed and solemnly declared before,

Witness's Signature

Date

Name:

Designation:

ABSTRACT

The first decade of the 21st century had seen a growing and increasing concern on the lasting effects of human activities towards the environment. Issues such as global warming as well as the dwindling reserves of non-renewable sources of energy have forced the human race to look for the best replacement or alternative solutions, across all fields of industries. In the automotive industry, various researches are being conducted to produce sustainable transportation systems, which can be divided into the development of renewable source of energy as well as the improvement of energy efficiency. The improvement of energy efficiency has seen the growth of hybrid vehicles, which is proven to reduce the consumption of fuel and emission of pollutant. Regenerative braking is one of the systems applied in hybrid vehicles, where the energy used during braking is recovered and stored for future use. This study evaluates a Regenerative Motor-Pump System for the application of a Hydraulic Hybrid Vehicle (HHV). The instrumentation and control for the system was developed, where the design was tailored specifically for a truck. The Regenerative Motor Pump System was found to be able to recover 40% of the braking energy, resulting in 60% less energy required to move a HHV truck from stationary to 10 km/h, as compared to the total dependence to Internal Combustion Engine (ICE). Additionally, HHV and conventional vehicle simulation drivetrains were developed based on the experimental data obtained and tested on two different drive cycle tests. Firstly, a stop-and-go drive cycle show that the HHV truck was able to save up to 33% of energy compared to a conventional truck. Moreover, a comparison between conventional and a HHV truck using the New York Garbage Truck Cycle (NYGTC) shows a saving of energy up to 29.6%. The results obtained shows that there are significant benefits for the implementation of hydraulic-based regenerative braking systems, especially for vehicles with large mass undergoing multiple stop-and-go driving cycles.

ABSTRAK

Dekad pertama abad ke-21 telah menyaksikan perkembangan dan peningkatan terhadap kesedaran terhadap kesan jangka panjang aktiviti manusia terhadap alam sekitar. Isu-isu seperti pemanasan global serta pengurangan simpanan sumber tenaga yang tidak boleh diperbaharui telah memaksa manusia untuk mencari pengganti ataupun penyelesaian alternatif dalam semua industri. Dalam industri automotif, banyak kajian telah dijalankan untuk membina sistem pengangkutan lestari yang boleh dibahagikan kepada pembangunan tenaga yang boleh diperbaharui dan juga peningkatan kecekapan tenaga. Peningkatan kecekapan tenaga menyumbang kepada pertambahan kenderaan hibrid, mengurangkan penggunaan bahan bakar dan pengeluaran asap pencemar. Brek regenerative merupakan salah satu daripada sistem yang digunakan dalam kenderaan hibrid, di mana tenaga yang digunakan semasa proses brek dikumpul dan disimpan untuk kegunaan akan datang. Kajian ini menilai sebuah Sistem Motor-Pam Regeneratif bagi kegunaan Kenderaan Hibrid Hidraulik (HHV). Instrumentasi dan kawalan bagi sistem tersebut telah dibangunkan, dimana rekaannya mengikut spesifikasi sebuah lori. Sistem Motor-Pam Regeneratif dapat mengumpul semula 40% tenaga, menyumbang kepada 60% pengurangan tenaga untuk menggerakkan HHV daripada pegun kepada 10km/j, berbanding dengan keadaan bergantung penuh dengan enjin biasa (ICE). Tambahan pula, simulasi kenderaan biasa dan HHV telah dibangunkan berdasarkan data eksperimen dan diuji menggunakan dua ujian kitaran panduan yang berbeza. Pertamanya, sebuah kitaran panduan henti-gerak menunjukkan yang HHV mampu menjimatkan sehingga 33% tenaga berbanding trak biasa. Selain itu, perbandingan antara trak biasa dan HHV dalam Kitaran Trak Sampah New York (NYGTC) menunjukkan penjumlahan sehingga 29.6%. Keputusan didapati menunjukkan kebaikan yang signifikan bagi implementasi sistem brek regeneratif berasaskan hidraulik, terutamanya bagi kenderaan yang berat serta menjalani kitaran panduan henti-gerak.

ACKNOWLEDGEMENT

First and foremost, all praises be to Allah, for His Kindness and Guidance are what made this Masters of Engineering Science studies a reality. This study has been partially funded by Malaysia Ministry of Science and Innovation under Science Fund, and partially funded by University of Malaya under student grant, Postgraduate Research Fund (PPP).

I would like to offer my deepest appreciation to my supervisor, Professor Dr. Mohd Hamdi Abd Shukor, for his advice and support in composing this study to completion.

I would also like to thank Dr Noor Azizi Mardi, Lecturer, Department of Engineering Design and Manufacture, Faculty of Engineering. I am greatly indebted to him for his expert opinion and sincere guidance extended to me.

I take this opportunity to thank all members of the Centre of Advanced Manufacturing and Material Processing (AMMP), University of Malaya for their help and encouragement.

Last but not least, my deepest appreciation to my beloved parents: *Abah* and *Emak*, my siblings, and my wife: Nurul Syuhadah Mohamed Dzarawi for keeping me on my toes to see this work through until completion and for bringing Hannah into our world.

CONTENTS

1.0 INTRODUCTION	1
1.1 Background	1
1.2 Research objectives	4
1.3 Scope and Limitation of Study	5
1.4 Organization of the thesis	6
2.0 LITERATURE REVIEW	8
2.1 Introduction	8
2.2 Types of Hybrid Vehicle	9
2.2.1 Electric – Internal Combustion Engine Hybrid	10
2.2.2 Electric – Fuel Cell Hybrid	14
2.2.3 Hydraulic – Internal Combustion Engine Hybrid	15
2.2.4 Hydraulic – Electric Hybrid	17
2.3 Energy Storage System (ESS)	19
2.4 Energy Management System Strategies	21
2.5 Regenerative Braking	24
2.5.1 Regenerative braking in Parallel Hydraulic Hybrid Vehicle	26
2.6 Conclusion	27
3.0 DESIGN AND INSTRUMENTATION	28
3.1 Introduction	28
3.2 Regenerative Motor-Pump System Description	29

3.2.1 HHV Vehicle Model	32
3.2.1 Hydraulic Diagram.....	34
3.2.2 Axial Piston Unit (APU)	37
3.2.3 Accumulators	42
3.2.4 Power Pack.....	43
3.2.5 Flywheel.....	45
3.2.6 Brake Assembly	47
3.2.7 Valves.....	47
3.2.8 Pressure Switches.....	51
3.3 Hydraulic Hybrid Vehicle Processes on Regenerative Motor-Pump System.....	52
3.3.1 OFF and Zero State	54
3.3.2 Charging State.....	55
3.3.3 Motor Mode State	56
3.3.4 Coasting State	57
3.3.5 Pump Mode State	57
3.3.6 STOP State.....	58
3.4 Development of Preliminary control for Regenerative Motor-Pump System	59
3.4.1 Development of Data Acquisition (DAQ) System	60
3.4.2 Development of Preliminary Controller in Simulink.....	61
3.4.3 Development of Switching Circuit for Data Acquisition and Control.....	68
3.5 Speed Sensor	73
3.5.1 Speed Sensor Conditioning.....	75

3.6 Pressure Transducer	79
3.7 Validation of the Preliminary Controller	84
3.7.1 Determining the best sampling number for Speed Sensor	87
3.7.2 Filtering Noise from Pressure Transducer Reading	91
3.7.3 Determining the better ramp time	94
3.7.4 Changing swashplate angles	96
3.8 Conclusion.....	98
4.0 CONTROLLER DEVELOPMENT AND VALIDATION	99
4.1 Introduction	99
4.2 Stateflow for Control Development	99
4.3 Controller Stateflow Chart	102
4.3.1 OFF State	106
4.3.2 Neutral State.....	106
4.3.3 Charging State	107
4.3.4 Motor Mode State	108
4.3.5 Pump Mode state.....	108
4.4 Controller Graphical User Interface.....	109
4.5 Safety Features	110
4.5.1 Charging mode pressure limiter	111
4.5.2 Valve Open check	112
4.6 Validations of the Controller.....	116
4.7 Conclusion	119

5.0 SIMULATION AND ANALYSIS	120
5.1 Introduction	120
5.2 HHV Conventional Driveline Model	121
5.2.1 Simulink model for NKR 71-E Conventional Driveline.....	121
5.2.2 ISUZU NKR 71-E Engine Model	132
5.3 HHV Hydraulic Driveline Model.....	136
5.3.1 Energy Recovery and Energy Delivery.....	136
5.3.2 Hydraulic Driveline Simulink Model.....	138
5.4 Simulation Results of the developed HHV Model.....	139
5.4.1 Comparison between Conventional truck and HHV truck	140
5.4.2 Comparison between ICE drivetrain and Hydraulic drivetrain.....	143
5.4.3 Simulations on Drive Cycles.....	147
5.5 Conclusion	156
6.0 CONCLUSIONS.....	157
6.1 Conclusions.....	157
RESEARCH OUTPUT	159
REFERENCES.....	161

LIST OF FIGURES

CHAPTER 2

Figure 2.1 Series Electric Hybrid Vehicle (Bossche, 2006c).....	11
Figure 2.2 Parallel Electric Hybrid Vehicle (Bossche, 2006b)	12
Figure 2.3 Series/Parallel Hybrid Electric Vehicle (Bossche, 2006a)	13
Figure 2.4 Example of Fuel Cell HEV topology (Ferreira et al., 2008)	14
Figure 2.5 An example of a Parallel Hydraulic Hybrid Vehicle drivetrain topology (Hilman et al., 2010)	16
Figure 2.6 New topology for PHHV with additional pump (Hui et al., 2009)	17
Figure 2.7 Hydraulic – Electric Energy Synergy Systems (HESS) drivetrain topology (Hui et al., 2009)	18
Figure 2.8 Comparison between energy storage technologies attributes for hybrid vehicles (Lukic et al., 2008, Nzisabira et al., 2009).....	20
Figure 2.9 (a) PHHV during braking (b) PHHV during acceleration	27
(M. Z. Norhirni et al., 2011).....	27

CHAPTER 3

Figure 3.1 Flow diagram of Regenerative Motor-Pump System emulation of HHV	31
Figure 3.2 ISUZU NKR 71 E truck used in this study	32
Figure 3.3 Hydraulic Diagram of the regenerative pump-motor system	35
Figure 3.4 Layout of the Regenerative Motor-Pump System	36
Figure 3.5 A4VSG Axial Piston Unit manufactured by Rexroth Corporation. (Right : Cross-sectional view of A4VSG Axial Piston Unit).....	37
Figure 3.6 Axial Piston Unit main ports; A and B	39
Figure 3.7 Proportional Valve position on the APU	40

Figure 3.8 Amplifier Card and its characteristics graph	41
Figure 3.9 Accumulators in the form of red tanks are positioned beside the power pack.	42
Figure 3.10 The power pack used for the regenerative motor-pump system. On the right is the top part of the power pack where Valve A and pressure gauge blocks are housed.....	44
Figure 3.11 The flywheel inside a steel cage for safety purposes.....	45
Figure 3.12 Pressure Relief Valve (blue block) with manual adjusting knob	48
Figure 3.13 Valve B (inside black block) with coil compartment on its right.....	50
Figure 3.14 Pressure Switch type HED 8	51
Figure 3.15 Charging State – Power Pack supply hydraulic fluid to the accumulator directly.....	55
Figure 3.16 Motor Mode – Accumulator releases high pressure hydraulic fluid to turn the flywheel.....	56
Figure 3.17 Pump Mode – The flywheel rotation pumps hydraulic fluid from reservoir back to the accumulator	58
Figure 3.18 Regenerative Motor-Pump System Connections.....	60
Figure 3.19 NI PCI-6229 DAQ card from National Instruments.	60
Figure 3.20 Preliminary Controller for Regenerative Motor Pump System	63
Figure 3.21 Flow of the processes of the basic testing for Regenerative Motor-Pump System.....	64
Figure 3.22 Simulink block arrangement for the switching modules (a) Turned off (b) Turned on	66
Figure 3.23 Simulink block arrangements for swivel angle	66
Figure 3.24 Simulink block arrangements for Pressure Switches	67
Figure 3.25 Switching Circuit for DAQ – Regenerative Motor Pump System Communications	70
Figure 3.26 Switching Circuit for Digital I/O Channel 1 to Channel 4.....	71

Figure 3.27 Switching Circuit for Digital I/O Channel 5 and Channel 6	72
Figure 3.28 Speed Sensor Dimension (Left) and Speed Sensor on mounting bracket (Right)	73
Figure 3.29 Speed Sensor position near the flywheel	75
Figure 3.30 Speed Sensor Conditioning – from pulses to RPM value	76
Figure 3.31 The effect of Edge Detector block (top) and the pulses received by speed sensor (below)	77
Figure 3.32 Pressure Transducer used in the system to evaluate the regenerative motor- pump system	80
Figure 3.33 Configuration setting for Pressure Transducer – NI PCI 6229 Analog Input	81
Figure 3.34 Pressure Transducer Simulink blocks.....	82
Figure 3.35 Analog Input block parameters.....	82
Figure 3.36 Pressure Subsystem block details	83
Figure 3.37 Pump Mode (top) and Motor Mode (below) in Regenerative Motor-Pump System.....	86
Figure 3.38 Flywheel Speed Measurement with sampling size, $N = 100$	87
Figure 3.39 Flywheel Speed Measurement with sampling size $N = 100$ in 1 second period.....	88
Figure 3.40 Flywheel speed measurement with sampling size, $N = 500$	89
Figure 3.41 Flywheel speed measurement with sampling size, $N = 1000$	89
Figure 3.42 Flywheel speed measurement with sampling size, $N = 1500$	90
Figure 3.43 Flywheel speed measurement with sampling size, $N = 2000$	90
Figure 3.44 Pressure Transducers reading with no filter	91
Figure 3.45 Pressure Transducer readings with 30 Hz cut-off frequency low-pass filter.....	92
Figure 3.46 Pressure Transducer readings with 25 Hz cut-off frequency low-pass filter.....	93
Figure 3.47 Pressure Transducer readings with 20 Hz cut-off frequency low-pass filter.....	93

Figure 3.48 Pressure Transducer readings with 15 Hz cut-off frequency low-pass filter.....	93
Figure 3.49 Pressure Transducer readings with 10 Hz cut-off frequency low-pass filter.....	94
Figure 3.50 Flywheel speed measurement from 0 rpm to 1260 rpm with ramp time of 5s.....	95
Figure 3.51 Flywheel speed measurement from 0 rpm to 1260 rpm with ramp time of 1s.....	95
Figure 3.52 Jumpers settings guidelines for the Amplifier Card	96
Figure 3.53 Motor Mode Speed Profile using different swashplate angle.....	97

CHAPTER 4

Figure 4.1 Simulink Diagram of the controller.....	104
Figure 4.2 STATEFLOW Chart of the controller.....	105
Figure 4.3 Off State of the Stateflow Chart	106
Figure 4.4 Neutral State of the Stateflow Chart.....	107
Figure 4.5 Charging State of the Stateflow Chart.....	107
Figure 4.6 Motor Mode state of the Stateflow chart	108
Figure 4.7 Pump Mode state of the Stateflow chart.....	109
Figure 4.8 GUI for the controller	110
Figure 4.9 Simulink block arrangements for pressure limiter switch	111
Figure 4.10 Switch block parameters settings.....	112
Figure 4.11 Voltage Regulator Circuit for Valve B ON/OFF indicator	114
Figure 4.12 Valve Open Check States – (a) Before and (b) after implementations.....	115
Figure 4.13 Validation of the controller on the 5 states (Pressure).....	117
Figure 4.14 Validation of the controller on the 5 states (Speed)	117
Figure 4.15 Validation of controller – Comparison between Pressure and Speed	118

CHAPTER 5

Figure 5.1 Simulink model of ISUZU NKR 71-E	122
Figure 5.2 Engine Subsystem modelled with blocks from the SimDriveline library of Simulink	124
Figure 5.3 WinPEP 7 GUI - Data Export Preview.....	125
Figure 5.4 Simulink Block – Generic Engine interface	126
Figure 5.5 Vehicle body block in Simulink	127
Figure 5.6 Tire block in Simulink.....	128
Figure 5.7 Simple Gear block in Simulink	129
Figure 5.8 Differential block in Simulink.....	130
Figure 5.9 Engine Data for ISUZU NKR 71 E: Power versus Time (Gear 1 - 4)	133
Figure 5.10 Engine Data for ISUZU NKR 71 E: Power versus Speed (Gear 1 – 4)	133
Figure 5.11 Simulated Engine Data for ISUZU NKR 71-E (Gear 1 – 4).....	134
Figure 5.12 Engine Data for Gear 1 – Speed (km/h) and Power (kW) versus Time	135
Figure 5.13 Driveline Subsystem for HHV.....	138
Figure 5.14 Speed comparison between Original truck and HHV truck	140
Figure 5.15 Power comparison between Original truck and HHV truck.....	141
Figure 5.16 Engine Speed Comparison between Original truck and HHV truck	142
Figure 5.17 Engine Power and Speed data from the Simulated HHV	144
Figure 5.18 Engine Power and Throttle data of the Simulated HHV	145
Figure 5.19 Power and RPM data of the Simulated HHV	146
Figure 5.20 Hybrid 1 Drive Cycle by New West and Bosch Rexroth.....	148
Figure 5.21 New York Garbage Truck Cycle (NYGTC).....	148
Figure 5.22 Stop-Go Drive Cycle based on Hybrid 1 drive cycle	149
Figure 5.23 New York Garbage Truck Cycle (NYGTC) on Signal Builder	150
Figure 5.24 Speed of NKR 71-E on Stop-Go Drive Cycle	151
Figure 5.25 Speed of Hybrid NKR 71-E on Stop-Go Drive Cycle.....	152

Figure 5.26 ICE Power comparison in conventional and hybrid NKR 71-E on Stop-Go
Cycle153

Figure 5.27 Speed of NKR 71-E on NYGTC154

Figure 5.28 Speed of Hybrid NKR 71-E on NYGTC.....154

Figure 5.29 ICE Power Comparison in conventional and hybrid NKR 71-E on NYGTC155

University of Malaya

LIST OF TABLES

CHAPTER 3

Table 3.1 Specifications of the ISUZU NKR 71 E truck.....	33
Table 3.2 Hydraulic symbols and its descriptions	34
Table 3.3 Specifications of the Axial Piston Unit.....	38
Table 3.4 Flow direction according to solenoid energized and APU rotation	41
Table 3.5 Inertia of the components in the flywheel assembly	46
Table 3.6 Technical Specification for Valve A.....	49
Table 3.7 Technical Specification for Valve B	50
Table 3.8 Technical specification of Pressure Switch type HED 8	51
Table 3.9 Comparison between processes in System and PHHV	53
Table 3.10 State and Processes in the System.....	54
Table 3.11 DAQ Modules used for the system	61
Table 3.12 Summary of DAQ Modules used for Preliminary Controller for Regenerative Motor Pump System	68
Table 3.13 Connections from Target PC to Switching Circuit (Channel 1 – 4)	71
Table 3.14 Connections to the Target PC to Switching Circuit (Channel 5 and Channel 6)	72
Table 3.15 Specifications of the Remote Optical Sensor.....	74
Table 3.16 Connection Detail for Speed Sensor and DAQ card.....	79
Table 3.17 Technical Specifications of the Pressure Transducer	79

CHAPTER 5

Table 5.1 Generic Engine block parameters settings	127
Table 5.2 Vehicle Body block parameters	128

Table 5.3 Tire block parameters	129
Table 5.4 Differential block parameters.....	131
Table 5.5 Engine Characteristics of NKR 71-E	135
Table 5.6 Energy and velocity data comparison between Motor Mode I and Motor Mode II.....	137
Table 5.7 Summary of Comparison between conventional and hybrid NKR 71-E truck	143
Table 5.8 Comparison between ICE and Hydraulic Drivetrain of the HHV	146
Table 5.9 Summary of Comparison between HHV ISUZU NKR 71-E Truck and Conventional ISUZU NKR 71-E truck on Stop-Go Drive Cycle.....	153
Table 5.10 Summary of Comparison between HHV ISUZU NKR 71-E Truck and Conventional ISUZU NKR 71-E truck on NYGTC	155

ABBREVIATION

AC	=	Alternating Current
AES	=	Auxiliary Energy System
AI	=	Analog Input
AO	=	Analog Output
APU	=	Axial Piston Unit
AW	=	Tread front
CVT	=	Continuous Variable Transmission
CW	=	Tread rear
DAQ	=	Data Acquisition
DC	=	Direct Current
DI	=	Digital Input
DIFF	=	Differential
DGND	=	Digital Ground
DO	=	Digital Output
DOH	=	Degree of Hybridization
EMS	=	Energy Management System
EV	=	Electric Vehicle
ESS	=	Energy Storage Systems
FC	=	Fuel Cell
GUI	=	Graphical User Interface
GUIDE	=	Graphical User Interface Design Environment
GVW	=	Gross Vehicle Mass
HEV	=	Hybrid Electric Vehicle
HESS	=	Hydraulic-Electric Synergy System
HH	=	Minimum Clearance
HHV	=	Hydraulic Hybrid Vehicle
HRBS	=	Hydraulic Regenerative Braking System
ICE	=	Internal Combustion Engine

IXEF	=	Polyarylamide (material)
LAN	=	Local Area Network
LED	=	Light Emitting Diode
NI	=	National Instruments
NRSE	=	Non-Referenced Single-Ended
NYGTC	=	New York Garbage Truck Cycle
OAL	=	Overall Length
OH	=	Overall Height
OW	=	Overall Width
PC	=	Personal Computer
PEMFC	=	Proton Exchange Membrane Fuel Cell
PHHV	=	Parallel Hydraulic Hybrid Vehicle
ROS	=	Remote Optical Sensor
RPM	=	Revolutions per minute
RSE	=	Referenced Single-Ended
SDI	=	Suction Diesel Injection
UC	=	Ultra-capacitors
WVU	=	West Virginia University Refuse Truck Cycle

1.0 INTRODUCTION

1.1 Background

Fluctuation of the oil price in the international market and the depletion of oil reservoirs have led the world to explore the untapped potentials of alternative energies such as solar energy, hydro-electricity, nuclear energy and biofuel. Researchers have predicted an energy crisis in the coming years as the world grew more and more dependent to oil (Kerr, 1998). Some estimated that the world will see its peak production of oil in the years of 2010 – 2020; when oil production will start to see a decline (Kerr, 1998). The current economic growth in China will also contribute to more demands of oil in the long term, as industries with high oil consumption are one of the contributors to the Chinese economy (Zou & Chau, 2006). The decline in oil production and higher demands of the commodity can only mean a trend of higher energy prices in the future.

This however, spurs the search of alternative energy sources. The world's largest construction project on energy is now situated in Alberta, Canada – where capitalists exploits Canada's great tar sands reserve to produce low quality fossil fuel (Nikiforuk, 2010). Production of oil from tar sands however, will yield high greenhouse gas emissions and resulted to high ecological footprint (Chavez-Rodriguez & Nebra, 2010). Other researchers are trying to develop cheaper solar cells – one of the reasons of why solar cells are yet to be widely implemented is because of its costs (Andersson & Jacobsson, 2000).

Nuclear power may be available to provide energy for a rapid growing economy as its previously did for Japan, but the recent March 11, 2011 Great East Japan Earthquake and the resulting Fukushima Daiichi nuclear plant accident has created

public outcry. Future development on nuclear energy should be implemented carefully with considerations for safety and general opinions of the public (Satoh, 2011).

Other alternatives such as biofuels, for instance ethanol from sugar cane and corn offer low greenhouse gas (GHG) emissions and low ecological footprint for its production (Chavez-Rodriguez & Nebra, 2010). But using food products as substitute to dirty fossil fuels will only increase the prices and eventually will only be produced for energy purposes. Other biofuels, known as biodiesel are also developed for diesel engines that use organic resources such as palm oil (Gokalp, Buyukkaya, & Soyhan, 2011; Hebbal, Reddy, & Rajagopal, 2006; Kannan, Karvembu, & Anand, 2011; Lin, Huang, & Huang, 2008; Sayin, 2011; Yusaf, Yousif, & Elawad, 2011) .

The automotive industry reacted to the rising fossil fuel prices trends by introducing solutions that generally show their interest in renewable energy and 'green' energy. The move was also in part influenced by the increase in environmental awareness in the general public. The solutions are mainly developed around the conventional Internal Combustion Engine – by improving it to use less fuel and emit less gaseous residues; or developing a cleaner oil (Carson & Vaitheeswaran, 2007).

Hybrid systems, while not entirely independent of oil, are aimed to make the classic internal combustion engine more effective. Hybrid systems are getting more popular now, ranging from various degree of hybridization (DOH), a term used to quantify how independent or dependent one hybrid system to oil. The DOH is calculated based on the ratio of energy conversion machines used in the hybrid system. While not solving the oil-dependency problem, hybrid systems have become the middle step for the world to go through the pathway of oil-independence. Hybrids are proven to be more fuel effective and produce fewer emissions (Fontaras et al., 2008).

Hydraulic hybrid vehicles (HHV), one of the approaches to reduce dependency on the ICE, are less developed due to the fact that it requires large sized components to generate substantial amount of power. There are few researches done on the hydraulic hybrid system rather than the electric hybrid systems. HHV has the advantage of delivering energy in higher densities with the usage of high pressure accumulators as compared to batteries, and can be charged and discharged in high rates (Hui, Ji-hai, & Xin, 2009).

A HHV system usually consists of a pump-motor for energy conversion, an accumulator to store the energy, a reservoir that stores hydraulic fluid and a control system that govern the whole system accordingly to the user's demands and parallel to the conventional ICE. This allows the HHV to employ regenerative braking that partially recovers braking energy to charge the energy accumulator. However, this results to large and bulky systems to be installed in vehicles. The system has to be sized accordingly to benefit from the high energy densities that are offered in HHV systems. This makes the HHV strategy to be more applicable to off-road and heavy vehicles (Hui et al., 2009).

However, there are less numbers of researches done on HHV as compared to the other hybrid vehicle systems. Current literatures are more focused on the energy management strategies, and most of the benefits of the HHV are determined based on simulation results. Development and instrumentation of HHV components may impart further understanding on HHV and its benefits. Furthermore, a working system using components of the HHV system can facilitate development of an actual HHV.

In this study, a Regenerative Motor-Pump System is developed using actual HHV components to emulate the hydraulic drivetrain of a HHV. The system will be able to demonstrate the processes in a real HHV and provide insights to further

developments. The system is proposed to be applied on ISUZU NKR 71-E truck and is developed based on the vehicle. The study is expanded to include simulation results to compare between conventional vehicle and HHV. The simulation model is made based on experimental results from the Regenerative Motor-Pump System to derive the benefits of implementing hydraulic drivetrain on a conventional truck. Most importantly, this study should add to the numbers of literatures available on HHV.

1.2 Research objectives

The study is aimed to be the starting point for an integration of a regenerative braking system into conventional truck driveline. The objectives of the study are:

- (1) To develop instrumentation and control of a Regenerative Motor-Pump System that is able to emulate hydraulic drivetrain of a Parallel Hydraulic Hybrid Vehicle.
- (2) To model a truck as the base vehicle for the HHV in a simulation and use the truck's engine data to effectively model the truck's engine in the simulation.
- (3) To evaluate the Regenerative Motor-Pump System in terms of energy recovery capabilities.
- (4) To compare between the energy delivery of Regenerative Motor-Pump System as the hydraulic drivetrain with the simulated engine model as the conventional drivetrain.

1.3 Scope and Limitation of Study

The study will be centred on a development of a Regenerative Motor-Pump System that will be used in the application of Hydraulic Hybrid Vehicle. The system is designed, planned and proposed to work on an ISUZU NKR 71-E commercial truck. A controller developed in the study is specifically made for the Regenerative Motor-Pump System. The truck engine has been modelled in a basic simulation using Simulink to evaluate the engine power and speed. The simulation data is then compared with the experimental data from the Regenerative Motor-Pump System as a means to compare between conventional drivetrain and hydraulic drivetrain. Evaluation of the Regenerative Motor-Pump System is made solely based on this comparison between experimental data and simulation data. It cannot be assumed that the same configuration can work with other systems as the work is done on case by case basis.

The instrumentation and control of the Regenerative Motor-Pump System are developed to emulate the operation of the hydraulic drivetrain of a HHV. The evaluation of the main drivetrain of the HHV is only made based on simulation results. The study only uses a simple rule as the HHV Energy Management System (EMS) used in the drive cycle simulation and is meant to roughly compare between NKR 71-E truck with HHV NKR 71-E. The present study only develops the control system for the Regenerative Motor-Pump System so that it is able to emulate processes on hydraulic drivetrain of the HHV.

1.4 Organization of the thesis

This thesis contains 6 chapters as described below:

Chapter 1 Introduction

This chapter describes the introduction of the study. A brief background of the study will be presented. This chapter will also include the study objectives, scope and outlined limitations of the study.

Chapter 2 Literature Review

This chapter consists of literature review, which summarizes past works done by others, which begins with the overall idea of hybrid vehicle technologies, its architecture, the development of EMS, the concept of regenerative braking with emphasis on the application of regenerative braking in Parallel Hydraulic Hybrid Vehicle (PHHV).

Chapter 3 Design and Instrumentation

This chapter describes the methodology employed to conduct the study. The chapter will present the design and instrumentation of the system and the development of Data Acquisition (DAQ) setup for the Regenerative Motor-Pump System. A preliminary controller is also discussed in the chapter.

Chapter 4 Controller Development and Validation

This chapter will describe in detail the development of a controller for the Regenerative Motor-Pump System. Safety features of the Regenerative Motor-Pump System are also discussed in this chapter.

Chapter 5 Simulation and Analysis

This chapter will describe the simulation tests and the results obtained. Results from the simulated HHV conventional engine and experimental results from the Regenerative Motor-Pump System will be presented and compared. Two drive cycle simulation is also used to compare between conventional NKR 71-E truck with HHV NKR 71-E.

Chapter 6 Conclusions

This chapter will summarize and conclude the study.

University of Malaya

2.0 LITERATURE REVIEW

2.1 Introduction

In this chapter, different hybrid systems are introduced. In the first section, Hybrid Electric Vehicles (HEV) and Hybrid Hydraulic Vehicles (HHV) are presented. As both HEV and HHV use different auxiliary energy sources, a comparison can be made between the drivetrain topology of the two. Previous works discuss on series, parallel and series-parallel hybrid vehicle architecture, and in this chapter, it will be illustrated in terms of HEV technology. For HHV technology, a study on Parallel Hydraulic Hybrid Vehicle (PHHV) will be discussed, and latest approach in synergizing HEV and HHV will be reviewed.

In the section that follows, an introduction to several Energy Storage Systems (ESS) technologies are presented. The energy storing technologies are compared and evaluated as well. Previous studies on different ESS are reviewed to be the ground work for the present study.

There are various strategies and approaches to energy management for hybrid vehicles. Past literatures that discuss different approaches to Energy Management System (EMS) are also presented in this chapter. Several systems such as On-line Fuzzy Management, Rule Based Energy Management, and Dynamic Programming are discussed, with example applications in Fuel Cell Vehicle, Hybrid Electric Vehicle and Hydraulic Hybrid Vehicle. Control strategies in the different vehicles involve distribution of torque, regenerating energy via regenerative braking and environmental prediction.

Lastly, the concept of regenerative braking, which is central to the PHHV will be explained as well. Previous works on the concept will be presented and discussed in this chapter. The study of past literature for Regenerative Braking concepts will provide the foundation for the development of an Energy Management System (EMS) for the PHHV. Selection of literature discussed includes other types of hybrid technology since they are more readily available as compared to specific PHHV literature.

2.2 Types of Hybrid Vehicle

There are different types of hybrid systems being developed and implemented in the automotive industries. The strategies differ in terms of approaches and objectives with regards to the governing systems, energy storage systems and auxiliary motorization. Most of the time, the only thing in common is the goals of the systems to reduce the usage of fossil fuel as the energy source of the vehicle, or to not depend on it altogether. This is usually related to the conventional Internal Combustion Engine (ICE). Generally, the different hybrid vehicle technologies can be categorized in several ways for example:

1. Drivetrain architecture

This categorization will divide the hybrid vehicle technologies in terms of its different topologies which are series, parallel and series-parallel (Kessels et al., 2008).

2. Degree of hybridization

This categorization will divide the hybrid vehicle technologies in terms of mild hybrid, plug-in hybrid and full hybrid (Sundstrom et al., 2010).

3. Medium of energy transfer

This categorization will group the hybrid vehicle technologies in terms of electric hybrid, hydraulic hybrid and many others.

In this study, the different vehicle technologies will be categorized by the nature of the energy. The groups are chosen based on the most recent development in vehicular technologies according to the literatures. The groups, in order of discussions, are:

1. Electric – Internal Combustion Engine Hybrid
2. Electric – Fuel Cell Hybrid
3. Hydraulic – Internal Combustion Engine Hybrid
4. Hydraulic – Electric Hybrid

2.2.1 Electric – Internal Combustion Engine Hybrid

Electric – Internal Combustion Engine Hybrid may be the most developed hybrid vehicle technology today. This is due to the fact that most of the early approaches to hybrid technology began with the improvement of conventional internal combustion engine with the addition of an electric motor as an auxiliary drivetrain. Furthermore, developments in electric and electronics and battery technologies help propel developments towards drive-by-wire.

Usually in these types of hybrid vehicle, the auxiliary drivetrain is an Electric Motor powered by battery, ultra-capacitor, or both (Karden, Ploumen, Fricke, Miller, & Snyder, 2007). These types of hybrid vehicle can be categorized into three different architectures which are series, parallel and series-parallel (Kessels et al., 2008).

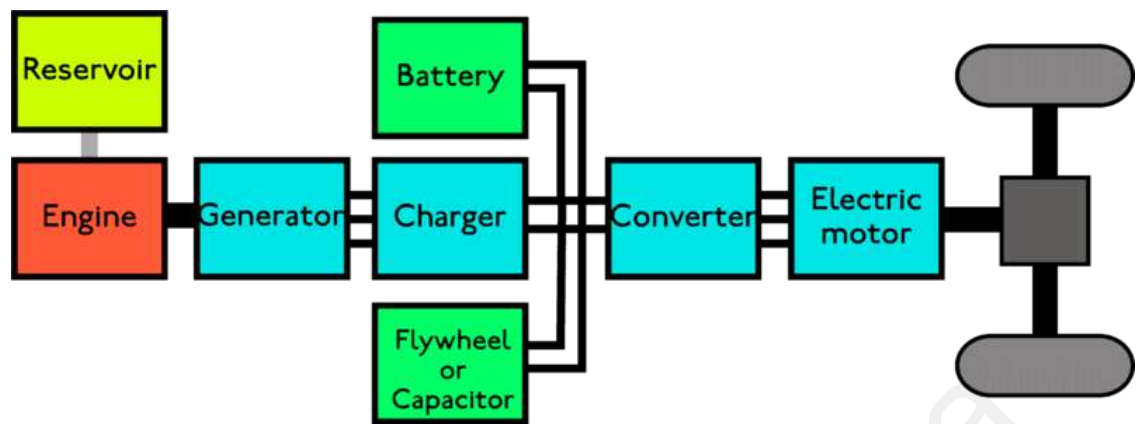


Figure 2.1 Series Electric Hybrid Vehicle (Bossche, 2006c)

Figure 2.1 shows the serial architecture of a HEV. In serial architecture, the main energy source that drives the vehicle is the electric motor. The conventional Internal Combustion Engine is used to drive a generator which in turn will either charge the Energy Storage System (ESS) or directly convert kinetic energy to electrical energy to power the electric motor. In this case, the vehicle has an electric transmission and only uses energy from the generator once the battery is depleted or the capacitor is fully discharged. Moreno et al. developed an Auxiliary Energy System or ‘AES’ by modelling the converter (buck-boost converter) and capacitor (ultra-capacitor) based on this topology (Moreno, Ortuzar, & Dixon, 2006).

This type of HEV is able to be driven as a 100% full electric vehicle when the travelling distance is not far. The development on this topology is based on improving the range of electric vehicle once the battery depletes. They are also possibilities of using the generator when the user demand on the system is high. Series HEV also may implement regenerative braking to recover braking energy so that the battery or capacitor can be charged during braking.

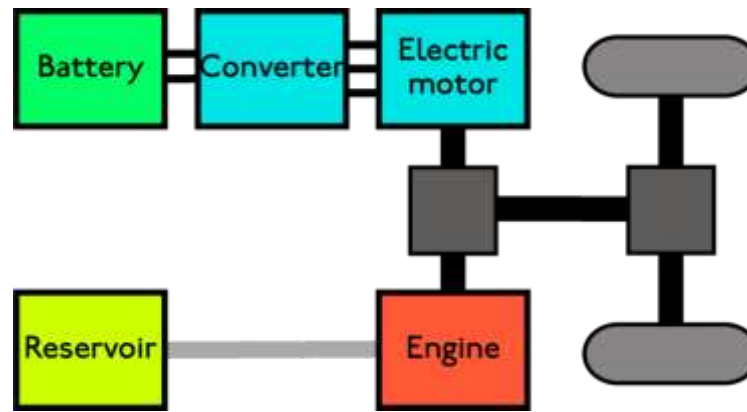


Figure 2.2 Parallel Electric Hybrid Vehicle (Bossche, 2006b)

Figure 2.2 shows a drivetrain topology for a parallel HEV. In this configuration, both the electric motor and the conventional ICE can supply torque to the vehicle independent of each other. This configuration sometimes is described as ‘mild hybrids’ as it mainly uses the ICE to supply torque especially when the electric motor is not capable of supplying torque on its own. In the case of mild hybrids, the electric motor is used as a booster to the conventional drivetrain and only used during peak loading. For instance, Sundstrom et al. developed a mild hybrid electric vehicle on parallel topology. There is no clutch that separates the ICE from the electric motor, making operating in 100% electric energy unattainable (Sundstrom et al., 2010). Zhang et al. also uses the same topology for a HEV that is set to maintain the operation of the ICE at its optimum point whereas an electric motor is used as supplementary power (J.M. Zhang et al., 2009).

It is also possible to implement regenerative braking in parallel drivetrain topology – so that whenever the vehicle brakes, negative loading is used to charge the battery. Recent research by Clarke et al. applied regenerative braking for a parallel HEV which uses a Skoda Fabia 1.9 SDI (Suction Diesel Injection) as the base vehicle and an electric motor that is connected to an ultra-capacitor via a DC-DC converter (Clarke et al., 2010).

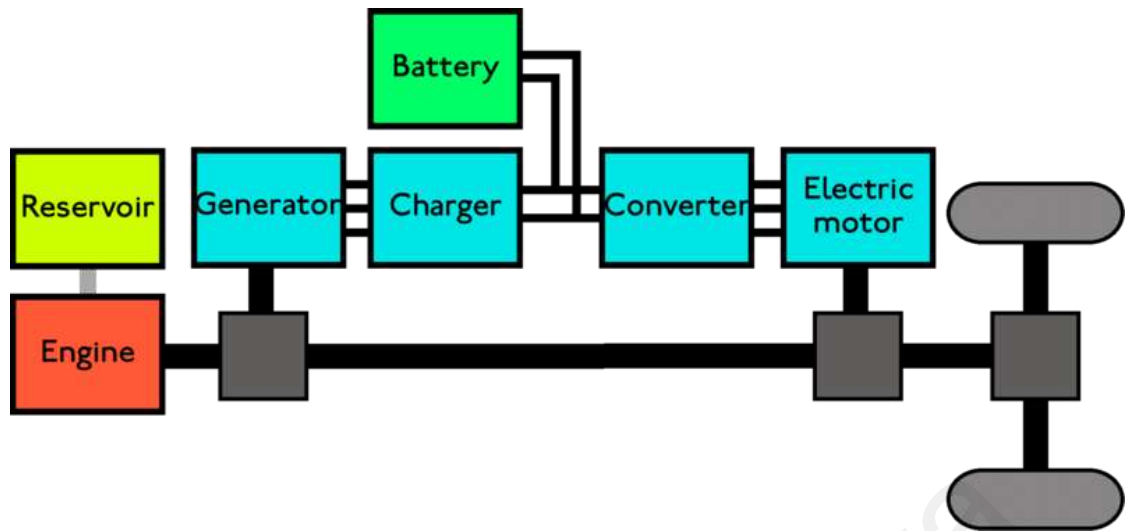


Figure 2.3 Series/Parallel Hybrid Electric Vehicle (Bossche, 2006a)

Figure 2.3 shows a power-split HEV which have a serial and parallel drivetrain topology. In this configuration, the vehicle can be driven by either the engine or the electric motor independently. Planetary gear is one existing power split device that is able to make use of series/parallel drivetrain configuration (Kessels et al., 2008). Additionally, Continuous Variable Transmission (CVT) can also be used to attain power splitting properties offered by this drivetrain configuration (Won, Langari, & Ehsani, 2005). The power splitting device allows either mechanical or electrical power to be supplied, thus, in this configuration, the torque generated by the ICE (or the electric motor) can be independent of the torque demanded by the driver.

Different drivetrain configurations demand different strategies in the development of the EMS. There are also different requirements in terms of integrating between the different drivetrains, especially in cases involving different types of energy. Study on various drivetrain configurations in HEV helps to understand the difference between configurations in other types of hybrid vehicles as well.

2.2.2 Electric – Fuel Cell Hybrid

Another popular hybrid vehicle technology is the fuel cell hybrid. This technology allows for the vehicle to be completely free of the ICE and implement total electric transmission. Usually, the main power is supplied by the fuel cell itself, for example; a Proton Exchange Membrane Fuel Cell (PEMFC) (Erdinc et al., 2009; Ferreira et al., 2008; Kisacikoglu et al., 2009; Thounthong et al., 2009) with supporting power from battery or ultra-capacitor, or both. The Proton Exchange Membrane Fuel Cell is selected mainly because of its low operating temperature and that it does not depend on fossil fuels (Ferreira et al., 2008). The HEV is driven by an electric motor.

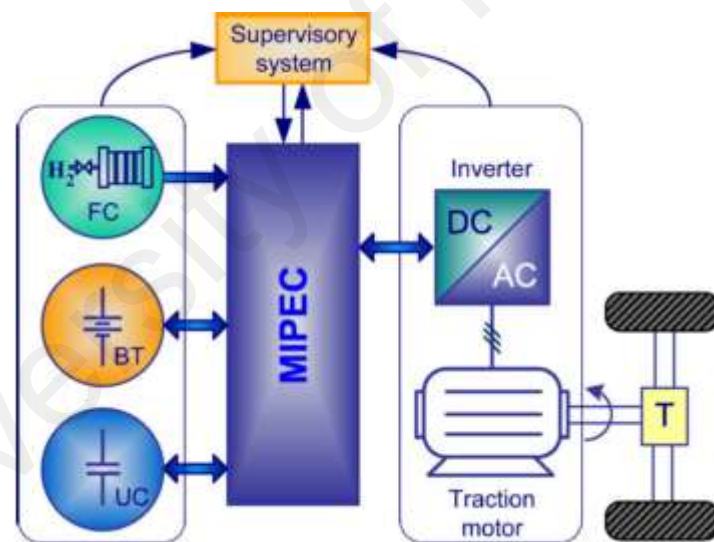


Figure 2.4 Example of Fuel Cell HEV topology (Ferreira et al., 2008)

Figure 2.4 shows an example of fuel cell hybrid topology. The multiple-input power electronic converter (MIPEC) is connected to three different sources which are fuel cell, battery and ultra-capacitor. The fuel cell act as the main drive, while the battery and the ultra-capacitor serves as the Energy Storage Systems (ESS) which stores energy from regenerative braking. The supervisory system is developed to govern and

balance between the load and the energy sources (Ferreira et al., 2008). Hybridizing conventional fuel cell vehicle with ESS such as battery and ultra-capacitor is viable mainly because fuel cell power is not reversible, and similar to ICE vehicle, needed fuel to continue operating (Bernard et al., 2009). Fuel Cell can also be made the main power supply that only supply the base load while the batteries and ultra-capacitor deals with transient and peak voltage events (Kisacikoglu et al., 2009).

Study on the Fuel Cell drivetrain configuration is important in the understanding of balancing the power supplies of different power densities. Batteries and ultra-capacitors for instance, complement each other during events with peak and transient loads. This is similar to hydraulic drivetrain and the ICE in the case of HHV. Further discussions on batteries and ultra-capacitors will be presented in section 2.4.

2.2.3 Hydraulic – Internal Combustion Engine Hybrid

Conventional Parallel Hydraulic Hybrid Vehicle (PHHV) usually consists of a hydraulic accumulator, a reservoir tank, and a variable displacement pump/motor which is coupled to the propeller shaft of the main drivetrain (Hui, Ji-hai, & Xin, 2009). Figure 2.5 shows an example of parallel hydraulic hybrid vehicle drivetrain topology. In PHHV, the main drivetrain is connected directly to the conventional ICE. The hydraulic pump/motor operates in two modes which are motor mode and pump mode (Hilman et al., 2010; Wu et al., 2004). During deceleration, the hydraulic pump/motor is able to assist deceleration by using the shaft rotation to pump hydraulic fluid to the high pressure accumulator. Similarly to deceleration, braking can involve the hydraulic pump/motor to charge the accumulator. The accumulator can discharge in the subsequent acceleration event.

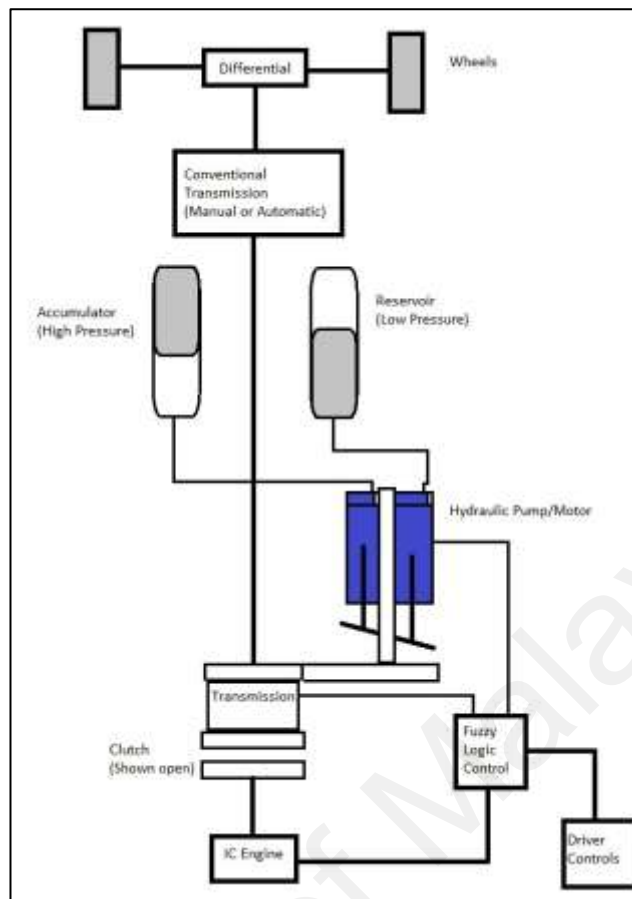


Figure 2.5 An example of a Parallel Hydraulic Hybrid Vehicle drivetrain topology (Hilman et al., 2010)

In contrast to having only one hydraulic motor/pump, using two hydraulic pumps can also help to recover more energy as proposed by Hui et al. To recover energy during cruise mode while allowing the ICE to operate as its optimum operating points, a secondary hydraulic pump will be used to recover excess energy (Hui et al., 2009). The excess can be caused by the difference between the demand from the driver in the cruise mode and the optimum ICE operating level. Figure 2.6 shows the topology as proposed by Hui et al.

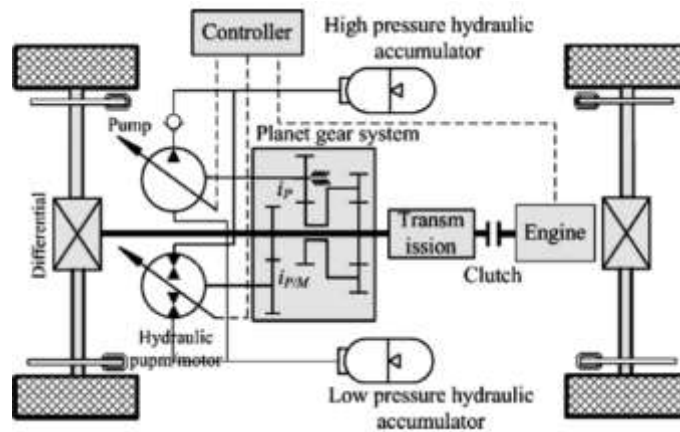


Figure 2.6 New topology for PHHV with additional pump (Hui et al., 2009)

The addition of another pump allows the PHHV to easily recover energy by other means than regenerative braking. This is similar to HEV strategy that allows the excess energy which emerges from the ICE to be used to charge a generator which in turn stores the energy in batteries or ultra-capacitors. However, there are other issues such as cost, maintenance and energy management strategy that should be taken into consideration by using this PHHV configuration.

2.2.4 Hydraulic – Electric Hybrid

One of the latest approaches in hybrid vehicle technology is the development of hydraulic – electric hybrid vehicle. For instance, Hydraulic-Electric Synergy System (HESS) has been developed that uses two types of Energy Storage Systems (ESS) which are hydraulic accumulator and electric battery (Hui et al., 2011). The different characteristics of two Energy Storage Systems play vital role on how the energy management system is developed. In this configuration, a battery and a hydraulic accumulator is used as the ESS. Active charging is always done to replenish the battery so to keep the ICE to operate as its optimum. Energy from braking is recovered by charging the hydraulic accumulator. This is due to the fact that hydraulic accumulator

2.3 Energy Storage System (ESS)

There are several different ESS that can be used in a hybrid vehicle. The ESS are usually chosen depending factors such as (1) the type of vehicle, (2) the mass of vehicle, (3) hybridization strategy and (4) cost of technology. In the previous section, different hybrid vehicle types have been introduced and some of the vehicular technology employs the usage of one or two ESS. There are 4 types of ESS that will be introduced in this section and they are:

- (1) Batteries
- (2) Ultra-capacitors (UC)
- (3) Hydraulic Accumulators
- (4) Flywheel

The selections of ESS are different in its characteristics and properties. A comparison between various storing technologies has been previously made; (1) comparison between batteries, ultra-capacitors and flywheel as ESS for HEV (Lukic et al., 2008) and (2) general comparison between batteries, ultra-capacitors, and hydraulic accumulators for hybrid vehicle (Nzisabira, Louvigny, & Duysinx, 2009). Figure 2.8 compiles the different attributes of energy storage technologies in a radar chart based on the works of Lukic et al. and Nzisabira et al.

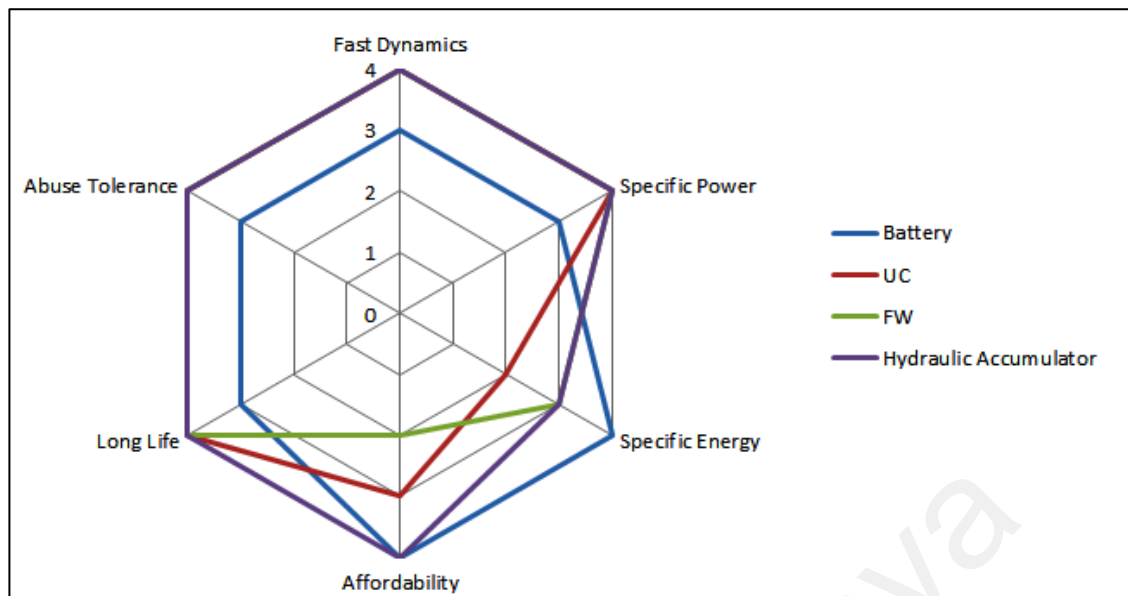


Figure 2.8 Comparison between energy storage technologies attributes for hybrid vehicles (Lukic et al., 2008, Nzisabira et al., 2009)

The first method of using batteries offers the advantage of being affordable, mobile and robust. However, batteries have low power density as compared to ultra-capacitors. Fuel cell technologies employ either batteries, ultra-capacitors or both of them altogether to store energies, improve response, and stabilise its output with regards to the fluctuations in the loading (Jin et al., 2009). Difference between power density and energy density between batteries and ultra-capacitors ensures that steady-state loading and transient loading system demands are well managed (Erdinc et al., 2009).

Next, applications of flywheels as ESS for automotive applications are novel. A revolving flywheel stores energy in the form of angular kinetic energy. Increasing the energy usually means using a heavier flywheel or one that moves in high speed. Automotive industries prefer higher angular speed flywheel as the energy stored is square of the flywheel angular speed and the fact that it comes in smaller sizes (Lukic et al., 2008). The only drawback is that due to friction, flywheel should operate in vacuum environment. Non-contact magnetic bearing applications to reduce bearing frictions have also been considered (Mulcahy et al., 1999). Higher energy storage capacity

flywheel will usually mean higher costs; therefore usage of flywheel is usually being considered only when other ESS costs higher (Lukic et al., 2008).

Applications of storage technologies vary from using only one ESS to using multiple ESS often with the considerations of how each of them interact within the system. For instance, PEM Fuel Cell uses both batteries and ultra-capacitors (Erdinc et al., 2009; Thounthong et al., 2009) and the Hydraulic-Electric Synergy System (HESS) employs batteries and hydraulic accumulators (Hui et al., 2011).

Study of different storage technologies that are presented provides an overview of the state of the art of hybrid vehicle development in terms of ESS. It also shows that different storing technologies require different handling and different strategies for the development of more effective hybrid vehicles. The present study will use hydraulic accumulator as the storing technology for the auxiliary energy supply for the HHV.

2.4 Energy Management System Strategies

An Energy Management System (EMS) is the brains behind the mechanisms of hybrid vehicle technologies. The EMS will govern the processes that take place at a specific time, by initiating and terminating the operations of devices under its control. Hybrid vehicles are often powered by more than one energy sources and many comprises of two different drivetrains. These put developing EMS for hybrid vehicle at higher stakes due to its complexity. In this section, different strategies in developing the EMS for hybrid vehicles are discussed.

EMS is developed for hybrid vehicle for often the same reason, which is to reduce the fuel (for ICE-hybrid) or hydrogen (for FC-hybrid) consumption by utilising energy supply from their own auxiliary drivetrain (Bernard et al., 2009; Caux et al., 2010; Kessels et al., 2008; Moreno et al., 2006; Silva et al., 2009; Sundstrom et al.,

2010; Wu et al., 2004). Other than reducing fuel, others are developed to reduce emissions from the ICE (Clarke et al., 2010; Silva et al., 2009).

In order to achieve these two objectives, often, two smaller objectives needed to be incorporated in the EMS which are to manage power sharing between different power sources (Ahn et al., 2009; Bernard et al., 2009; Erdinc et al., 2009; Hui et al., 2010; Kisacikoglu et al., 2009; Taghavipour et al., 2009; Won et al., 2005) and retaining charge for its auxiliary power sources (Hui et al., 2010; Jin et al., 2009; Moreno et al., 2006; Sundstrom et al., 2010; Won et al., 2005). Another objective for the developed EMS is the drivability of the vehicle – it is important to make sure that the driving experience does not deteriorate upon introduction of hybrid drivetrain in the system. Some drivability issues discussed are requirement of high quality power (Ferreira et al., 2008), maintain the engine to operate at its highly effective region (Hui et al., 2010; J. M. Zhang et al., 2009), antiskid regenerative braking system (J. L. Zhang et al., 2010) and slowing down the vehicle using regenerative braking (Seki, Ishihara, & Tadakuma, 2009).

The different objectives are implemented in the EMS using different strategies. There are generally two types of different strategies in developing an Energy Management System for a hybrid vehicle. Past researches suggested that the different strategies can be grouped into two which are (1) Optimization-based strategies and (2) Rule-based strategies.

For optimization-based strategies, the most popular is Dynamic Programming (DP) which has been discussed in various literatures (Caux et al., 2010; Dosthosseini, Kouzani, & Sheikholeslam, 2011; Geng, Mills, & Sun, 2011; Johannesson, Pettersson, & Egardt, 2009; Kessels et al., 2008; Saeks, Cox, Neidhoefer, Mays, & Murray, 2002; Wu et al., 2004). In developing EMS for hybrid vehicles, DP often used offline since

DP optimization can only be done with the whole power profile known (Caux et al., 2010). Furthermore, there are also requirement of large computations for the optimization process, making it even difficult to be used on-line (C. Zhang, Vahidi, Pisu, Li, & Tennant, 2010).

Other than DP, there are also other optimization-based strategies such as global optimization (Bernard et al., 2009), reducing multi-objective non-linear problem to single objective linear objective for optimization (Won et al., 2005) and training neural network (NN) on power profiles provided by previous cycle tests (Moreno et al., 2006).

The second strategy for EMS is rule-based strategies. Rule-based strategies can usually be used on-line, during the vehicle operations. Rule-based strategies include fuzzy logic, deterministic strategy and artificial intelligence. In past literatures, much has been discussed about fuzzy logic (Caux et al., 2010; Erdinc et al., 2009; Ferreira et al., 2008) and Equivalent Consumption Minimization Strategy (ECMS) (Chasse & Sciarretta, 2011; Geng et al., 2011; Geng, Mills, & Sun, 2012; Kim, Cha, & Peng, 2011; Sezer, Gokasan, & Bogosyan, 2011; Sinoquet, Rousseau, & Milhau, 2011; Xu, Li, Hua, Li, & Ouyang, 2009a, 2009b; C. Zhang et al., 2010) for the application of designing an EMS for hybrid vehicles. Most of the time, rule-based strategies are used as preliminary strategies before development of optimal control. ECMS for example, establishes a set of rules for the EMS before minimization of equivalent consumption for different power sources can be calculated.

Additionally, there are also other rule-based strategies used for this application such as Dynamic Classification – in hybrid fuel cell vehicle where the fuel cell states are determined the voltage of the battery (Thounthong et al., 2009), Transmission Actuated Energy Management (Sundstrom et al., 2010) and Nonlinear Power Balance

Control which modelled 6 different control modes in Bond Graph (Taghavipour et al., 2009).

From the study of the different EMS on different hybrid vehicles, it can be summarized that there are many approaches and strategies to be considered when it comes to developing an EMS. The current study develops a Regenerative Motor-Pump System and employs regenerative braking as a way to store energy in the system. Previous literatures studies on different EMS on different hybrid vehicle provide general ideas on how the control for Regenerative Motor-Pump System should be developed.

2.5 Regenerative Braking

Recently, regenerative braking has been a really popular way of reducing emissions and fuel consumption of internal combustion engine (ICE). Regenerative Braking is a braking mechanism that recovers mechanical energy and stores it for later use. Applications of regenerative braking as auxiliary energy in a vehicle differ in terms of the storage of recovered energy. Energy storage system (ESS) for vehicle that applies regenerative braking can be different, according to its primary motorization. Electric-based vehicle may have batteries, fuel cells or super-capacitors as its ESS (Ahn et al., 2009; Clarke et al., 2010; Jin et al., 2009; Kisacikoglu et al., 2009; Silva et al., 2009). Rotating flywheel is a mechanical ESS (Lukic et al., 2008), while highly pressurized hydraulics can store energy using the concept of regenerative braking (Hui et al., 2011). Other than applications on hybrid vehicles, regenerative braking has also been implemented on wheelchairs (Seki et al., 2009).

Regenerative braking has been considered as one of the “low-cost” solutions to the problems of emissions and fuel consumption other than fuel cut while coasting, engine stop/start, engine downsizing and turbocharging (Silva et al., 2009).

Regenerative braking is found to be effective if the reduction of fuel consumption can compensate the increment in weight of the vehicle due to the instalment of electrical pathway to the original vehicle. However if the typical efficiency of 73% is able to be reached by the regenerative braking system, a resultant of 10% fuel saving is possible (Silva et al., 2009).

Clarke et al. also proposes regenerative braking to cut vehicle emissions (Clarke et al., 2010). In their study, the authors discuss two different architectures for regenerative braking systems which are (1) regenerative braking systems operating in parallel with Internal Combustion Engine and (2) regenerative braking system that is used inside an electric vehicle. The authors tested the first architecture on a Skoda Fabia 1.9 SDI (Suction Diesel Injection) which incorporates the usage of electric motor that is connected to the ultra-capacitor via a DC-DC converter. They have found out that there is a higher increase in efficiency in the vehicle during city driving as compared to rural driving. In city driving, the Skoda Fabia succeeds to reduce emissions of CO₂ from 144.8g/km to 67g/km (Clarke et al., 2010).

The second architecture involves regenerative braking in an electric vehicle. For that purpose, the authors chose an electric scooter (EVT 4000E) to be tested with regenerative braking. The regenerative braking architecture incorporates an ultra-capacitor as an auxiliary energy storage system (to support the original battery power). The ultra-capacitor is connected to the motor controller via a DC-DC converter, while the original electric scooter battery is connected directly to the motor controller. The scooter, tested in a city driving test shows increase of 18.1% in efficiency, where the energy consumed would reduce from 0.056kWh/km to 0.039kWh/km (Clarke et al., 2010).

2.5.1 Regenerative braking in Parallel Hydraulic Hybrid Vehicle

Regenerative braking has been applied in Hybrid Electric Vehicle (HEV) and in Electric Vehicle (EV) and has shown significant savings in terms of fuel consumption and gas emissions as mentioned previously. The present study meanwhile based its foundations on Parallel Hydraulic Hybrid Vehicle (PHHV). In PHHV, the implementations of regenerative braking differ greatly from its electrical counterparts. Firstly, there's a difference in terms of transmission. PHHV adds an extra hydraulic transmission to the original ICE mechanical transmission as compared to electrical transmission in HEV. Secondly, PHHV uses hydraulic accumulator as ESS as compared to batteries and ultra-capacitors.

Hydraulic Regenerative Braking System (HRBS) that has been developed by Norhirni et al. implemented regenerative braking by converting kinetic energy to potential energy in the form of high pressure hydraulics in hydro-pneumatic accumulators (M. Z. Norhirni et al., 2011). HRBS will determine the modes of the operation from the user demands. Usually during braking, user will press the brake pedal resulting to the vehicle slowing down from the friction of the brake pad on the brake disc (or brake shoe on the brake drum – depending on the type of brakes). While this slows the vehicle down, some of the energy is converted to heat which usually accumulated along the brake linings. In contrast, HRBS will slow the vehicle down by allowing an axial piston pump/motor to operate as pump, and its output is supplied to a hydraulic accumulator. The conversion of energy to the hydraulic accumulator produces the braking effect (M. Z. Norhirni et al., 2011).

On the other hand, during acceleration, HRBS will decide; depending on the State of Charge (SOC) whether to use the accumulated charges in the pressurized accumulator to drive the main shaft of the vehicle. In this matter, the high pressure

accumulator will discharge the hydraulic fluid to the low pressure accumulator via the axial piston pump/motor unit (M. Z. Norhirni et al., 2011). This is illustrated in Figure 2.9

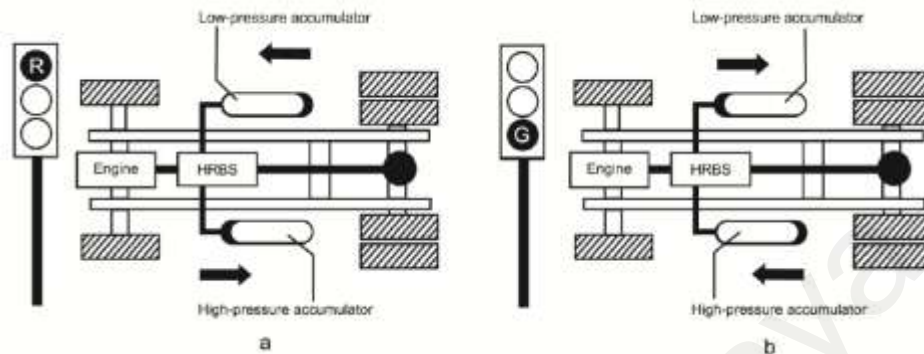


Figure 2.9 (a) PHHV during braking (b) PHHV during acceleration (M. Z. Norhirni et al., 2011)

2.6 Conclusion

In the present study, a regenerative motor-pump system is developed for the applications of Hydraulic Hybrid Vehicle (HHV). Based on previous research, HHV has great application potentials, especially when it comes to heavy vehicles having start-stop driving cycle. Regenerative braking is a part of the mechanism on the regenerative motor-pump system and hydraulic accumulator has high energy conversion efficiency to hugely capture braking energy, as well as high power density to accelerate heavy vehicles from stationary position. The next chapter will discuss on the instrumentation and control of the regenerative motor-pump system.

3.0 DESIGN AND INSTRUMENTATION

3.1 Introduction

This chapter describes the development of the Regenerative Motor-Pump System for the hydraulic hybrid vehicle (HHV). The Regenerative Motor-Pump System was developed to simulate hydraulic motorization in a HHV. The developed system will be discussed and elements from actual hydraulic hybrid vehicle will be compared. Processes from the actual hydraulic hybrid vehicle will be emulated using the system. Then, methods of evaluating the performance of the regenerative motor-pump system is discussed, and the measuring devices are introduced. Speed of flywheel and the pressure in accumulator tank are two of the examples of output signals retrieved from the system.

A Data Acquisition (DAQ) system is used to read and measure these signals and the relationship between the DAQ and the system is discussed. Signals retrieved from the system will also undergo signal conditioning using hardware and software before it can actually be used as an accurate evaluation of the controller. Actual testing of the controller will be in terms of demonstrating the processes in hydraulic hybrid vehicle. Further testing and evaluation of the controller with regards of the system will be discussed in the next chapter.

The controller developed is able to show that the processes in hydraulic hybrid can be emulated using a system, and that further evaluation of a hydraulic hybrid vehicle can be done using the system. The preliminary controller developed will also be able to anticipate problems that may arise when installing fully automated controller.

3.2 Regenerative Motor-Pump System Description

A hydraulic hybrid vehicle can be driven using two different motorizations, the first one is using conventional internal combustion engine (ICE); and the other is hydraulic motorization. The hydraulic motorization is driven by storing high pressure (charges) in the accumulator. In this study, the regenerative motor-pump system is designed to also recover energy during braking and store it in the accumulator for later use.

For this study, a Regenerative Motor-Pump System has been developed to emulate the hydraulic motorization of a hydraulic hybrid vehicle. The system serves as a substitute to installing hydraulic hybrid drivetrain on an actual truck. The system was designed for future applications and installation on an actual target vehicle. One of the advantages of using the system instead of directly installing the system on an actual truck is that the HHV controller can be tweaked, modified and tested without using the actual vehicle. The system can also be re-used to test a different controller for the HHV. This allows some flexibility in terms of controller development, that a lot of factors can be considered before finalizing the system and fixing it on the actual vehicle. Furthermore, testing can be done without moving from the Regenerative Motor-Pump System location. This way, the HHV system behaviour can be observed while many of the environment and external factors is kept constant.

The system developed is able to emulate two important process of a HHV hydraulic motorization, which are motor mode and pump mode. In motor mode, the system will emulate the process of using energy inside a HHV while in pump mode the system will emulate the process of braking energy recovery. Figure 3.1 shows the flow diagram of the Regenerative Motor-Pump System used to emulate processes on a HHV.

Prior to demonstrating processes on a HHV, the Regenerative Motor-Pump System needs to be charged with energy. Charging process in an actual HHV will occur during braking, using regenerative braking to charge the energy storage system (ESS). After the ESS had enough charge to start the demonstration, the Regenerative Motor-Pump System can start to emulate actual processes on HHV.

The motor mode is the process where the ESS starts to discharge energy to be used by the vehicle, in the case of HHV, during acceleration. Coasting is a process where the system do not discharge or charge the ESS. Pump mode is a process where the ESS is being charged, in the case of HHV, during braking and deceleration. The process of charging and discharging can be done continuously according to demand, which is simulated using cycle tests, or actual user input. The accumulated charge during pump mode can be used in the subsequent motor mode to support the main energy source, in the case of HHV, the Internal Combustion Engine.

These processes that are shown in Figure 3.1 are used to emulate actual processes on a HHV. Details on how actual devices are controlled and responded will be discussed in Section 3.4.2. Validation of the controller developed for the Regenerative Motor-Pump System will use this flow and the results are discussed in Section 3.7. The next sections will discuss on the components of the Regenerative Motor-Pump System in more details.

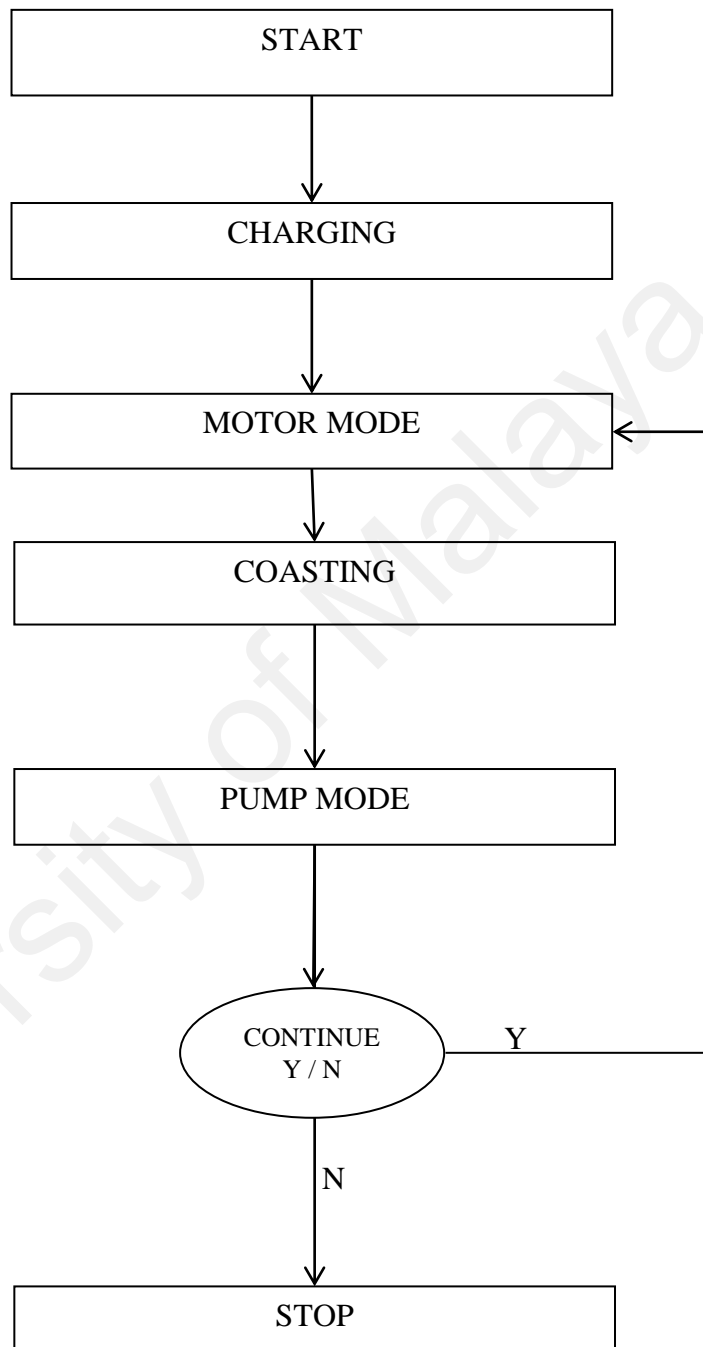


Figure 3.1 Flow diagram of Regenerative Motor-Pump System emulation of HHV

3.2.1 HHV Vehicle Model

To actually realize the full potential of regenerative braking in HHV, the base vehicle that is used should be heavy and preferably will operate on a stop-go cycle. Therefore, the system that was developed was designed to represent an actual HHV. The system consists of a 108.33-kg flywheel that is used to emulate the dynamics of a heavy truck. From the revolution speed of the flywheel, we can approximate the speed of the truck.

For this study, a commercial 5-ton truck is chosen to be the base vehicle for the hydraulic hybrid vehicle. Figure 3.2 shows a picture of the truck. The truck chosen is ISUZU made with model name NKR 71 E.



Figure 3.2 ISUZU NKR 71 E truck used in this study

Table 3.1 shows the specification of the ISUZU NKR 71 E truck which is used as the basis of the HHV. The truck has gross vehicle mass (GVW) of 8250 kg and curb weight (total weight of vehicle without cargo) of 2180 kg. For this study, the curb weight will

be considered in the simulation. A simulation of a HHV discussed later on in Chapter 5 is based on results of a dynamometer testing for the truck without load.

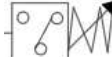
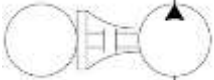
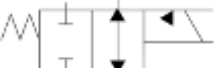
Table 3.1 Specifications of the ISUZU NKR 71 E truck

Dimension		
Overall Length (OAL)	mm	5830
Overall Width (OW)	mm	1860
Overall Height (OH)	mm	2120
Wheelbase (WB)	mm	3360
Min. Clearance (HH)	mm	200
Tread Front (AW)	mm	1400
Tread Rear (CW)	mm	1425
Engine		
Engine Model		4HG1-T
Bore and stroke	mm	115 x 110
Piston Displacement	cc	4570
Max Output	PS/rpm	125/2900
Max Torque	kgfm/rpm	35/1200-2200
Transmission		
Transmission Model		MYY5T
1 st		5.315
2 nd		3.053
3 rd		1.655
4 th		1.000
5 th		0.721
Rev		5.068
Final Gear Ratio		5.875
Suspension		
Front		Semi elliptical laminated leaf spring
Rear		With double force shock absorbers
Tire		
Front		7.50-16-14PR
Rear		7.50-16-14PR
Dish Wheel Size		16 x 6.00 GS
Weight		
Curb Weight	kg	2180
Gross Vehicle Mass (GVW)	kg	8250
Others		
Fuel Tank Capacity	Litre	100
Min. Turning Radius	m	7.5
Max. Gradability	%	38
Max. Speed	Km/hr	115
Accu	V-AH	12-65 x 2
Alternator	V-A	24-35
Power Steering		Yes
Tilt Cabin		Yes
Reverse Parking Camera		Yes

3.2.1 Hydraulic Diagram

A hydraulic flow diagram has been designed for the development of Regenerative Motor-Pump System. The system is designed so that it can emulate processes on an actual HHV. The design is represented with a hydraulic diagram as shown in Figure 3.3. Table 3.2 describes some of the symbols in the hydraulic diagram.

Table 3.2 Hydraulic symbols and its descriptions

Hydraulic Symbols	Description
	Work line
	Accumulator
	Ball valves
	Pressure Switch
	Filter
	Power Pack Motor Assembly
	Reservoir
	Check Valve
	Spring loaded Check Valve
	Throttling, depending on viscosity
	Variable pump
	Manometer
	4/3 Proportional Valve
	2/2 Valve (Valve B)
	3/2 Valve (Valve A)
	Pressure Limiting Valve, fixed

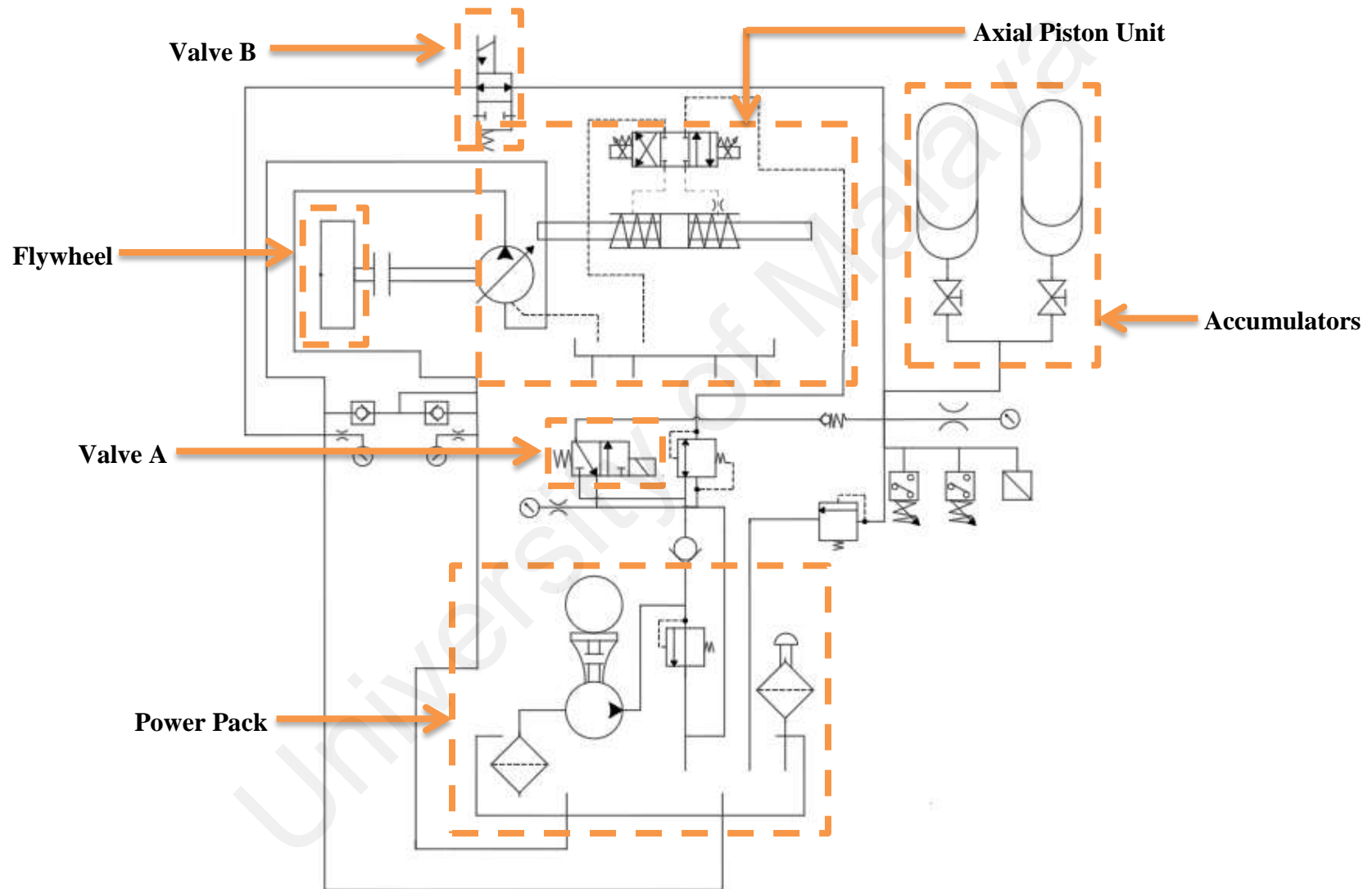


Figure 3.3 Hydraulic Diagram of the regenerative pump-motor system



Figure 3.4 Layout of the Regenerative Motor-Pump System

Figure 3.4 shows the layout of the Regenerative Motor-Pump System. The Regenerative Motor-Pump System is assembled based on the designed hydraulic diagram. The main components in the system are:

- (1) Axial Piston Unit
- (2) Accumulators
- (3) Power Pack
- (4) Flywheel
- (5) Brake Assembly
- (6) Valves
- (7) Pressure Switches

In the next sections, all these important components of the Regenerative Motor-Pump System will be discussed.

3.2.2 Axial Piston Unit (APU)

The APU is the most important component in the regenerative motor-pump system for HHV. The flywheel in the system is generally driven by the APU, and at the same time, the APU is the component that emulates the two modes in HHV which are pump mode and motor mode. The APU determines whether the hydraulic fluid will be stored in the accumulator (regenerative braking) or released to the reservoir tank (energy using – accelerating). The APU that is being used is “A4VSG Proportional Pump” manufactured by Rexroth Corporation. The unit is controlled with an amplifier card supplied to control the APU. By manipulating input signals on the amplifier card, we can determine the swash plate angle for motor mode and pump mode processes. Determining the swash plate angle affect the amount of fluid that travel via the APU. Manipulating the swash plate varies the flow rate and affects the power conversion from the high pressure accumulator to the speed of flywheel.

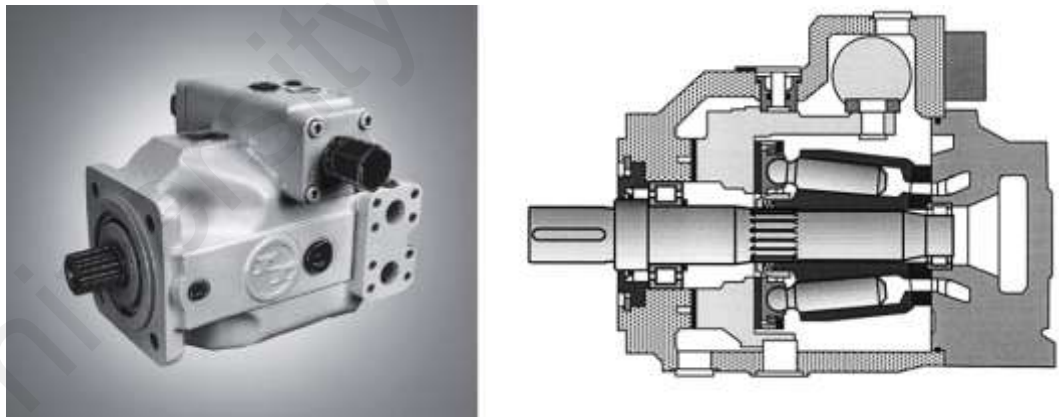


Figure 3.5 A4VSG Axial Piston Unit manufactured by Rexroth Corporation. (Right : Cross-sectional view of A4VSG Axial Piston Unit)

The APU that is used in this study is a variable displacement pump with swashplate design. The model that is selected is mostly used in industrial applications. The swashplate is hydraulically controlled by a proportional valve. Figure 3.5 shows a

diagram on the A4VSG Axial Piston Unit. Table 3.3 shows the specifications of the A4VSG Axial Piston Unit.

Table 3.3 Specifications of the Axial Piston Unit

Pump Model	A4VSG 71E01/10R – PPB10N00		
Axial Piston Unit	A4VS – Variable pump, swashplate design, industrial applications		
Mode of operation	Pump, closed circuit		
Control and adjustment devices	Hydraulic control, with proportional valve		
Series	10		
Direction of rotation (as viewed from shaft drive)	clockwise		
Seals	Buna N/ Shaft seal: FPM (Fluorocarbon)		
Shaft end	Metric keyed shaft per DIN 6885		
Mounting flange	ISO 4-bolt		
Port connections	Port A,B: SAE on the side, same side, UNC mounting threads		
Through drive	Without auxiliary pump, without through drive		
Displacement, $V_{g \max}$	cm^3/rev		71
Max. speed, n_{\max}	rpm		3200
Max flow at n_{\max} , Q_{\max}	L/min		227
Max flow at $n_E = 1200 \text{ rpm}$, Q	L/min		85
Max flow at $n_E = 1800 \text{ rpm}$, Q	L/min		128
Max power at n_{\max} , P_{\max}	kW		132
Max power at $n_E = 1200 \text{ rpm}$, P	kW		50
Max power at $n_E = 1800 \text{ rpm}$, P	kW		75
Max torque at $V_{g \max}$, T_{\max} $\Delta p = 350 \text{ bar}$	Nm		395
Torque at $V_{g \max}$, T $\Delta p = 100 \text{ bar}$	Nm		113
Moment of inertia about drive axis, J	kgm^2		0.012
Filling volume (case)	L		2.5
Approx. weight, m	kg		60
Permissible loading of drive shaft	Max axial Force, $F_{ax \max}$	N	800
	Max radial Force, $F_{q \max}$	N	1200

To ensure that the APU serves its purpose in the Regenerative Motor-Pump System, there is a need to control the swashplate angle of the APU. Controlling the swashplate angle is directly related to the flow direction of the hydraulics in the system. This ensures that the system can operate in both motor mode (hydraulic fluid discharges from accumulator to the reservoir) and pump mode (hydraulic fluid from reservoir charging

the accumulator) even when the APU shaft is rotating at the same direction. Controlling the swashplate angle enable the system to apply negative load to the system thus slowing down the flywheel rotation and at the same time recovering some braking energy. Figure 3.6 shows the APU main ports which are Port A and Port B.

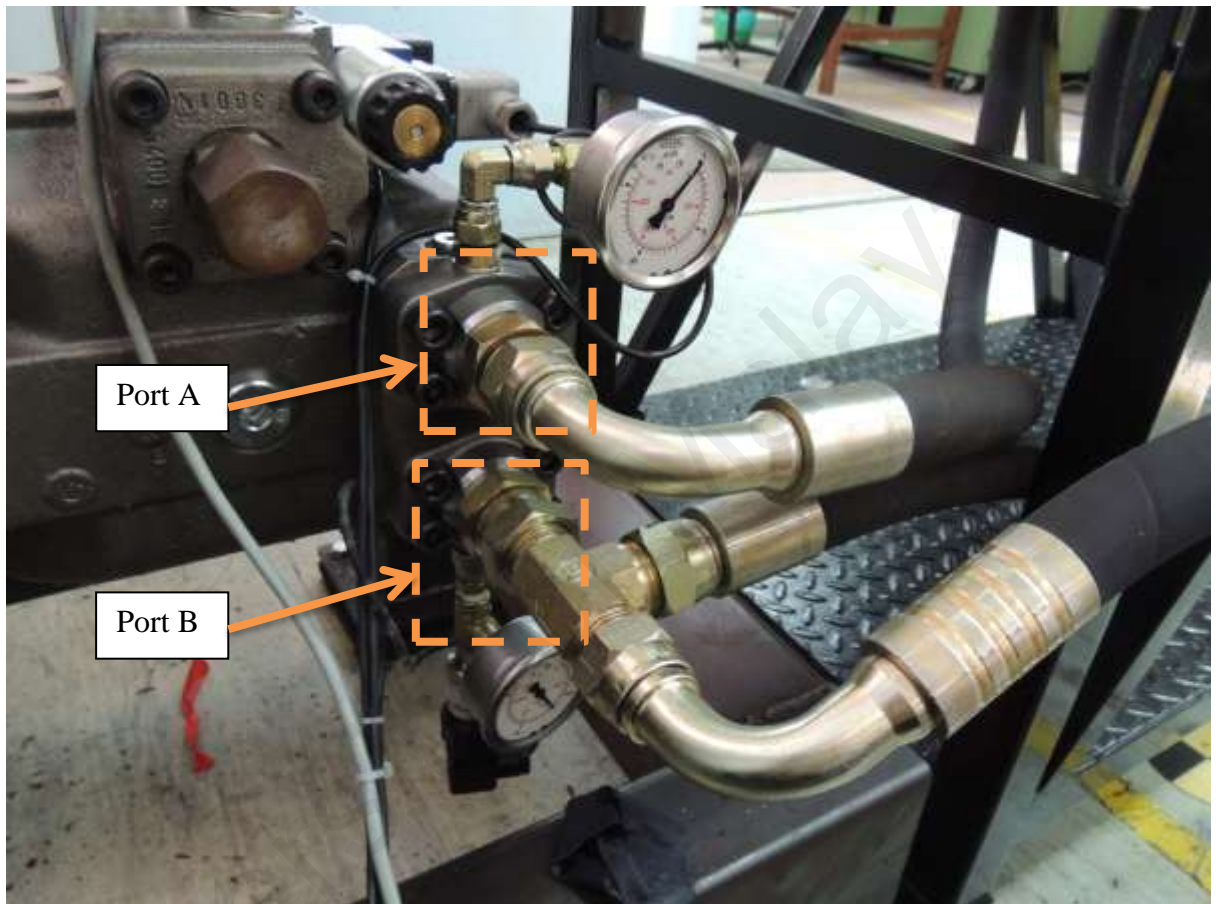


Figure 3.6 Axial Piston Unit main ports; A and B

Port A is directly connected to the reservoir while Port B is connected to the accumulator. To control the flow direction however, the proportional valve needed to be controlled to adjust the swashplate angle. The proportional valve is adjacent to the APU. The position of the APU's proportional valve can be seen in Figure 3.7.

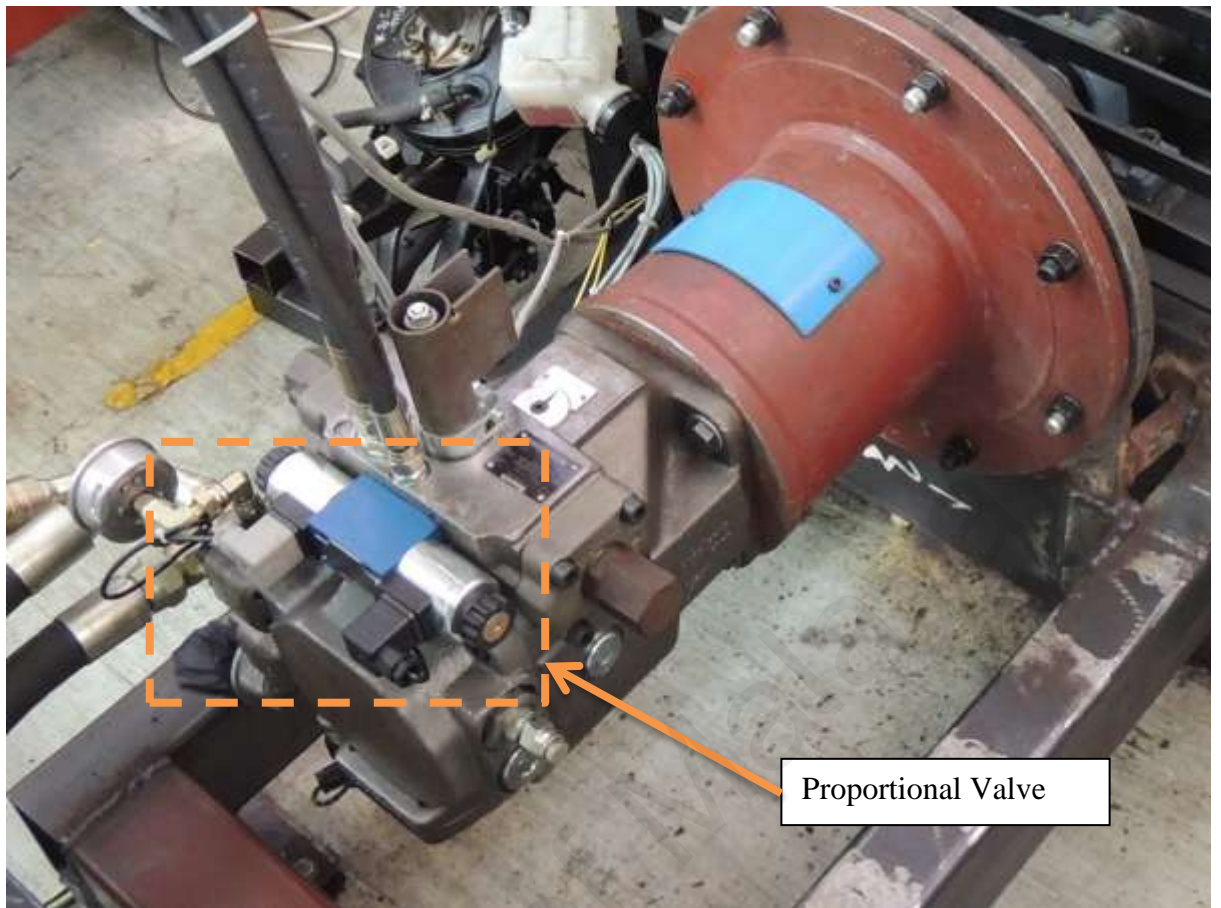


Figure 3.7 Proportional Valve position on the APU

As mentioned previously, the displacement of the proportional valve is controlled via an electric amplifier VT 5035. This amplifier card is specifically made for the APU and will amplify signals from external controller to adjust the flow of the APU. Figure 3.8 shows the amplifier card with its characteristics graph. The characteristics graph shows the ratio of the voltage (V_g/V_{gmax}) on the x-axis and the ratio of the swashplate angle (U/U_{max}) on the y-axis where the relationship is linear. Therefore, we can easily calculate the voltage required to get the desired swashplate angle. The calculation can be simplified as in Equation 3.1.

$$V_g = \frac{U}{U_{max}} \times V_{gmax} \quad (3.1)$$

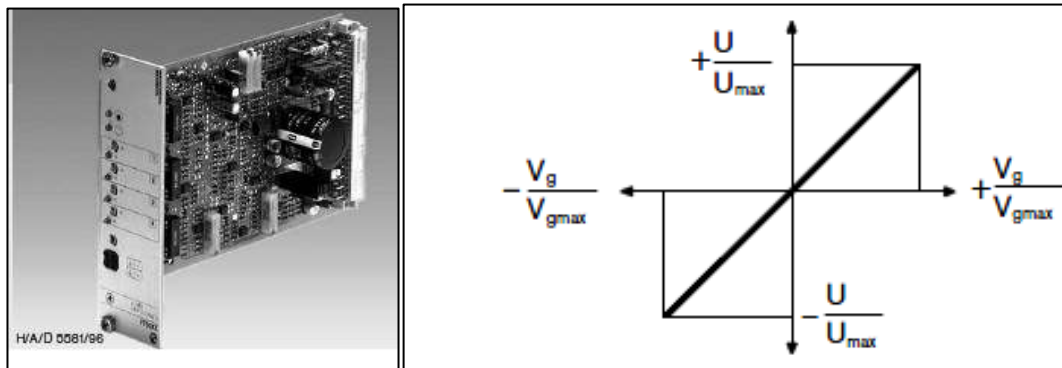


Figure 3.8 Amplifier Card and its characteristics graph

The direction of hydraulic fluid flow can be controlled by changing the swashplate angle, but it also depends on the direction of the rotation of the APU. Table 3.4 shows the direction of the flow according to the direction of rotation of the APU.

Table 3.4 Flow direction according to solenoid energized and APU rotation

Solenoid Energized	Clockwise	Counter-Clockwise
Right / b	B to A	A to B
Left / a	A to B	B to A

3.2.3 Accumulators



Figure 3.9 Accumulators in the form of red tanks are positioned beside the power pack.

Figure 3.9 shows a picture of two accumulators assembled for the regenerative motor-pump system. These accumulators serve as storing energy in the form of high pressure nitrogen gas. These accumulators are hydro-pneumatic bladder type accumulator that weigh 90 kg each, with nominal volume of 32 L. The maximum flow rate of the accumulators is 1800 L/min. For this study, only one of the accumulators is being used. The other accumulator is separated from the system by closing the ball valves underneath it. The ball valves being used are flange type steel ball valve (MKH-DN50).

3.2.4 Power Pack

In the HHV system, during release of stored energy inside the accumulator to the system, the hydraulic fluid would need to be collected in a low pressure reservoir. During motor mode, the Axial Piston Unit will allow high pressured hydraulic fluid to be released into the reservoir. In this study, the regenerative motor-pump system has one 90-L capacity reservoir for this purpose. This reservoir meanwhile is a part of a power pack.

The power pack has two functions. These functions are not a part of the functions of an actual HHV, but they are needed for the operation of the regenerative motor-pump system. The two functions are:

(1) Supplying 15 bar pilot pressure to the Axial Piston Unit.

The Axial Piston Unit (A4VSG Displacement Pump) is hydraulically operated, and therefore needed external pressure to be supplied to it. This external pressure is called as the pilot pressure. The proportional valve that controls the swash plate needed to be supplied with the pilot pressure so that it can operate. The supplied pressure is 15 bars and needed to be supplied continuously. The power pack is equipped with a 3-phase motor (5.5 kW, 8cc) that will pump the necessary pressure to the Axial Piston Unit.

(2) Charging the accumulator to begin the test cycle

The regenerative motor-pump system is developed without connecting it to an external engine that can drive the flywheel shaft in order to pump hydraulic fluid (store energy) into the high pressure accumulator. Therefore, the power pack also functions to charge the high pressure

accumulator with hydraulic fluid so that it can later be used to turn the flywheel, and simulate the speed of an actual HHV.

During charging process, the hydraulic fluid inside the reservoir will be pumped into the accumulator. The fully charged accumulator then can release energy into the system and therefore the testing cycle may begin.

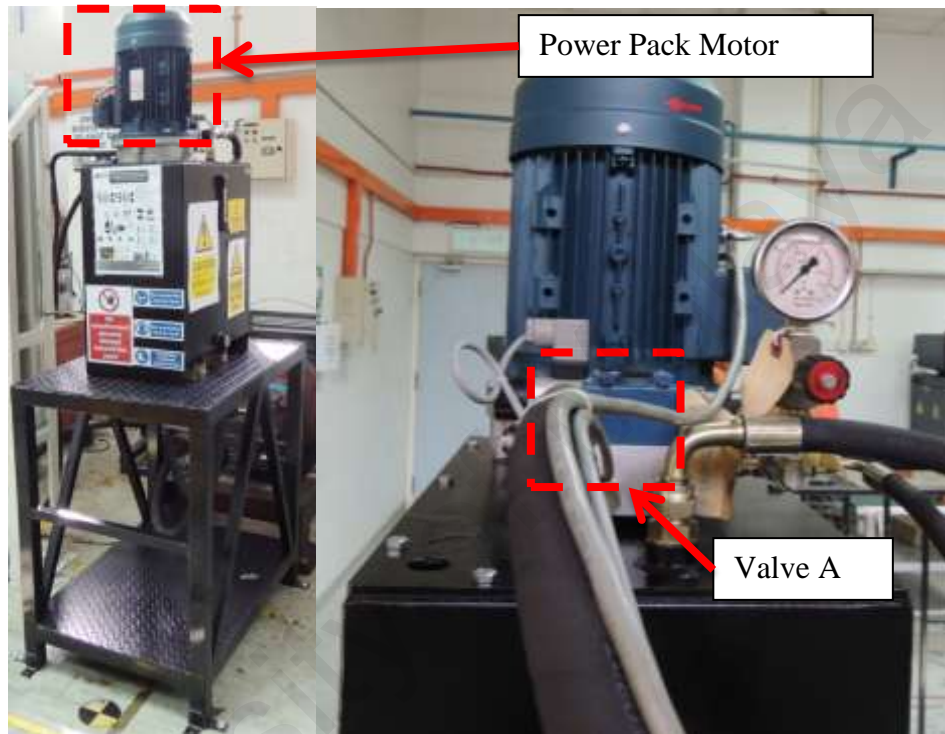


Figure 3.10 The power pack used for the regenerative motor-pump system. On the right is the top part of the power pack where Valve A and pressure gauge blocks are housed.

Figure 3.10 shows a picture of the power pack. The power pack is housed on a platform because the reservoir needed to be situated higher than the Axial Piston Unit. The reservoir is the black tank directly on the platform. The 3-phase motor for the power pack is the blue component directly on the tank. The top part of the power pack is also assembled with the Valve A, which controls the charging process for the system.

3.2.5 Flywheel



Figure 3.11 The flywheel inside a steel cage for safety purposes

Figure 3.11 shows a picture of the flywheel used in the system for the system. The flywheel is used to simulate the mass of the truck. From the revolution speed of the flywheel, we can approximate the speed of the truck using calculation. Energy in a moving truck is given by:

$$E_{vehicle} = \frac{1}{2} m_t v_t^2 \quad (3.2)$$

Where;

m_t = Mass of the truck, kg

v_t = Velocity of the truck, m/s

And meanwhile, energy in a moving flywheel is given by:

$$E_{flywheel} = \frac{1}{2}I\omega^2 \quad (3.3)$$

Where;

I = Inertia of the flywheel, $kg.m^2$

ω = Angular velocity of the flywheel, rad/s

To approximate the speed of the truck, we can arrange both equations to give:

$$v_t = \sqrt{\frac{I\omega^2}{m_t}} \quad (3.4)$$

Equation 3.4 approximates the velocity of a truck for any given flywheel angular velocity. The approximation is made by equating the energy inside a rotating flywheel and the energy in a moving truck. Evaluation on the regenerative motor-pump system will be made later based on this approximation.

To make this approximation, the inertia of the flywheel assembly needed to be considered. The flywheel weighs 108.33 kg and measures 50 cm in diameter. Table 3.5 shows the values of inertia for components of the flywheel assembly.

Table 3.5 Inertia of the components in the flywheel assembly

Components	Inertia ($kg.m^2$)
Flywheel	2.928
Drumbrake	0.00133
Pump Coupling	1.1262×10^{-3}
Shaft Coupling	3.2173×10^{-3}
Total	2.9456

3.2.6 Brake Assembly

The brake assembly consists of two components. One component which is the drum brake, is directly attached on the flywheel shaft and is considered as one of the flywheel assembly components as stated in the previous section. Another component is the brake pedals. For this study, only consideration on the inertia of the drum brake is included with the total inertia of the flywheel assembly. For this study, the brake pedal, even though is connected to the regenerative motor-pump system, is not used.

3.2.7 Valves

The regenerative motor-pump system has several valves that allow or block hydraulic fluid during certain processes. The valves are:

- (1) Ball valves for each accumulator (MKH – DN 50)
- (2) 3/2 valve to control the flow of hydraulic fluid from the power pack to the accumulator. Involves in charging the accumulator before beginning any testing cycle. Denoted in this study as Valve A.
- (3) 2/2 valve to control the flow from Power Pack (Reservoir) – Axial Piston Unit – Accumulator. This valve involves in motor mode and pump mode for the system. This valve is denoted as Valve B in this study.
- (4) Pressure Relief Valve to control the maximum pressure allowed into the accumulator. During pump mode, this pressure relief valve will allow hydraulic fluid from the reservoir to return back to the reservoir once the pressure inside the accumulator reached the pre-set pressure. For this study, the pre-set pressure is 80 bar.

The ball valves for each accumulator can be closed or open manually by pulling the lever that controls it. In this study, only one accumulator is being used from the two available, therefore one of the ball valve is open while the other is closed. Valve A and

Valve B are both electrically controlled. To open the valves, a voltage of 24V needed to be applied. The pressure relief valve is adjusted manually by manipulating the knob indicating the pressure. Figure 3.12 shows the pressure relief valve with the adjustment knob. There is also an analog pressure gauge assembled next to the pressure relief valve as shown in the figure. The analog pressure gauge is used to manually determine the pre-set pressure. For this study, the pressure relief valve will only allow charging the accumulator to 80 bars.



Figure 3.12 Pressure Relief Valve (blue block) with manual adjusting knob

3.2.7(a) Valve A

Valve A is 3/2-way directional poppet valve which is actuated using solenoid. Valve A is used to start charging process in the regenerative motor-pump system. Valve A connects the reservoir (power pack) directly with the accumulator so to charge the

accumulator directly. In an actual hydraulic hybrid vehicle, this connection is not available. Valve A requires 24V supply to open it since it is normally closed.

Table 3.6 Technical Specification for Valve A

Maximum Operating Pressure	350 bar (5000 psi)
Actuator Ports	3
Valve type	Poppet valve, wet pin solenoid actuated with removable coil
Coil Nominal Voltage	24V DC
Voltage Tolerance	+/- 10
Electrical connection	Individual connection; with component plug DIN 43560-AM2, without plug-in connection (with protected manual override)
Ambient Temperature Range	-30 to +50 °C
Weight	1.5 kg
Max flow	25 L/min
Power Consumption	30 W
Frequency	15000 cycles/hour
Protection to DIN 40 050	IP 65
Max coil temperature	150 °C

3.2.7(b) Valve B

Valve B is poppet type 2-way double lock normally closed solenoid operated valve. Valve B is used in the regenerative motor pump system to control the hydraulic flow from the accumulator to the axial piston unit. The valve will be open during the motor mode and pump mode. Valve B requires 24 V (90% nominal voltage) to open as it is normally closed. Table 3.7 shows the technical specifications for valve B. Figure 3.13 shows a picture of the solenoid valve.

Table 3.7 Technical Specification for Valve B

Maximum Operating Pressure		350 bar (5000 psi)
Fatigue Cycle Life at 300 bar (5000 psi) and 0.5 Hz (1s ON – 1s OFF)		10 million cycles
Rated Flow		70 L/min
Weight		0.220 kg
Minimum Voltage Required		90% nominal
Coil		
Weight		0.180 kg
Encapsulating Material		IXEF
Ambient Temperature Range		-30 to +60 °C
Heat Insulation	Class H	180 °C
Voltage, V	Nominal	24 DC
Resistance, Ω	Ta = 20 – 25 °C	28.5
Power, W	Cold Coil	20
Current, A	Cold coil	0.85
	Hot Coil	0.61



Figure 3.13 Valve B (inside black block) with coil compartment on its right.

3.2.8 Pressure Switches

The regenerative motor-pump system employs two pressure switches to track pressure in the accumulator. The pressure switch signal also acts as one of the safety measures in the system. In developing the system, two different pressure switches is calibrated and connected to the system. Both pressure switches is connected as to detect the reading of the pressure inside the accumulator. The pressure switches are calibrated to turn 'on' when the pressure reaches 15 bar and 90 bar respectively.

The pressure switches being used are Mannesmann Rexroth's type HED 8 hydro-electric pressure switch. Table 3.7 shows the technical specifications of the pressure switches used in this study. Figure 3.14 shows a picture of the pressure switch.

Table 3.8 Technical specification of Pressure Switch type HED 8

Weight	0.8 kg
Maximum settable pressure	200 bar
Maximum operating pressure	350
Pressure setting range	5 to 200
Switching accuracy	$< \pm 1\%$ of settable range
Permissible switching frequency	4800/h
Maximum connection cross sectional area	1.5 mm ²
Maximum contact load (V DC)	50V/1A, 125V/0.03A, 250V/ 0.02A



Figure 3.14 Pressure Switch type HED 8

3.3 Hydraulic Hybrid Vehicle Processes on Regenerative Motor-Pump System

The system is developed to simulate the processes that occurred on an actual hydraulic hybrid vehicle. The processes on an actual HHV can be categorized into two most important states:

1. Motor Mode (Energy Release)
2. Pump Mode (Energy Recovery)

In an actual HHV, regenerative braking will supply the needed pressure in the hydraulic accumulator. In the system, since it is stationary, there is a requirement of charging the accumulator before any of the modes can be simulated. For the system, the charging process is introduced. In this process, a power pack will directly charge the accumulators so that the simulation can begin.

The amount of charge inside the accumulator can be controlled manually using pressure relief valve and automatically using programming. Other than the charging process, two different states were introduced to represent Idle Mode in the actual HHV. Lastly, a STOP mode is also introduced in the system to signal end of simulation. Table 3.9 shows the comparison between the states in the system with the processes that occurred in an actual Hydraulic Hybrid Vehicle (HHV).

Table 3.9 Comparison between processes in System and PHHV

States in Regenerative Motor-Pump System	Processes in PHHV
OFF State	Idle Mode
Zero State	Idle Mode
Charging State	No corresponding process in PHHV
Motor Mode	Motor Mode
Coasting	Pure ICE motorization
Pump Mode	Pump Mode
STOP	Idle Mode

In previous section, Figure 3.3 shows the hydraulic diagram of the assembly of the regenerative motor-pump system. To understand the processes in the regenerative motor-pump system, the hydraulic diagram will be referred to and discussed according to the processes. Figure 3.3 can also be referred to, to check the connection between different devices in the system. In the diagram however, the flywheel assembly is simplified as the diagram serves to highlight the hydraulic connectivity of the system.

The different process will require different devices to behave differently in one state and the other. For example, the 2/2 valve is only OPEN during motor mode and pump mode. The 2/2 valve needs to be CLOSED during charging to ensure that the hydraulic fluid flow directly into the high pressure accumulator. Table 3.10 shows the different devices and how it behaves according to the processes. In the table, the processes are being grouped into states, where states correspond to the events (processes) that occurred in an actual HHV.

Table 3.10 State and Processes in the System

State	Processes	Device Behavior
OFF State	Turn OFF	E-STOP OPEN All Switch OFF Main Supply OFF 3 Phase Disconnect
Zero State	Control everything OFF	E-STOP OPEN All Switch OFF
	Begin Setup	Turn ON Extension Cable Power Turn ON TargetPC Turn ON Remote Control (Laptop) Load xpcexplr in MATLAB
	Turn ON motor	DO2 ON (Contactor)
	Turn ON Amplifier Card	DO1 ON (ENABLE)
Charging State	OPEN Valve A	DO3 ON (3/2)
	Charge until 85 bar	Check pressure gages Alternative (Pressure Transducer reading – Auto-Stop)
	After 85 bar CLOSE Valve A	DO3 OFF
Motor Mode	Swash Angle –ve Max	A1 -10V (Matlab)
	OPEN Valve B	DO4 ON (2/2)
	After 15 bar CLOSE Valve B	DO4 OFF (2/2)
Coasting	Flywheel run	Caution
	Swash Angle Return '0'	A1 0V (Matlab)
	Flywheel Speed Read	Speed Sensor Reading
Pump Mode	Swash Angle +ve	A1 5V (Matlab)
	OPEN Valve B	DO4 ON (2/2)
	After flywheel stop CLOSE Valve B	DO4 OFF (2/2)
STOP	Check Accumulator Pressure	Check Pressure Gages Alternative (Pressure Transducer Reading – Auto Read)

3.3.1 OFF and Zero State

OFF state is the default state of the system. In this state, the system is not supplied with any power. Zero state, is the second state, where the system is not actually emulating any of HHV processes. In this state, the system is being setup. All the devices are devoid of power except the main control terminal which is the Target PC, and the remote control computer (user terminal). The control program is also being

loaded from the remote control computer to the Target PC in this state. The power pack motor is also turned on in this state.

3.3.2 Charging State

Figure 3.15 shows the flow of the hydraulic fluid during charging state. In the charging state, Valve A is opened to allow the power pack to charge the accumulator. In this way, the system will have high state of charge (SOC) before the testing starts. This charging state also does not have any corresponding process in an actual PHHV. In real PHHV, the charging of the accumulator happened along with braking. Since the system does not incorporate an engine, the accumulator has to be charged in order to make the first run.

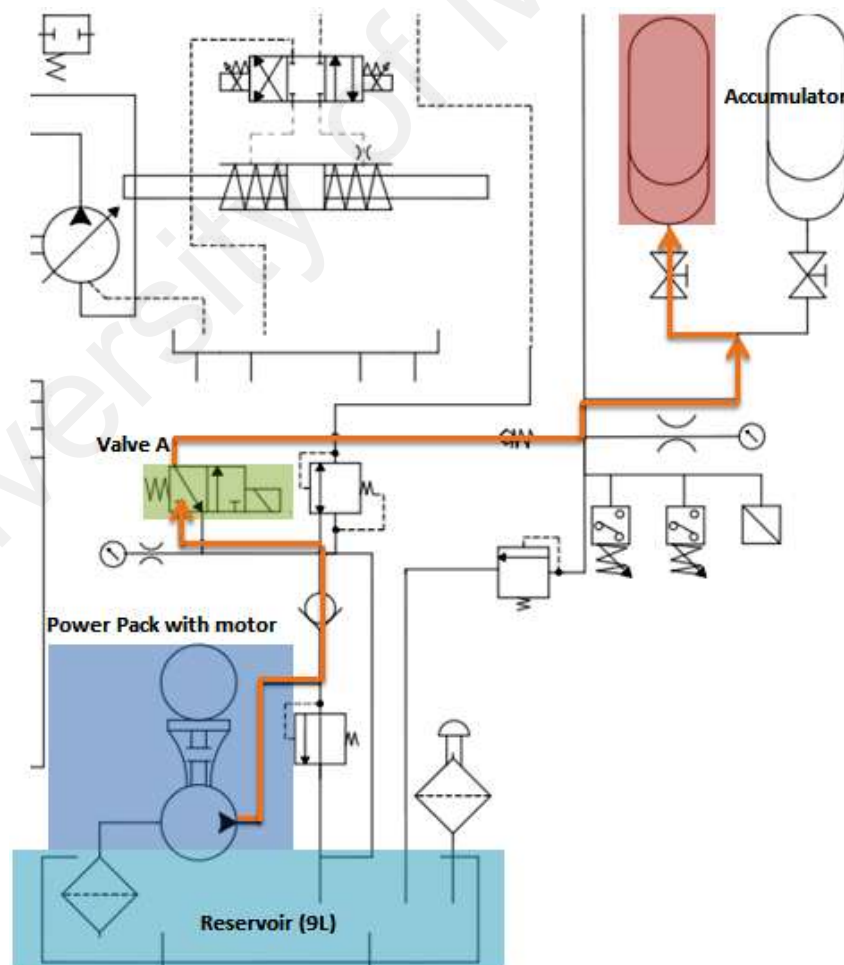


Figure 3.15 Charging State – Power Pack supply hydraulic fluid to the accumulator directly

3.3.3 Motor Mode State

The next state is motor mode. Figure 3.16 shows the flow of the hydraulic fluid in the motor mode state. In an actual PHHV process, the accumulator will release the high pressure fluid to the reservoir tank. This will supply the energy for the APU to revolve, thus supplying torque to the vehicle. In the system, this process will also allow APU to revolve thus supplying the torque to the flywheel - which has been carefully selected to represent an actual vehicle weight. To initiate this state, Valve A will be closed, while Valve B will be opened to allow the pressure built up to flow via the APU. The hydraulic fluid will then flow to the reservoir tank, and the flywheel will continue moving due to its inertia. To allow the fluid to flow to the right direction, the swashplate angle is set to be -15° , which is the maximum negative angle of the APU.

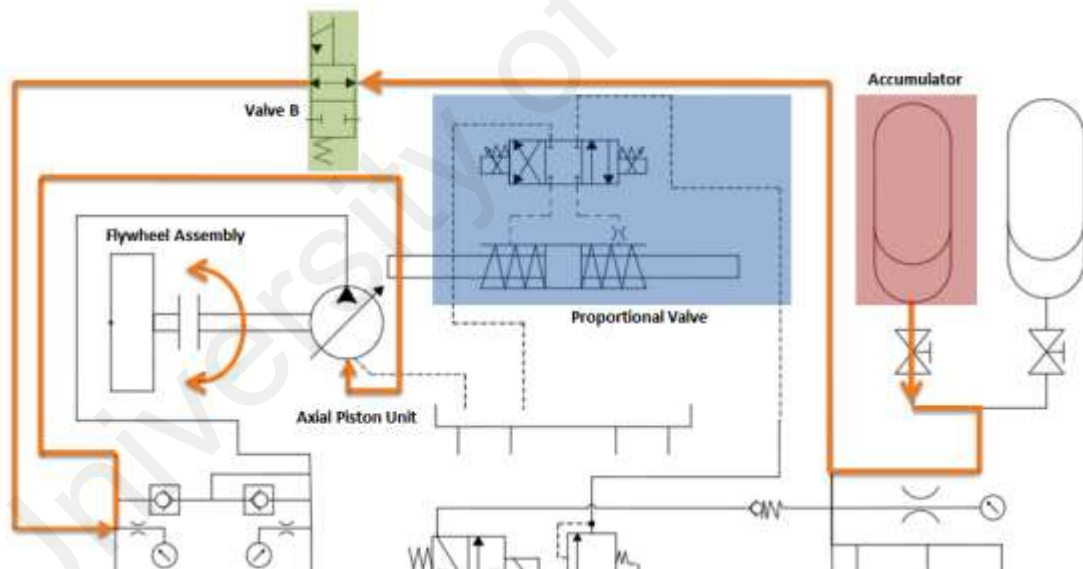


Figure 3.16 Motor Mode – Accumulator releases high pressure hydraulic fluid to turn the flywheel

3.3.4 Coasting State

The next state is the coasting state. This state is entered if the SOC of the system is low. In actual PHHV, this state will allow the vehicle to be driven purely with the Internal Combustion Engine. But in the Regenerative Motor-Pump System, once there is no charge in the system, there will not be any more torque supplied to the system. This state will be a transition state between the motor and pump modes. In this state, the flywheel is allowed to revolve freely without moving any fluid from any location. The swash plate angle for this state is 0° , which is the neutral location of the swash plate for the APU.

3.3.5 Pump Mode State

The pump mode state is a state that emulates the actual pump mode in PHHV. Figure 3.17 shows the flow of hydraulic fluid in pump mode state. In this state, similarly like the actual PHHV, the braking energy will be used to pump back the hydraulic fluid from the reservoir to the accumulator. In this state, Valve B will be opened to allow fluid from the APU to flow to the accumulator. By doing so, the flywheel will slow down as energy is being used to pump the fluid. This correspond to the actual PHV where activating the regenerative braking will slow down the vehicle. The swashplate angle of the APU will be set to 5° so that the fluid will flow from the reservoir to the accumulator even when the APU is revolving at the same angular direction during motor mode. This different swash plate angle made the different direction flow possible (reservoir to accumulator/accumulator to reservoir) even when the APU is turning in the same angular direction (counter-clockwise). But instead of the APU revolving in the opposite direction, changing the fluid flow will slow down itsk revolutions which in turn slow down the flywheel.

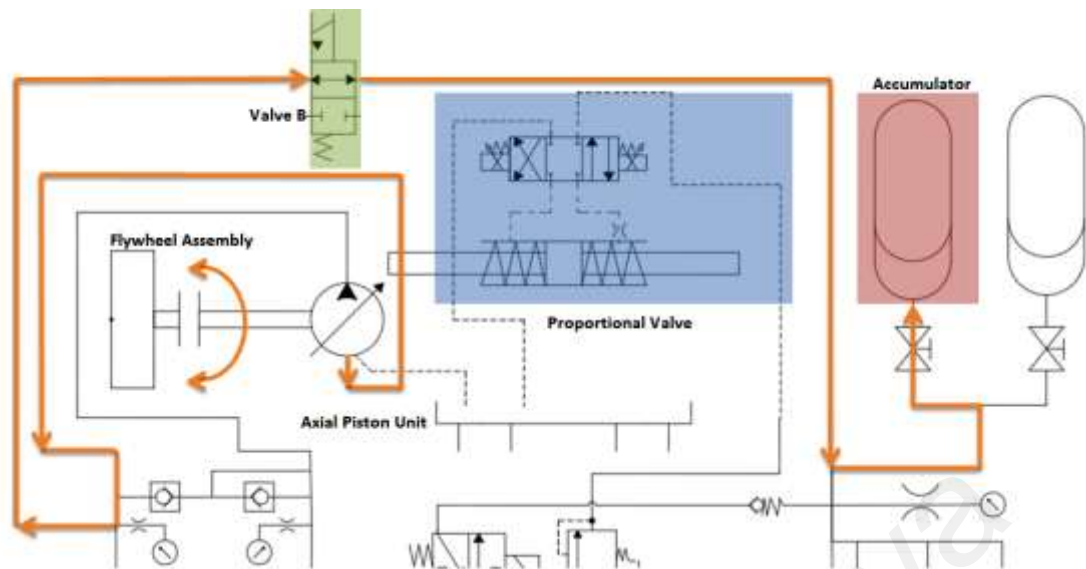


Figure 3.17 Pump Mode – The flywheel rotation pumps hydraulic fluid from reservoir back to the accumulator

3.3.6 STOP State

The Regenerative Motor-Pump System slows down to a halt after the Pump Mode. The STOP state in the system is for the purpose of ending the simulation. This state will allow the data collected from the system (Target PC) to be downloaded to the remote control (user terminal) to be analysed later.

3.4 Development of Preliminary control for Regenerative Motor-Pump System

As previously discussed, there are many advantages of Regenerative Motor-Pump System when used to evaluate HHV controller as compared to directly implementing the controller on the actual HHV. In previous sections, the components and parts of the Regenerative Motor-Pump System have been discussed, and in most cases, the components on the system are the actual component proposed to be on the actual HHV. Also in the previous section, the processes on the system has also been discussed. Most of the processes resembles the actual processes on the HHV and needed to be controlled so that it can emulate the flow of processes on the actual HHV.

In order to achieve that objective, a controller for the Regenerative Motor-Pump System was developed. The controller initiates processes on the system by communicating with the components and devices on the system, while at the same time acquire feedback from the system. In this study, a preliminary controller has been developed in MATLAB/Simulink environment.

Figure 3.18 shows the connections between the systems to the Target PC and finally to the Host PC which can be situated remotely. The controller developed was executed in a PC that is connected to a Target PC that is then connected directly to the components of the system via a Data Acquisition (DAQ) card. In this study, the Target PC and the Host PC is connected through LAN cable. The two PC can also be connected via Wi-Fi; data can be transferred between the two PC as long as they can establish LAN connections.

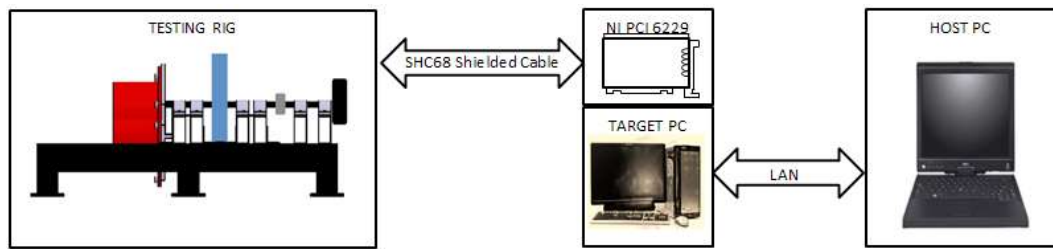


Figure 3.18 Regenerative Motor-Pump System Connections

3.4.1 Development of Data Acquisition (DAQ) System

Data from the system will be collected as a feedback to the controller to help evaluate the system being developed. The DAQ card that is used to cater to this function is an M-series NI PCI-6229 made by National Instrument. The DAQ card has four 16-bit analog output and 48 digital input/output. It was selected due to its high sampling rate and high accuracy. It is also low cost and able to be integrated with the developed controller, due to its compatibility with MATLAB integrated development environment. Figure 3.19 shows a snapshot of the DAQ card.



Figure 3.19 NI PCI-6229 DAQ card from National Instruments.

The modules for the DAQ card can easily be accessed from MATLAB's Simulink environment, making it easier to develop the system using MATLAB and Stateflow. For the system, there are several modules that are used to acquire data and to transmit data. They are 7 Digital I/O, 3 Analog Input and 1 Analog Output modules. For the digital I/O, 3 are for input and the rest are for output. Table 3.11 shows the assignments of the different I/O signals to the actual physical functions.

Table 3.11 DAQ Modules used for the system

Modules	Device	Function
Digital Output 1 (DO1)	Amplifier Card	ENABLE signal
Digital Output 2 (DO2)	Motor Contactor	To turn on the power pack motor
Digital Output 3 (DO3)	Valve A	To OPEN valve
Digital Output 4 (DO4)	Valve B	To OPEN valve
Digital Input 1 (DI1)	Pressure Switch 1	Indicate that pressure reached 15 bar
Digital Input 2 (DI 2)	Pressure Switch 2	Indicate that pressure reached 90 bar
Digital Input 3 (DI 3)	Speed Sensor	Measure the frequency of reflection on the flywheel to convert it to flywheel angular speed.
Analog Output (AO1)	Amplifier Card	Change the swash plate angle
Analog Input (AI1)	Pressure Transducer 1	Only one of analog module is supported in MATLAB's Simulink, so the DAQ will have to scan both channels alternately.
Analog Input (AI 2)	Pressure Transducer 2	

3.4.2 Development of Preliminary Controller in Simulink

Figure 3.20 shows the Preliminary Controller developed for the HHV Regenerative Motor-Pump System. The controller also features some virtual LED to determine the states of the devices. During test runs, switching a manual switch to 'ON' or 'OFF' will cause a virtual LED to light up in red colour. Virtual displays are also available on the Simulink controller. Voltage for swivel angle of the swashplate is

displayed in one, along with two on flywheel rotational speed, two for pressure transducers and one that shows the converted value of the flywheel rotational speed in kilometres per hour (km/h).

Additionally, there are also Target Scope blocks on the Simulink diagram of the controller. The blocks represent the scope that is displayed on the monitor of the Target PC. For instance, pressure transducer readings are displayed on the Target PC monitor in the form of graph. These virtual indicators and Target PC displays helps the operator of the Preliminary Controller to understand the conditions and states of the system allowing informed decisions to be made.

There is also one subsystem block for workspace variables, where all the data collected during the test runs are saved. Data collected using DAQ from the speed sensor and pressure transducers are saved in a generic variable that are easily transferred to other formats where it can be analysed and manipulated.

Using this controller, some basic runs have been made to test the controller and the response of all the system components. Figure 3.21 illustrates the flow of processes done in the basic testing for the Regenerative Motor-Pump System. The basic testing consists of charging the accumulator up to 85 bar of pressure, then change into motor mode until the pressure reached 15 bar before revolving the flywheel in coasting mode. In coasting mode, the swivel angle of the Axial Piston Unit/ Swashplate Proportional Pump will be 0 °.

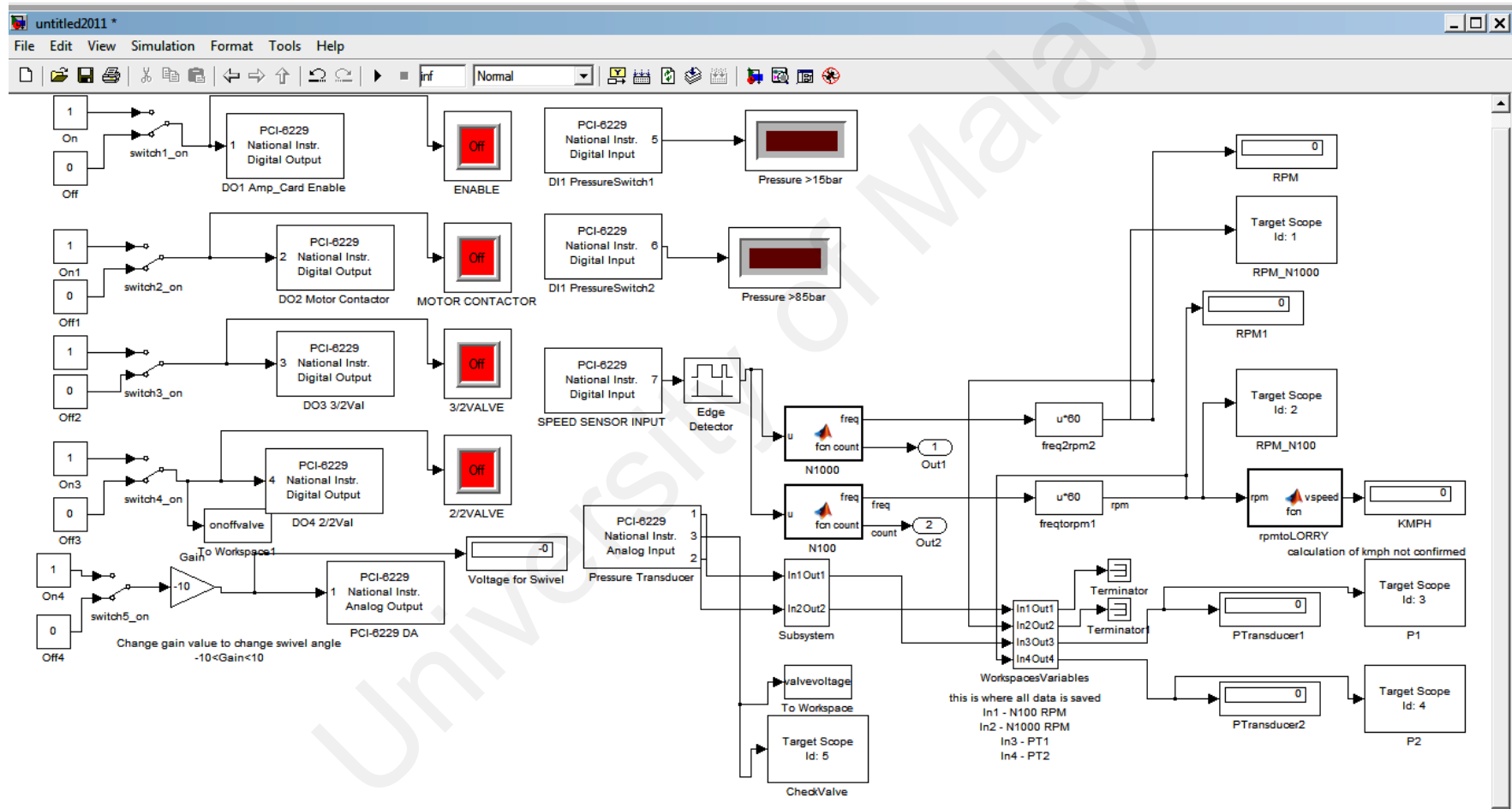


Figure 3.20 Preliminary Controller for Regenerative Motor Pump System

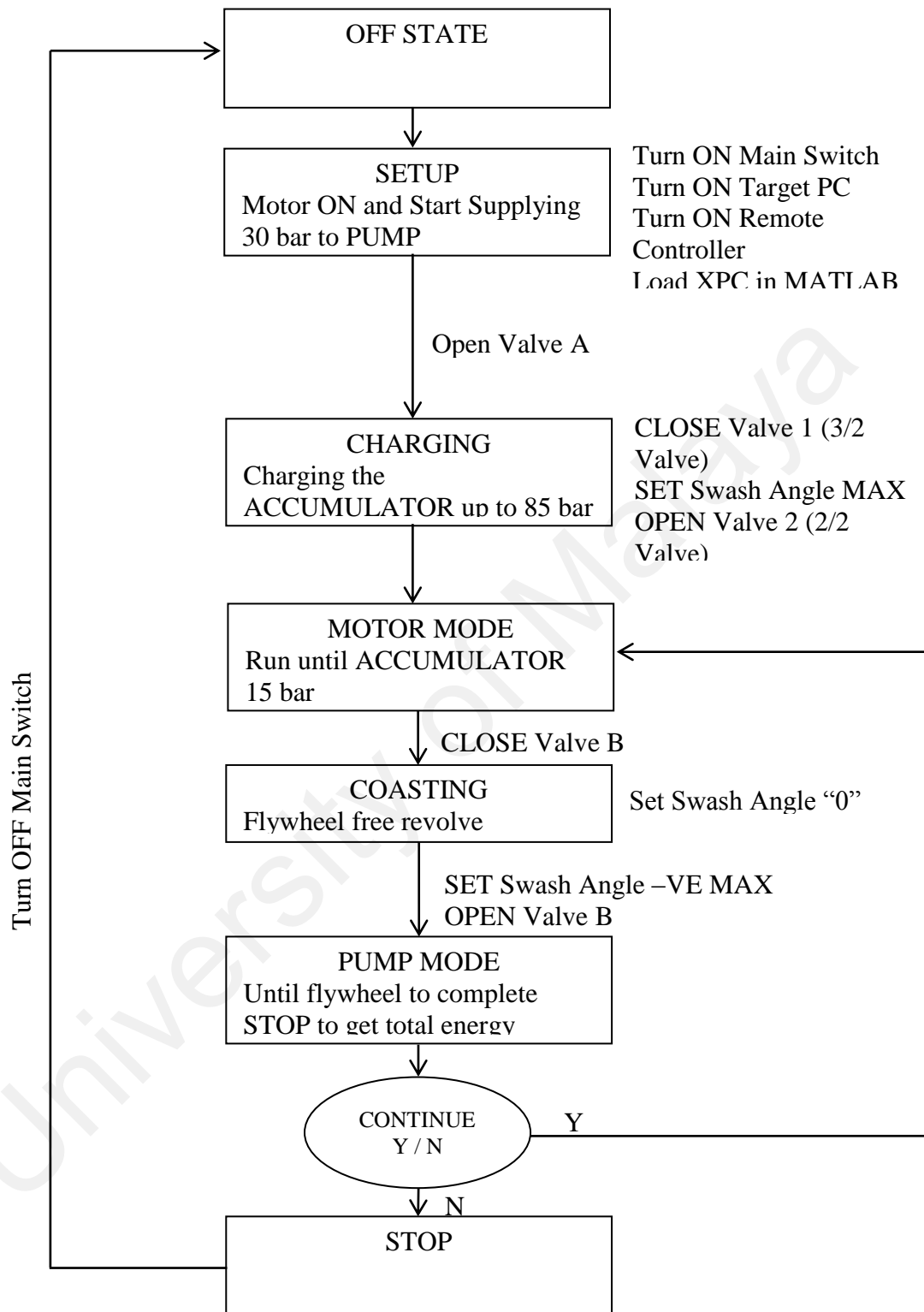


Figure 3.21 Flow of the processes of the basic testing for Regenerative Motor-Pump System

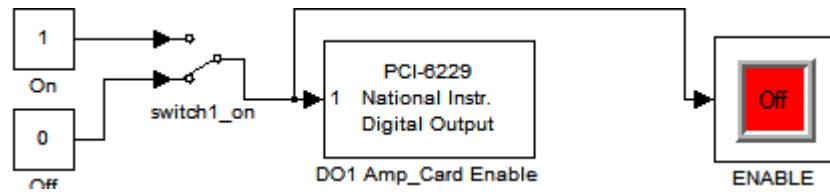
After that, the system will be changed into Pump Mode while the flywheel is still revolving to see the charging process done by the revolving flywheel. This testing will be done manually; switching the valves and changing the angle will be determined by the operator by looking at available feedbacks.

The preliminary controller consists of switches that will be controlled by the operators.

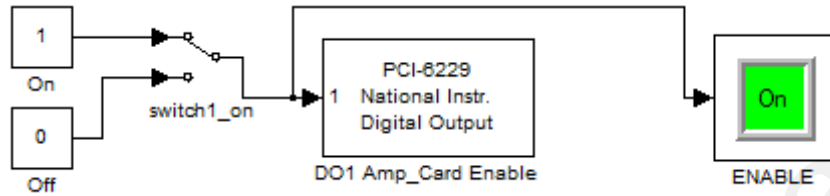
The preliminary controller can be divided by modules. The modules are:

1. Digital Output for Amplifier Card
2. Digital Output for Motor Contactor
3. Digital Output for Valve A
4. Digital Output for Valve B
5. Digital Input for Pressure Switch A
6. Digital Input for Pressure Switch B
7. Digital Input for Speed Sensor
8. Analog Output for Swivel Angle
9. Analog Input for Pressure Transducers

Among these modules, the first four modules are equipped with switches. In Simulink/MATLAB environment, these translate into having manual switch block on the Simulink diagram connected to two inputs which are zero and one. Figure 3.22 shows an example of the Simulink block arrangements for one of the Digital Output modules. In the diagram, the Enable Amplifier Card module is being shown. The “On” switch and “Off” switch is actually passing “1” and “0” respectively to the “PCI-6229 National Instrument Digital Output” block.



(a)



(b)

Figure 3.22 Simulink block arrangement for the switching modules (a) Turned off (b) Turned on

For the swivel angle, the operator can change the voltage needed to be supplied by the DAQ card by changing the Swivel Voltage gain block value as shown in Figure 3.23. For this controller, changing the gain block value is done manually, and in Figure 3.23, the Swivel Voltage gain block has a value of -10.

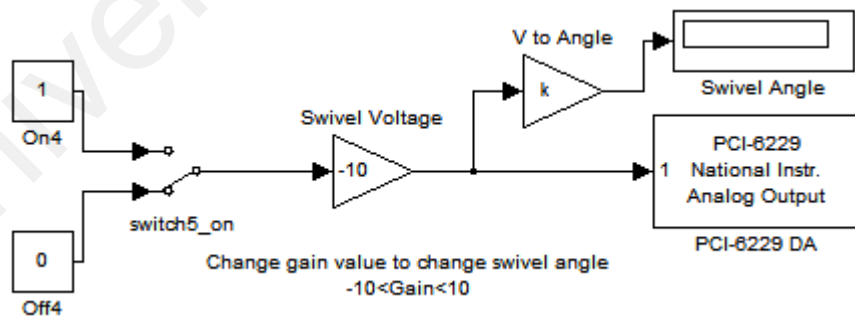


Figure 3.23 Simulink block arrangements for swivel angle

The swivel angle is calculated by:

$$\frac{\text{Maximum Swashplate Angle}}{\text{Maximum Voltage}} \times \text{Swivel Voltage} \quad (3.5)$$

Where;

$$k = \frac{\text{Maximum Swashplate Angle}}{\text{Maximum Voltage}}$$

And since the Maximum Swashplate Angle is 15° in both directions, and that the maximum voltage range for the DAQ Analog Output module is $-10V$ to $10V$, the Maximum Voltage has a value of 10. This made the value k in the Simulink block arrangements to be equal to 1.5.

Therefore, the Swivel Angle value that can be used as input in the Simulink block arrangements ranges from -10 to 10 . The Swivel Angle display block will display the swivel angle currently required from the system.

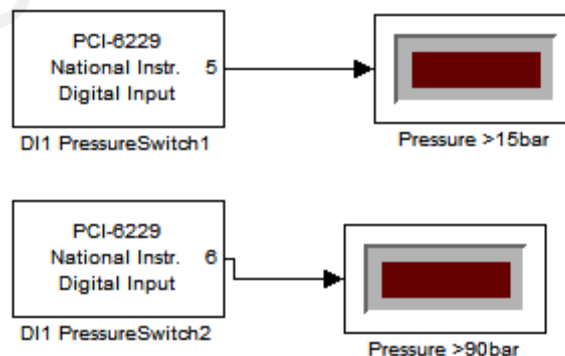


Figure 3.24 Simulink block arrangements for Pressure Switches

The manual controller also employs two Digital Input modules that will return value from pressure switches in the system. One of the pressure switches will be turned on once the pressure inside the accumulator reaches 15 bar, while another will light up once the pressure inside the accumulator is 90 bar. This is illustrated in Figure 3.24. Both pressure switches are supplied with 24V and will be turned on when the accumulator reached the respective pressures.

The modules discussed in this section for preliminary controller for Regenerative Motor Pump System is summarized in Table 3.12. In the table, there is information on the connected terminals. The speed sensor and pressure transducers modules will be discussed in later sections.

Table 3.12 Summary of DAQ Modules used for Preliminary Controller for Regenerative Motor Pump System

DAQ NI 6229 Modules	DAQ NI 6229 Terminal (+ve)		DAQ NI 6229 Terminal (-ve)		Item/Device
Channel 1 Digital I/O	52	P 0.0	18	DGND	ENABLE (Amplifier Card)
Channel 2 Digital I/O	17	P 0.1	18	DGND	Contactora
Channel 3 Digital I/O	49	P 0.2	18	DGND	Valve A
Channel 4 Digital I/O	47	P 0.3	18	DGND	Valve B
Channel 5 Digital I/O	19	P 0.4	53	DGND	Pressure Switch A
Channel 6 Digital I/O	51	P 0.5	53	DGND	Pressure Switch B
Channel 1 Analog Output	22	AO 6	55	AO GND	SWIVEL ANGLE (Amplifier Card)

3.4.3 Development of Switching Circuit for Data Acquisition and Control

There is also a need to design a circuit that can act as a mediator between the Target PC (DAQ card) and the devices and components of the Regenerative Motor Pump System. Some of the devices are switched “on” and “off” using the DAQ card,

but sometimes, the DAQ card couldn't supply the necessary voltage/current to the devices. Some of the problems are:

- (1) The ENABLE signal for the Amplifier Card needed to be supplied by short-circuiting 22a and 22c terminals in the Amplifier Card.
- (2) The Contactor needed to be supplied with 24V DC to turn it 'ON' so that it can allow 3 phase supply to power up the motor.
- (3) Valve A and Valve B needed to be supplied with 24V DC to 'OPEN' them, and de-energize to 'CLOSE' them.
- (4) Pressure Switches A and B are supplied with 24V DC and will allow it to flow once the pre-set pressure is reached which are 15 bar and 90 bar respectively.

Figure 3.25 shows the switching circuit developed to assist the communications between the Target PC (DAQ card) with components and devices on the Regenerative Motor Pump System. The switching circuit modules can be divided into two different types. Figure 3.26 show the switching circuits used for Channel 1 to Channel 4 of the DAQ Digital I/O. For this type of circuit, the relay being used is a 5V relay. This is because the DAQ card will energize the relay to complete the load circuit.

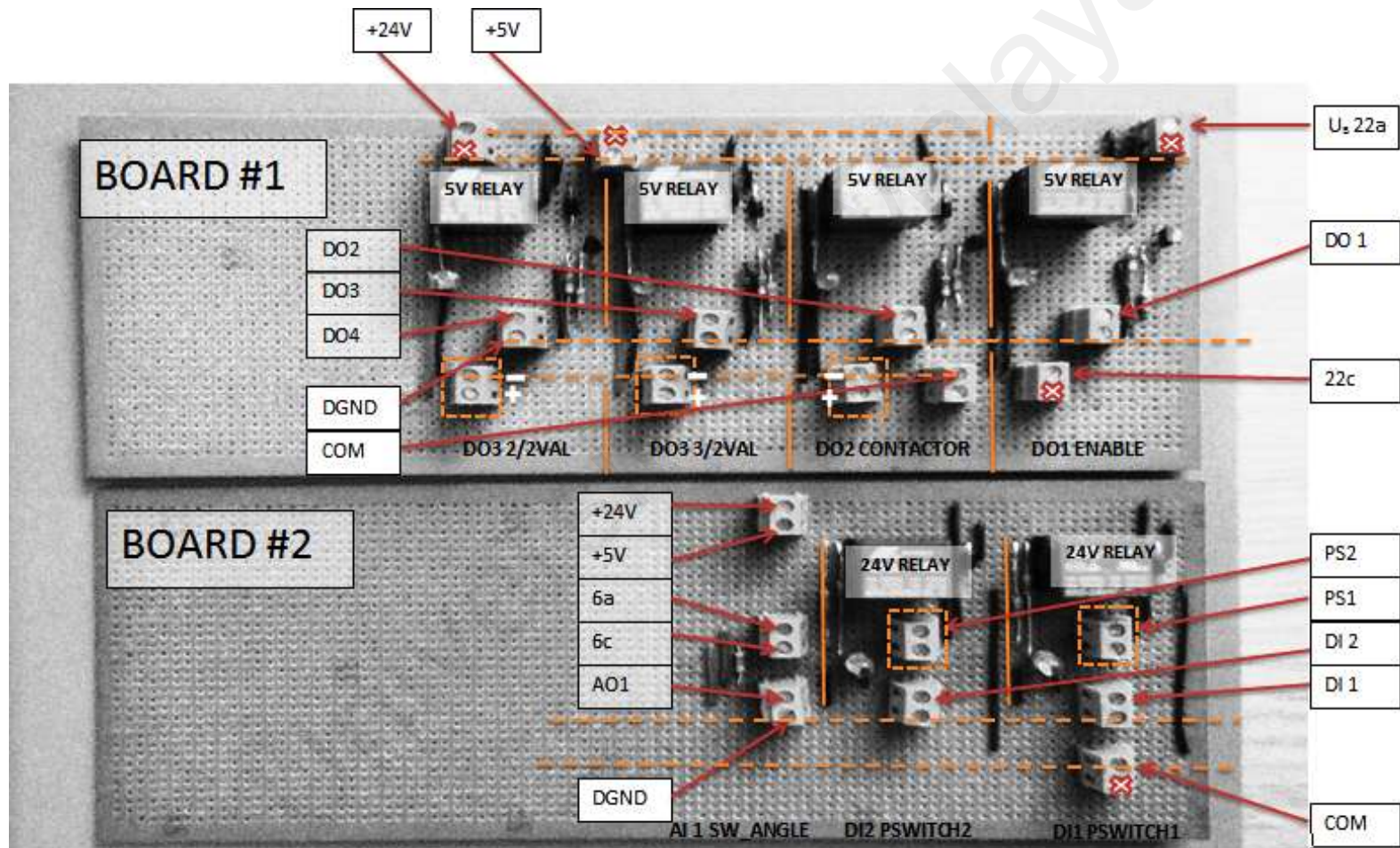


Figure 3.25 Switching Circuit for DAQ – Regenerative Motor Pump System Communications

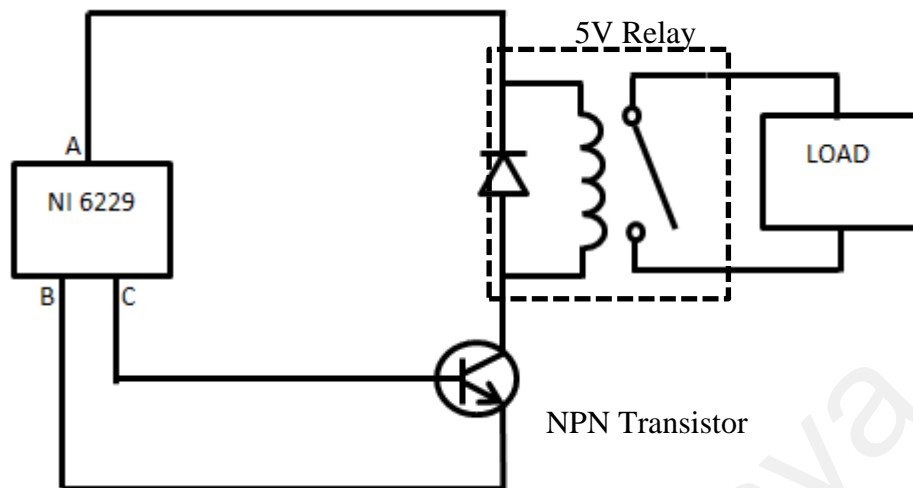


Figure 3.26 Switching Circuit for Digital I/O Channel 1 to Channel 4

For Channel 1 to Channel 4, the connections to the Target PC (DAQ) card can be summarized in Table 3.13.

Table 3.13 Connections from Target PC to Switching Circuit (Channel 1 – 4)

Channel	Load	DAQ Terminal		
		A	B	C
1	ENABLE	+5V	P 0.0	DGND
2	Contactora	+5V	P 0.1	DGND
3	Valve A	+5V	P 0.2	DGND
4	Valve B	+5V	P 0.3	DGND

The second type of switching circuit is for DAQ Digital I/O Channel 5 and Channel 6 which is connected to the Pressure Switches. Both pressure switches are supplied with 24V, therefore in this type of switching circuit, the relay being used is 24V relay. Figure 3.27 shows the switching circuit of this type. The connections to the Target PC (DAQ card) are as summarized in Table 3.14.

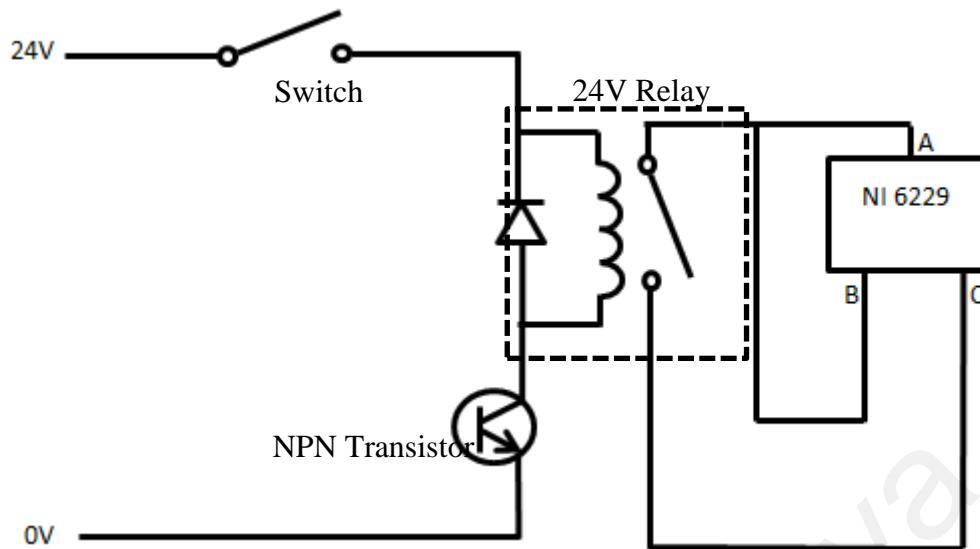


Figure 3.27 Switching Circuit for Digital I/O Channel 5 and Channel 6

Table 3.14 Connections to the Target PC to Switching Circuit (Channel 5 and Channel 6)

Channel	Switch	DAQ Terminal		
		A	B	C
5	Pressure Switch A	+5V	P 0.4	DGND
6	Pressure Switch B	+5V	P 0.5	DGND

The development of the switching circuit allows the problems stated earlier to be solved. Using the switching circuit, controlling ENABLE signal for the Axial Piston Unit (APU) can be done using the Preliminary Controller. Devices that require voltage supplies that are unable to be supplied directly by the DAQ card such as the contactor, Valve A and Valve B can now be controlled via the switching circuit. Signals that come with higher voltage than the acceptable voltage of the DAQ can also be measured and detected via switching using the circuit. For instance, signal from the Pressure Switches are in 24V – the voltage supply will activate a relay which in turn allow a voltage of 5V to pass and signal the DAQ system.

3.5 Speed Sensor

In order to gauge and evaluate the performance of the regenerative motor-pump system for HHV, the system will need to measure the revolving speed of the flywheel. As discussed in the previous section, the flywheel assembly will be an alternative to an actual hydraulic hybrid vehicle dynamics. The speed of the actual vehicle can be approximated based on the revolving speed of the flywheel.

The speed sensor that is used in the system is a Monarch Instrument Remote Optical Sensor (ROS-W). This speed sensor is able to measure speed up to 250,000 rpm with low power requirement of 3 to 15 VDC at 40 mA. It has a visible red LED to illuminate the surface of measurement, and require a reflective marker for it to able to measure the frequency of the reflection which in turn converted to the speed of the flywheel in revolution per minutes. Figure 3.28 shows a picture of the speed sensor. Table 3.15 lists the specifications of the speed sensor.

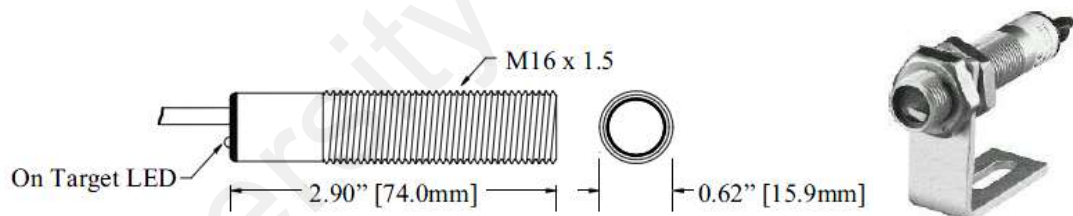


Figure 3.28 Speed Sensor Dimension (Left) and Speed Sensor on mounting bracket (Right)

Table 3.15 Specifications of the Remote Optical Sensor

Speed Range	1-250,000 RPM
Illumination	Visible Red LED
Operating Temperature	-10 to 70 C
Operating Range	Up to 0.9m and 45 degrees from target
Cable Length	2.4 m
Connection	Tinned wires
Material	303 Stainless Steel plus two M16 Jam Nuts and Mounting Bracket
Lens	Acrylic Plastic
Dimension	Threaded Tube [M16 x 1.5 x 7.4 mm] long
Power Requirement	3.0 – 15V DC @ 40mA
Output Signal	Negative Pulse input voltage (+V) to 0
On target indicator	Green LED on end cap

Since the speed sensor would require a visual tracking of the flywheel, it has been positioned near the flywheel to accurately record the frequency of the flywheel revolution. Figure 3.29 shows the position of the speed sensor on the system. The speed sensor has been mounted directly on the system to avoid inaccurate results due to distance. Figure 3.29 also shows the position of the reflective marker that is used to measure the revolution speed of the flywheel.

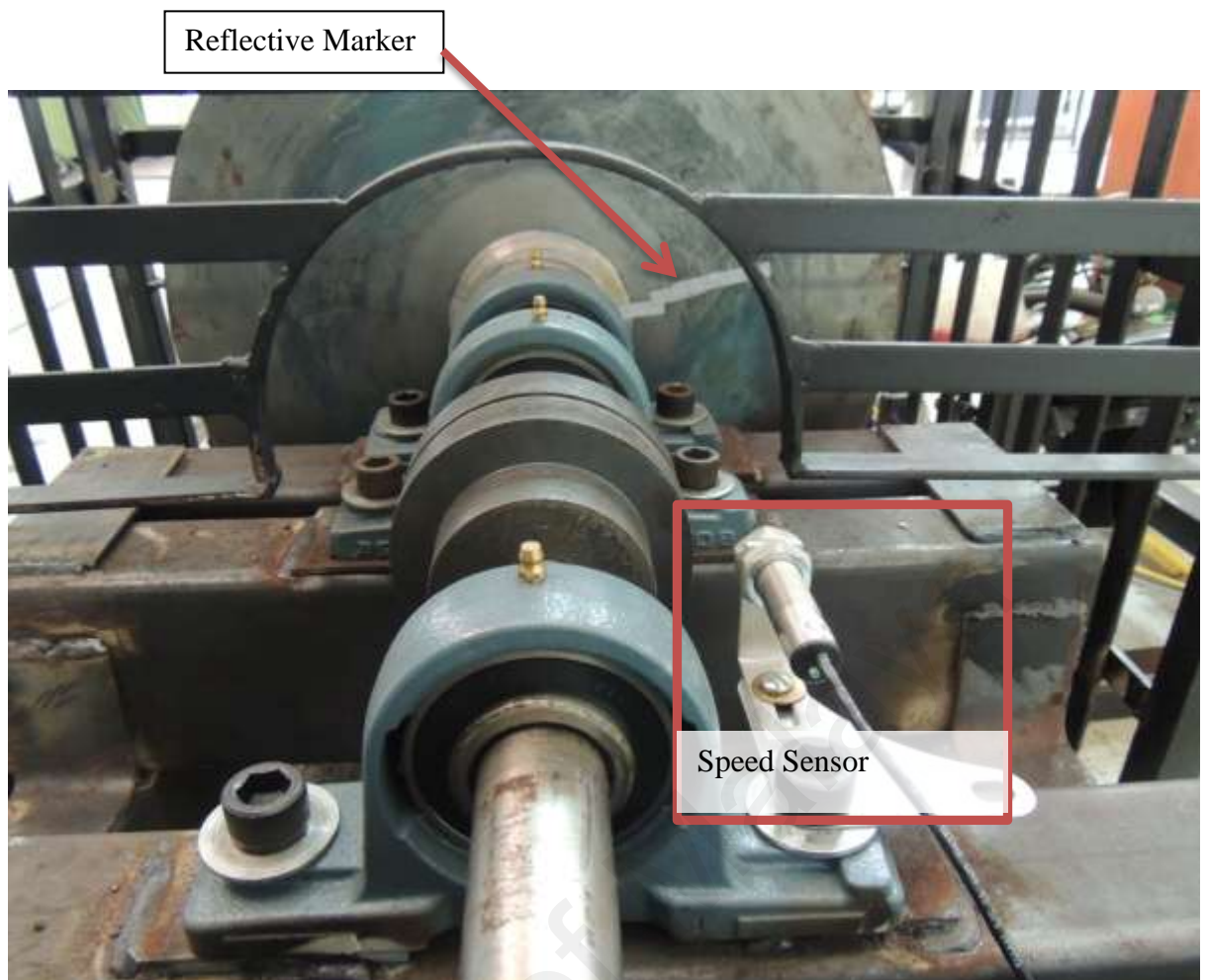


Figure 3.29 Speed Sensor position near the flywheel

The speed sensor detects the reflective marker sent out negative pulses of the input voltage. In this way, the speed sensor actually captures the frequency of the instance where the speed sensor is on target with the reflective marker. This signal is then needed to be translated into the speed of flywheel in revolutions per minute. To make sure that the signal received by the system is accurate, the signals from the speed sensor should be conditioned.

3.5.1 Speed Sensor Conditioning

The speed sensor needed to be powered at the same time during the transmission of signals. The speed sensor is connected to the system via the DAQ card. Figure 3.30 shows the conditioning process of the speed sensor. The speed sensor signals will be

read by the DAQ card and can be viewed in Matlab/Simulink environment. A PCI-6229 Digital Input block is selected as the input channel from the DAQ card. The block is connected to an Edge Detector block which will transform the pulsed signals from the speed sensor to single values as shown in Figure 3.31. These values are then passed via an Embedded MATLAB Function block which will turn the truncated pulses to frequency values. Finally, the frequency values are multiplied by 60 sec/min to convert the values to revolution per minute.

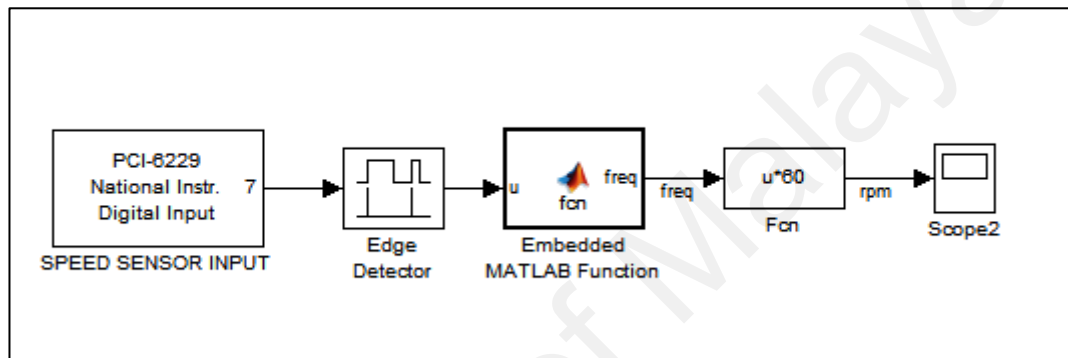


Figure 3.30 Speed Sensor Conditioning – from pulses to RPM value

The Embedded Matlab Function block houses some codes that change the truncated pulses to frequency. The block can be simplified with an equation:

$$f = \frac{1}{N \cdot T_s} \sum_{i=0}^N u_i \quad (3.6)$$

Where;

f = frequency, Hz

N = sampling size

T_s = sampling time, s

u_i = input pulse

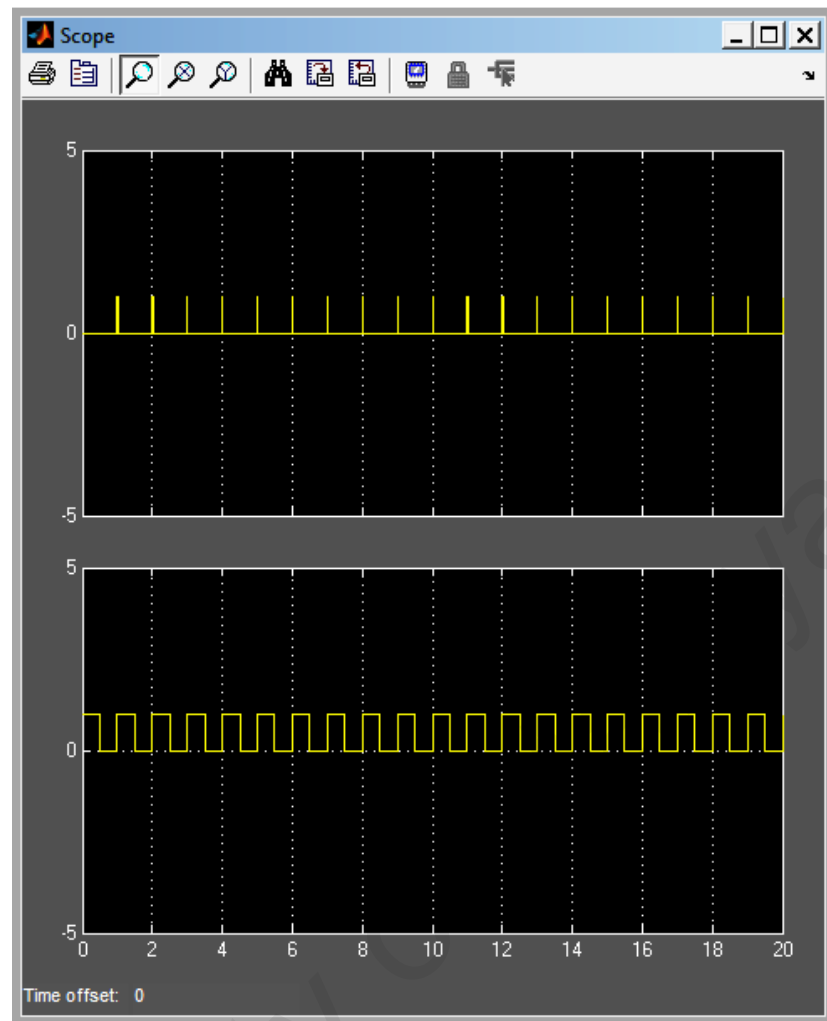


Figure 3.31 The effect of Edge Detector block (top) and the pulses received by speed sensor (below)

However in Matlab/Simulink environment, the summation can be presented with an array structure that will store the input values. The size of the array depends on the sampling size stated in the Embedded Matlab Function block. In the case that there are no input pulses from the system, an array filled with zeros will be created.

Using Simulink blocks as in Figure 3.30, the pulses captured by the speed sensor can be turned into the revolution speed of the flywheel. The operation of the speed sensor and to the extent, the practicality of the Simulink codes can be tested by pointing the speed sensor to conventional fluorescent light to detect a 100Hz frequency (twice the mains frequency of 50 Hz) that yield a speed of 6000 RPM.

Another important consideration when dealing with the speed sensor sampling is the Nyquist rate. Nyquist rate is the minimum sampling rate required in signal sampling to avoid aliasing. The Nyquist frequency is given by:

$$f_N = 2B \quad (3.7)$$

Where;

f_N = Nyquist frequency

B = Highest frequency of the sample

$$f_s > f_N \quad (3.8)$$

Where;

f_s = sampling frequency

From earlier test runs with the system, the flywheel speed has a maximum speed of 1200 RPM. This translates to a frequency of 20Hz. Therefore, the Nyquist frequency; f_N is 40 Hz. The suggested sampling time for the system is 0.025 s. However, for this study, the sampling time is set to 0.001 s. This smaller sampling time is even more sufficient to be used to sample the signal from the speed sensor to avoid aliasing.

The speed sensor is powered with 5V DC from the NI PCI-6229 DAQ card. At the same time, the pulsed signal is connected to the Digital Input module of the DAQ card. Table 3.16 shows the connection details between the speed sensor wires to the terminals in the DAQ card.

Table 3.16 Connection Detail for Speed Sensor and DAQ card

Remote Optical Sensor		NI PCI 6229 DAQ card	
Function	Wire Colour	Terminal	Function
Positive Power Supply (+V)	Brown	+5V	Power Supply
Common	Blue	DGND	Common
Signal (+V to 0V DC Pulse)	Black	P0.0	Digital Input Channel 1
Housing Ground	Shield	-	-

3.6 Pressure Transducer

The regenerative motor-pump system is also equipped with two pressure transducers. The system has two HDA 4445-B-250-000 Pressure Transmitter manufactured by HYDAC ELECTRONIC GMBH. The two transducers are positioned in before and after Valve B to measure the pressure loss in the system. One of the transducers will be measuring the pressure inside the pressure accumulator. Another will measure the hydraulic pressure near the APU. The two transducers are able to measure pressure up to 250bar and require 12 to 30 V DC at 25mA. The signal that comes out from the pressure transducer ranges from 0V to 10V. Table 3.17 lists the technical specifications of the pressure transducer used in this study. Figure 3.32 shows a picture of the pressure transducer.

Table 3.17 Technical Specifications of the Pressure Transducer

Measuring Range	250 bar
Overload pressures	400 bar
Burst pressure	1000 bar
Mechanical connection	G1/4 A DIN 3825
Torque value	20 N.m
Output signal	0 to 10 V, 3 conductor
Permitted Resistance	$R_{Lmin} = 2 \text{ k } \Omega$
Compensated temperature range	0 to +70 °C
Operating temperature range	-25 to +85 °C
Storage temperature range	-40 to 100 °C
Fluid temperature range	-40 to 100 °C
Power supply	10 to 30 V
Current consumption	Approx. 25mA
Weight	Approx. 145 g



Figure 3.32 Pressure Transducer used in the system to evaluate the regenerative motor-pump system

Both pressure transducers are connected directly to NI PCI-6229 DAQ card on the Analog Input module. There are two types of analog input sources that can be connected to the analog input terminals of the DAQ card. The sources are (1) Floating signal sources and (2) Ground-Referenced Signal sources. In this study however, the pressure transducer is considered as Ground-Referenced Signal Sources as the devices are powered externally with 24V DC. The external power supply however is connected to the building system ground. The Target PC also shares the same ground since it is plugged into the same power system as the external power supply. The pressure transducers then can be connected to the analog input terminals with 3 different configurations. The configurations settings are:

- (1) Differential (DIFF)
- (2) Non-Referenced Single-Ended (NRSE)
- (3) Referenced Single-Ended (RSE)

For this study, the DIFF configuration settings are used to connect the pressure transducers to the Target PC. The DIFF configuration is used when the channel meets some of these conditions:

- (1) Low level input signal
- (2) The connections between the signal and device are greater than 3 m long.
- (3) The signal requires a separate ground-reference point or return signal
- (4) Noisy environments
- (5) Two analog input channels, AI + and AI – are available.

Since the pressure transducer uses separate ground-reference point with the NI PCI 6229 DAQ card, DIFF configuration setting is used. Two analog input channels AI+ and AI- are also available to be used. Figure 3.33 shows the configuration settings for both pressure transducers.

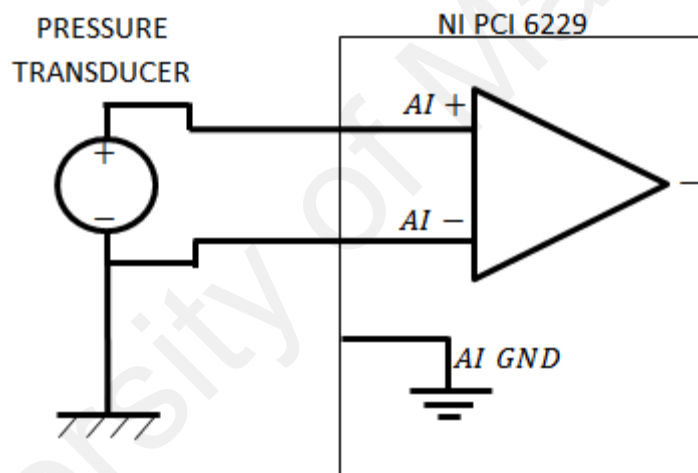


Figure 3.33 Configuration setting for Pressure Transducer – NI PCI 6229 Analog Input

For Analog Inputs, the DAQ card will scan one channel at a time. For two pressure transducers, the DAQ card will scan one pressure transducer for its signal before scanning the other one. Therefore, for analog input, there is a requirement to specify sampling time and scan interval. For the Analog Input module, the sampling time is set to be 0.1s, therefore, the scan interval is half the sampling time owing to the fact that the DAQ card will need to switch between the two transducers within one sampling. Figure 3.34 shows the Pressure Transducers Simulink blocks, while Figure 3.35 shows the parameters for the Pressure Transducer Analog Input block. Selection of

configuration settings for the Analog Input can be made by changing the parameter values in the Analog Input block. Change can be made in the input coupling vector panel where 0, 1, 2 is the value corresponds to RSE, NRSE and DIFF respectively.

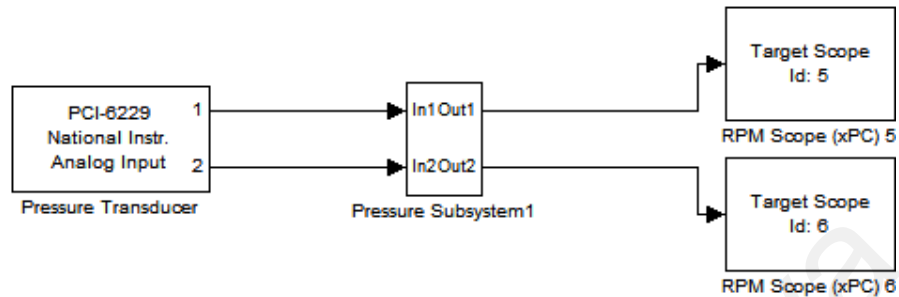


Figure 3.34 Pressure Transducer Simulink blocks

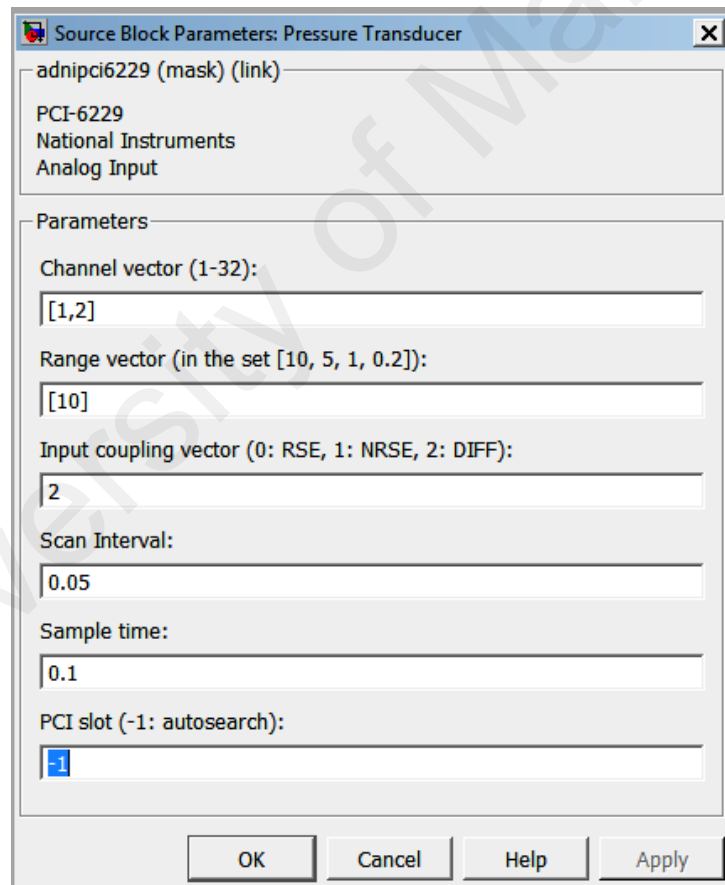


Figure 3.35 Analog Input block parameters

The Pressure Transducer will send a signal in the form of voltage, according to the ranges acceptable to the NI PCI 6229 DAQ card. The ranges can be set by changing the Range vector panel in the Analog Input block parameter window as shown in Figure 3.36. Range vector of “10” corresponds to getting signals from -10V to 10V.

The signals need to be calibrated to show the values of Pressure instead of the values of voltage. The pressure subsystem block in Figure 3.33 is doing just that. Figure 3.35 shows the content of the subsystem. The subsystem has two inputs, one from each pressure transducers. Since the pressure transducer has the capability to detect up to 250 bar of pressure, the maximum voltage is scaled to the maximum pressure. The input is then divided by the maximum voltage and multiplied to the maximum measurable pressure to yield the pressure reading of the two inputs.

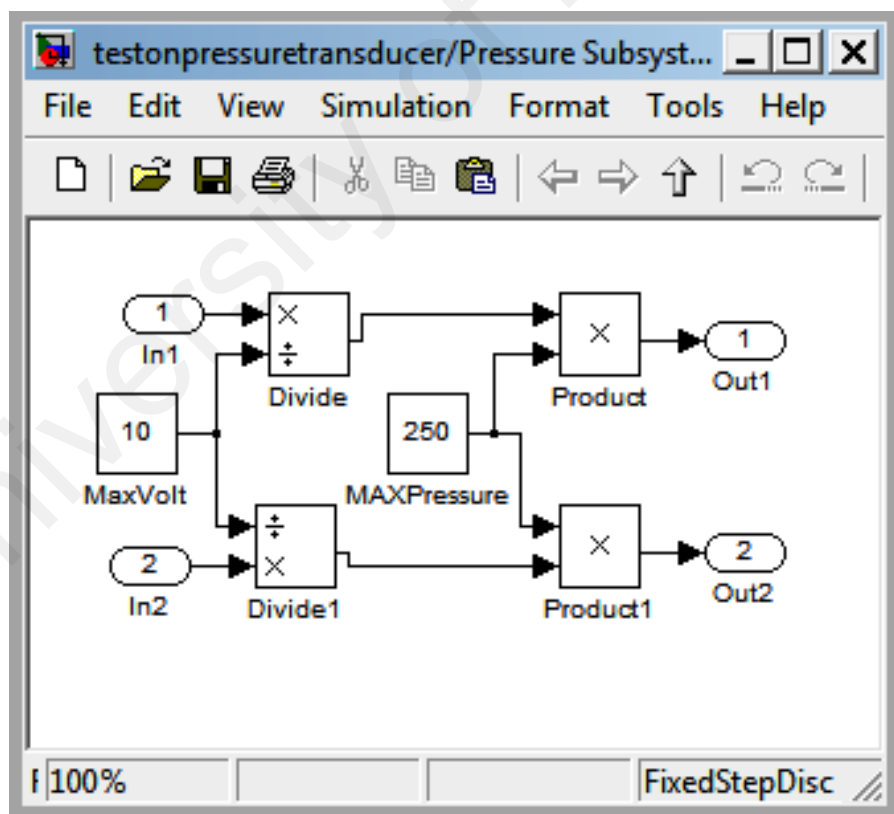


Figure 3.36 Pressure Subsystem block details

The block in Figure 3.36 can be simplified using this equation:

$$P = \frac{V_i}{V_{MAX}} \times P_{MAX} \quad (3.9)$$

Where;

P = Pressure

V_i = Input voltage (Pressure Transducer signal)

V_{MAX} = Maximum voltage range of the devices, 10V

P_{MAX} = Maximum pressure that can be measured by the Pressure Transducer, 250 bar.

3.7 Validation of the Preliminary Controller

After all the setting and configurations of the Preliminary Controller has been finalized, the system is tested by operating it through the various modes as discussed in Section 3.3. The tests will ensure that the Regenerative Motor Pump System is able to emulate the processes of an operational Hydraulic Hybrid Vehicle (HHV). The most important validation is on whether the system is able to emulate motor mode (energy release) and pump mode (energy recovery).

However, the system is limited in terms of energy recovery. As previously explained, the system emulates motor mode by allowing high pressure hydraulic fluids to flow from the accumulator to the reservoir. In real applications, this will move the HHV from stationary position to moving. When the state of charge of the accumulator is low, the HHV will continue moving by switching the drive from APU to the conventional ICE. For motor mode, the system does not have any problems to emulate the real process on HHV.

Energy recovery in HHV depends on braking of the vehicle. At that moment, the HHV will usually be driven by the ICE instead of APU. Therefore, the energy recovered during braking will use the make use of the fact that the vehicle is already moving, and slow the vehicle by putting a negative work that is done by transferring hydraulic fluid from the reservoir to the high pressure accumulator. In the developed system, however, there is no ICE attached, therefore, the only possible way to emulate pump mode is by evaluating the energy recovered after the flywheel is turned using the pressure from the accumulator.

Figure 3.37 shows the two modes emulated by the system. In pump mode, the flywheel revolved around 1100 rpm and slows down to around 200 rpm during pump mode, while the pressure recovered by the system is 40 to 50 bar. On the other hand, the motor mode shows a rise of flywheel revolution from 0 rpm to 1100 rpm while the accumulator pressure drops from 80 bar to 0 bar.

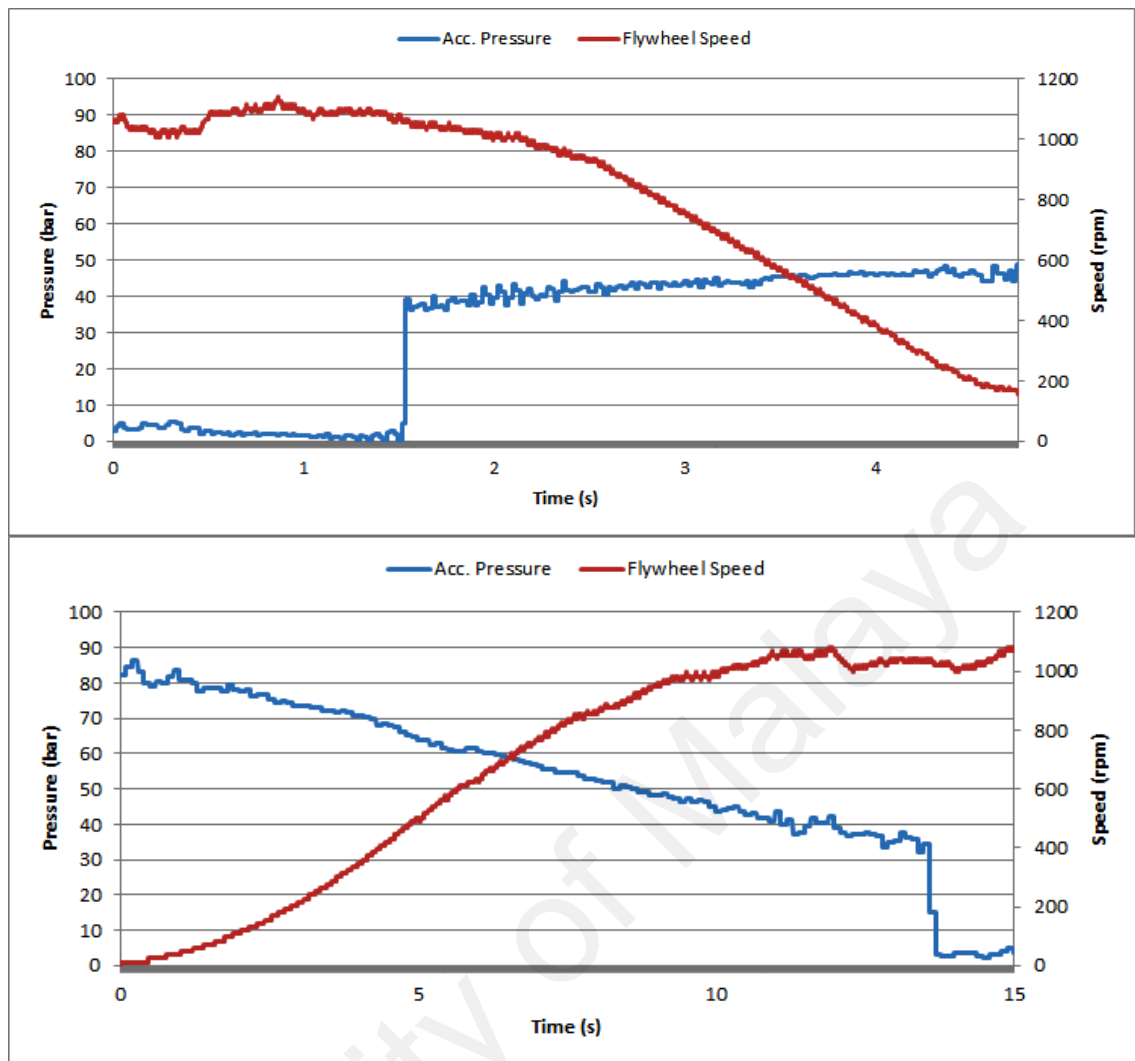


Figure 3.37 Pump Mode (top) and Motor Mode (below) in Regenerative Motor-Pump System

This difference in pressure levels suggest that the system is capable of capturing around half of the original pressure used to revolve the flywheel on the same speed. Further discussions on the energy recovery capability will be discussed in Chapter 5.

There are several tests done to evaluate the Preliminary Controller. Other than finding out whether the system is able to emulate the two important modes, several other tests are:

1. Finding the best number of samples to accurately measure speed
2. Filtering noise from the pressure transducer reading

3. Determining the better ramp time

3.7.1 Determining the best sampling number for Speed Sensor

In the previous sections, the study has established on the configurations and conditioning of the speed sensor. In this section, the speed reading from the speed sensor will be evaluated to see whether the measurement is accurate and deterministic. In previous sections, it is also established that the sampling time for the speed sensor is set to be 0.001s based on consideration of ‘aliasing’ effect and calculations compared to the Nyquist rate.

Another parameter to be considered to measure the speed accurately is the sampling size of the speed sensor. To evaluate the accuracy of the speed sensor reading based on the sampling size, different sampling size has been used to operate the system to undergo a charging – motor mode – pump mode – motor mode event.

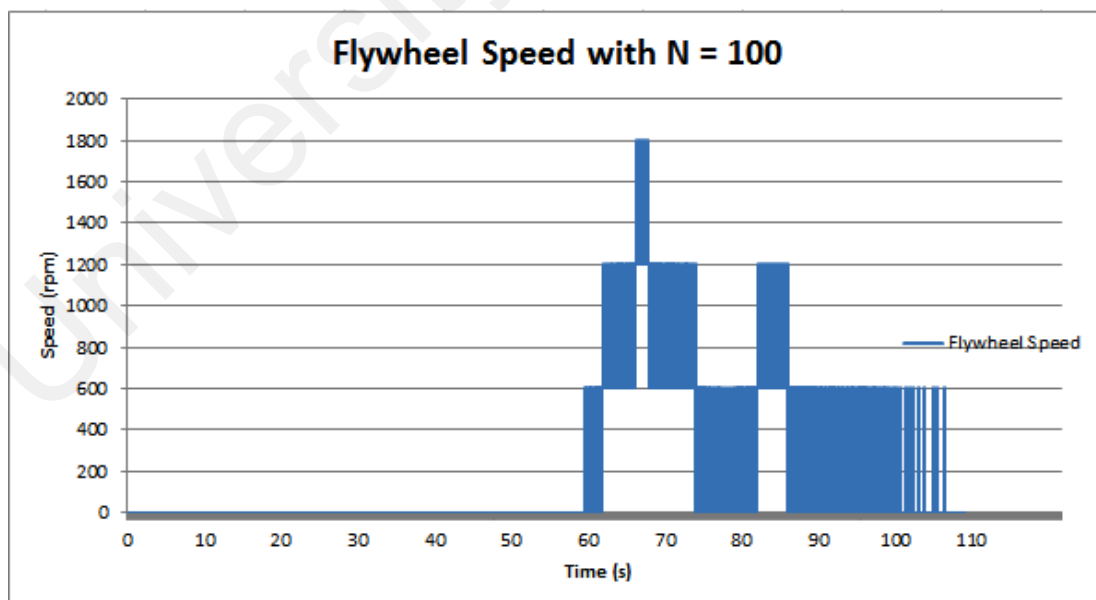


Figure 3.38 Flywheel Speed Measurement with sampling size, N = 100

Figure 3.38 shows the flywheel speed measurement with sampling time of 0.001 s with sampling size of N = 100. This means that the system will consider up to 100

samples before calculating the frequency as in Equation 3.5. With $N = 100$, this also means that the speed of the flywheel will always be updated every 0.1 seconds. This causes the measurement of the speed to fluctuate quickly and is not accurate. Figure 3.39 demonstrates the fluctuation. A closer look in the flywheel speed diagram with sampling size of $N = 100$ shows that the measurement fluctuates in the ranges of 0 rpm to 600 rpm multiple times in 1 second.

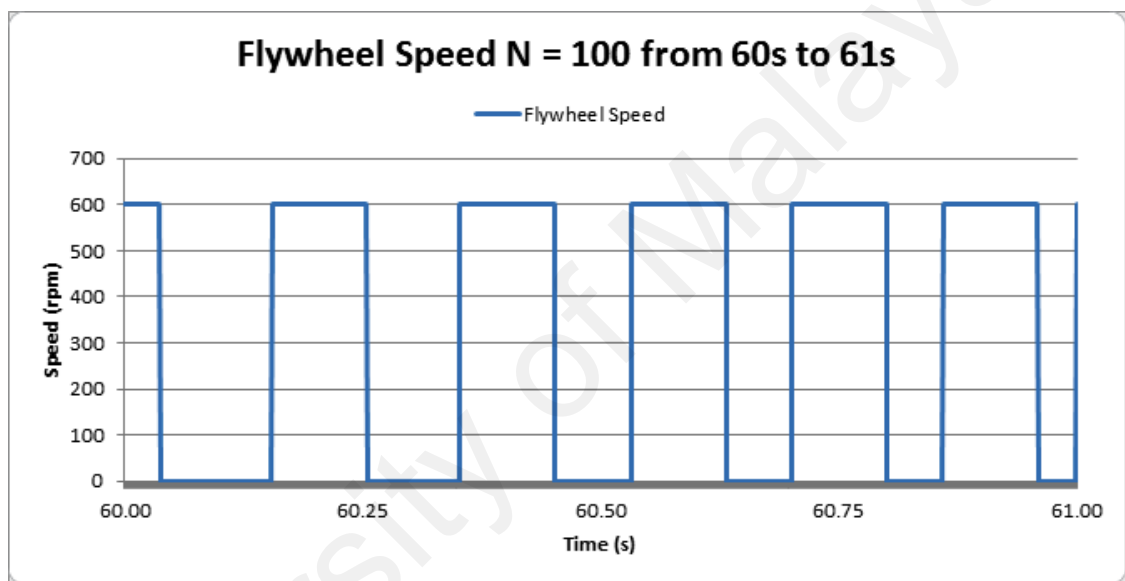


Figure 3.39 Flywheel Speed Measurement with sampling size $N = 100$ in 1 second period

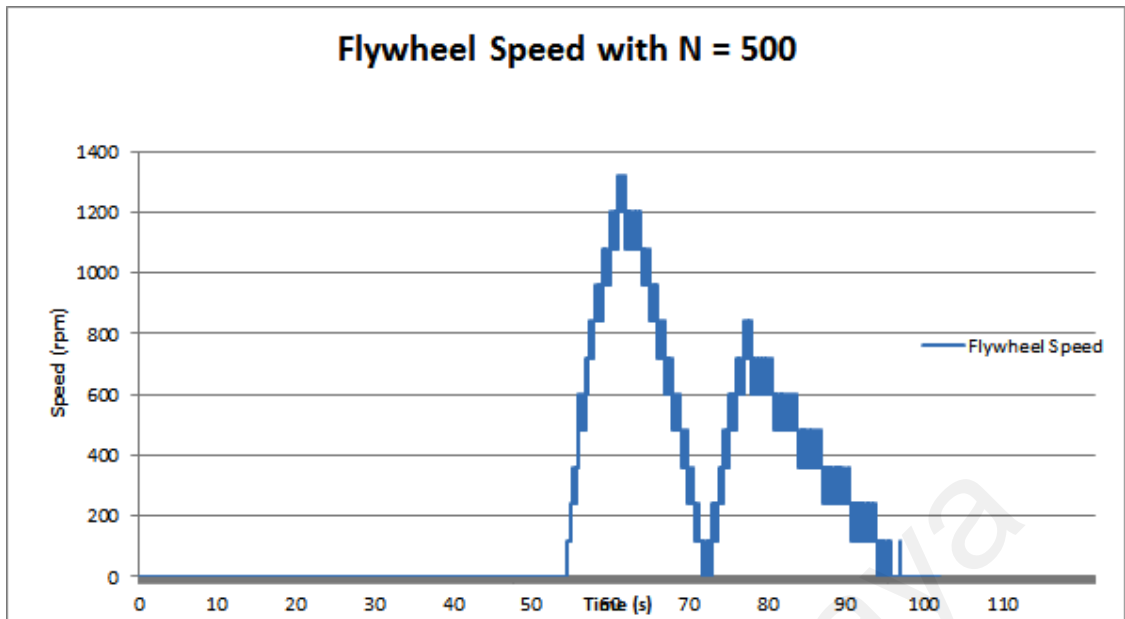


Figure 3.40 Flywheel speed measurement with sampling size, N = 500

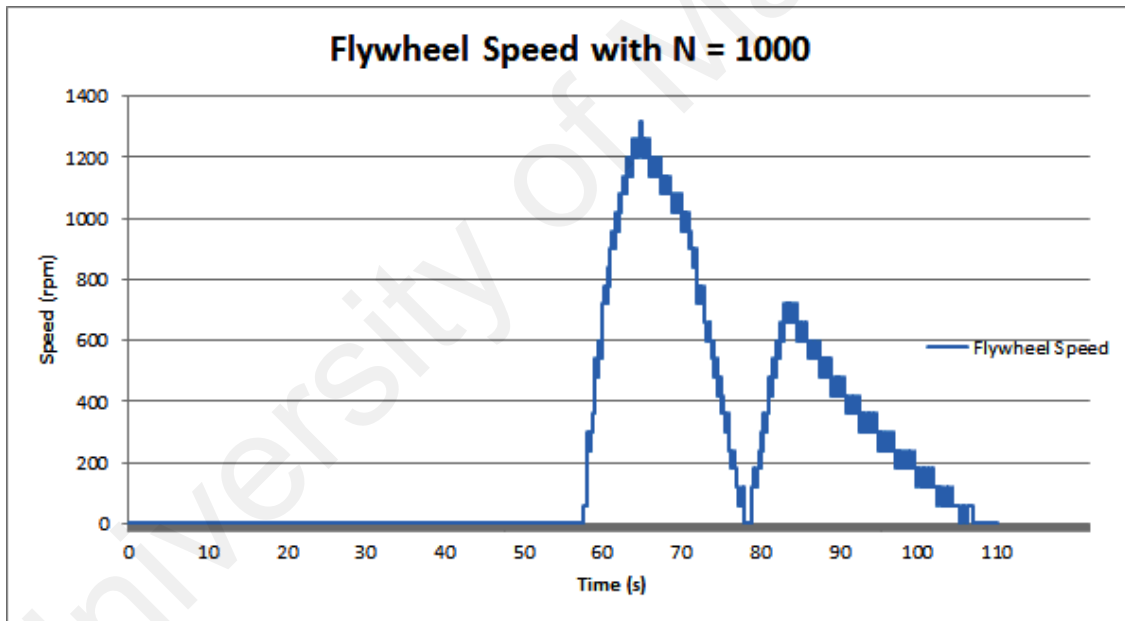


Figure 3.41 Flywheel speed measurement with sampling size, N = 1000

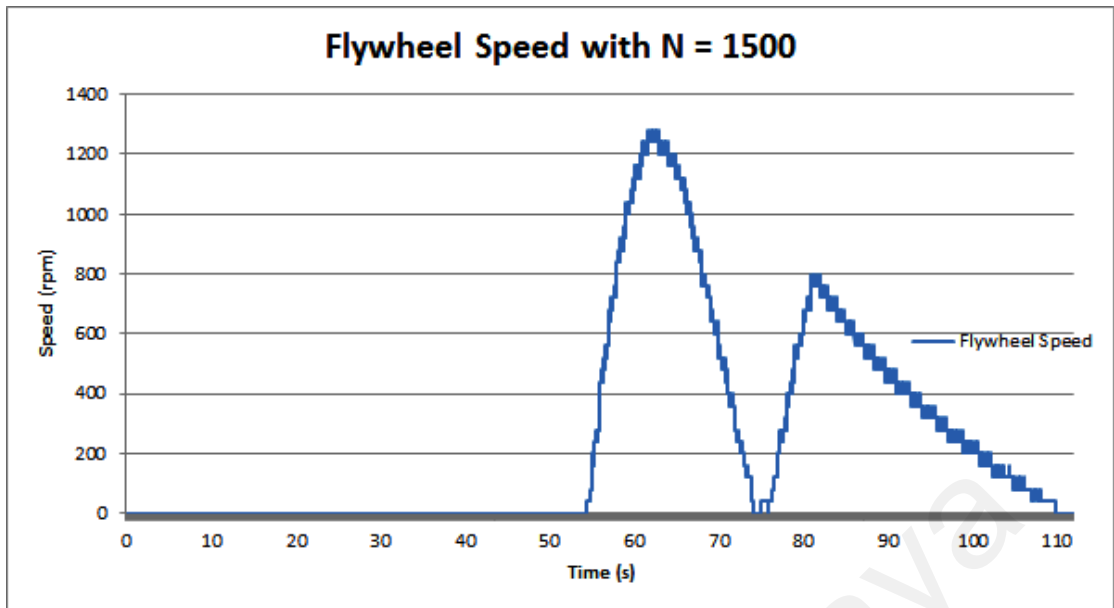


Figure 3.42 Flywheel speed measurement with sampling size, $N = 1500$

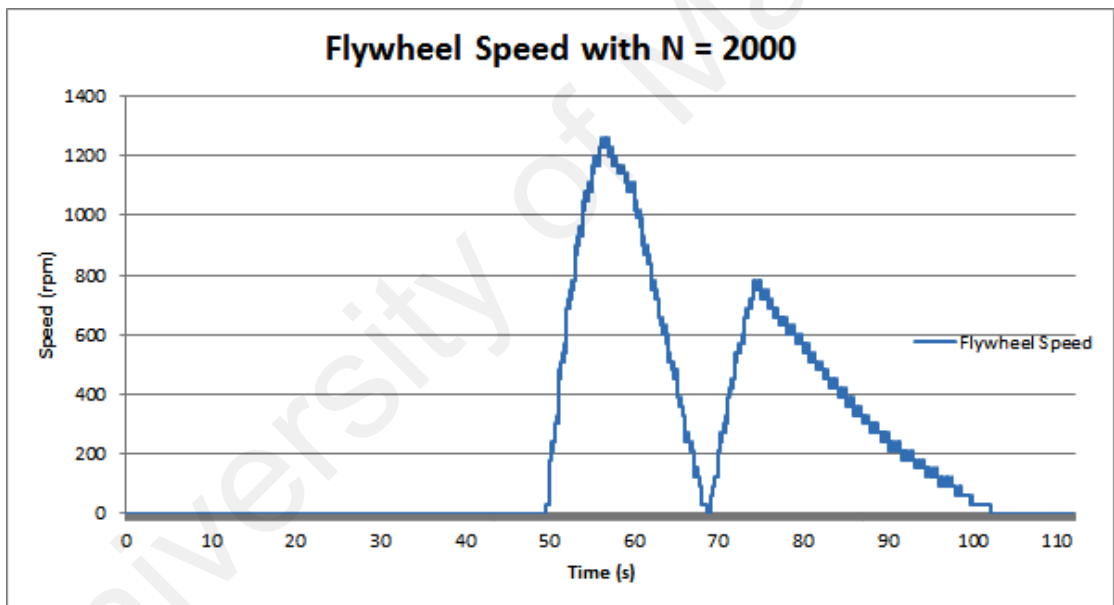


Figure 3.43 Flywheel speed measurement with sampling size, $N = 2000$

Similarly, Figure 3.40 to Figure 3.43 shows the speed measurement with sampling time of 0.001 s and sampling size of $N = 500$, $N = 1000$, $N = 1500$ and $N = 2000$. They represent speed measurement update rate of 0.5 seconds, 1 second, 1.5 seconds and 2 seconds respectively. By adding more samples, it can be seen that there are smaller fluctuations each time the sampling size is added. But, in the case of more samples, the measurement update rate will be slower, thus the measurement will not be accurate.

In this study, the sampling size of $N = 1000$ has been chosen so that the system will be updated with the new measurement data every 1 second.

3.7.2 Filtering Noise from Pressure Transducer Reading

In Section 3.6, the configuration settings and calibration of the pressure transducers has been discussed. However, there are still some measures to be done in order to make sure that the pressure transducer can produce accurate measurement reading that can be used in the study. The system that is developed in this study consists of two pressure transducers; one is measuring the pressure in the accumulator directly, while the other is measuring the pressure near the pump. The two pressure transducer actually is connected and can show similar pressure reading, but it is separated to each other by Valve B. Therefore, when Valve B is closed, we can see that the pressure between the two transducers is different. When Valve B is opened meanwhile, the pressure is about the same, and the difference between the pressures can be regarded as pressure loss after the high pressure hydraulic fluid enters Valve B.

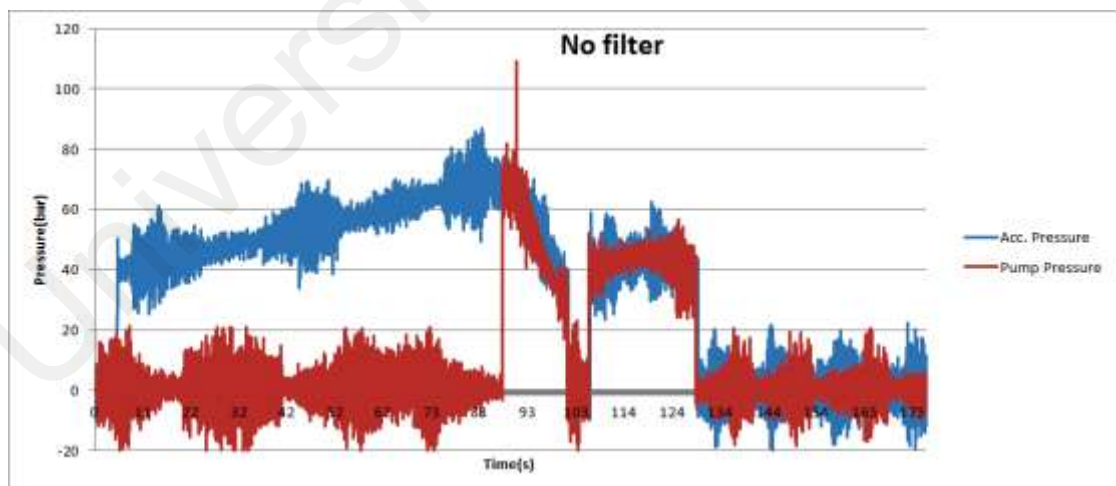


Figure 3.44 Pressure Transducers reading with no filter

Figure 3.44 shows two pressure readings from the two different pressure locations. The measurements are as a result of testing done similar to what was done for speed sensor. In Figure 3.44, the pressure reading for the pressure transducer located at the accumulator is denoted in blue, while the one that is near the pump is denoted in red. In the early stages, it can be seen that there's an increase in pressure at the accumulator. This is because the system is undergoing a charging process. The other transducer should record a '0' pressure reading, but as seen in Figure 3.43, that is not the case. Both the pressure reading at the pump and at the accumulator have a noisy reading consists of high frequency noise and low frequency noise.

In this section, the implementation of low-pass filter on the pressure transducer reading is discussed. A low-pass filter attenuates frequencies higher than the pre-set cut-off frequency and allows lower frequency signals to be read.

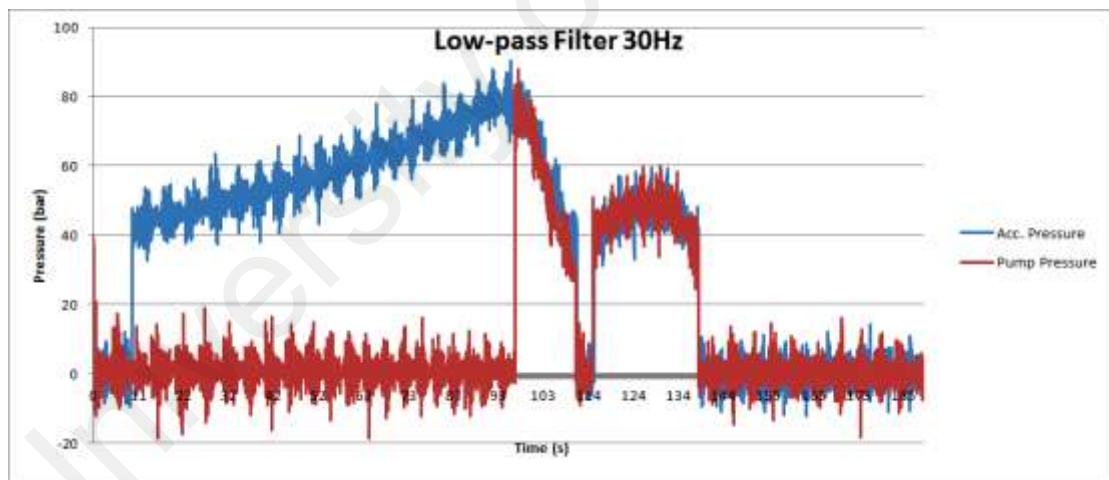


Figure 3.45 Pressure Transducer readings with 30 Hz cut-off frequency low-pass filter

To determine the best cut-off frequency for the low-pass filter, different frequencies has been used to investigate the effects of the filters to the pressure reading. Figure 3.45 shows the pressure reading once a 30Hz cut-off frequency low-pass filter is applied to the pressure transducer readings.

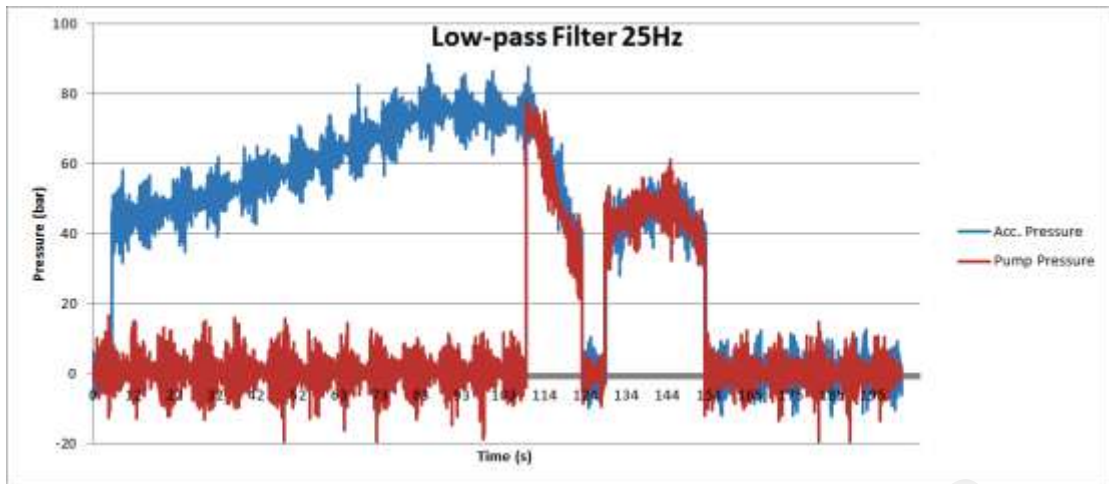


Figure 3.46 Pressure Transducer readings with 25 Hz cut-off frequency low-pass filter

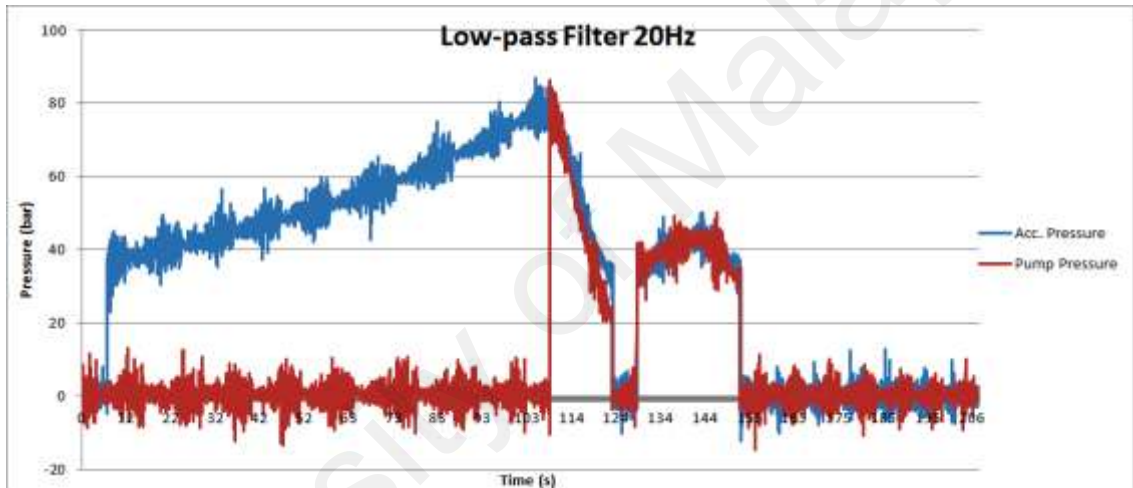


Figure 3.47 Pressure Transducer readings with 20 Hz cut-off frequency low-pass filter

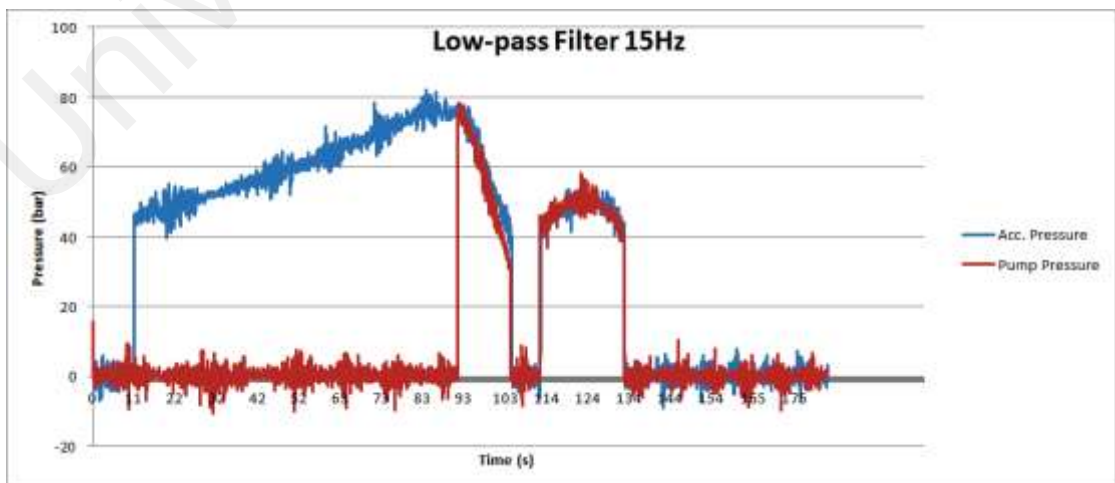


Figure 3.48 Pressure Transducer readings with 15 Hz cut-off frequency low-pass filter

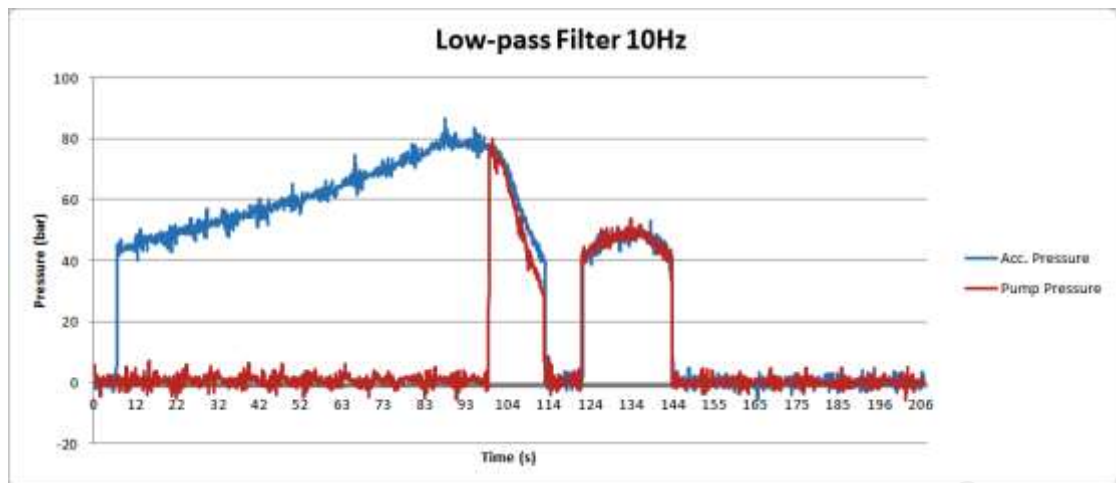


Figure 3.49 Pressure Transducer readings with 10 Hz cut-off frequency low-pass filter

Figure 3.46, Figure 3.47, Figure 3.48 and Figure 3.49 shows pressure reading when a low-pass filter of cut-off frequency of 25 Hz, 20 Hz, 15 Hz and 10 Hz is applied to the pressure transducer readings. For lower cut-off frequency, the graphs shows smoother curves even though many of them still retain some fluctuations. For this study, a low-pass filter of 10 Hz is used to condition the pressure transducer reading. A 10 Hz low-pass filter will allow change in the system within 0.1 second period. A lower cut-off frequency low-pass filter, even though desirable, will not allow the system to be fast enough to capture significant changes in the system.

3.7.3 Determining the better ramp time

The amplifier card is equipped with a ramp generator that functions to change a step-input signal to a ramp-shaped input signal. The ramp time corresponds to the time taken for the command value input to get to 100% of its value. For the regenerative motor-pump system, this applies to changing of the swashplate angle. The ramp time can be changed by using a potentiometer on the amplifier card. The maximum ramp time can be set to be approximately 1 second or 5 seconds, by changing the jumper setting on the amplifier card itself.

For the development of this regenerative motor-pump system, the different ramp time has been tested to see the effect of different ramp time on the flywheel speed. Figure 3.50 and Figure 3.51 shows the speed measurement of a flywheel rotating from 0 rpm to 1260 rpm with ramp time of 5 s and 1 s respectively.

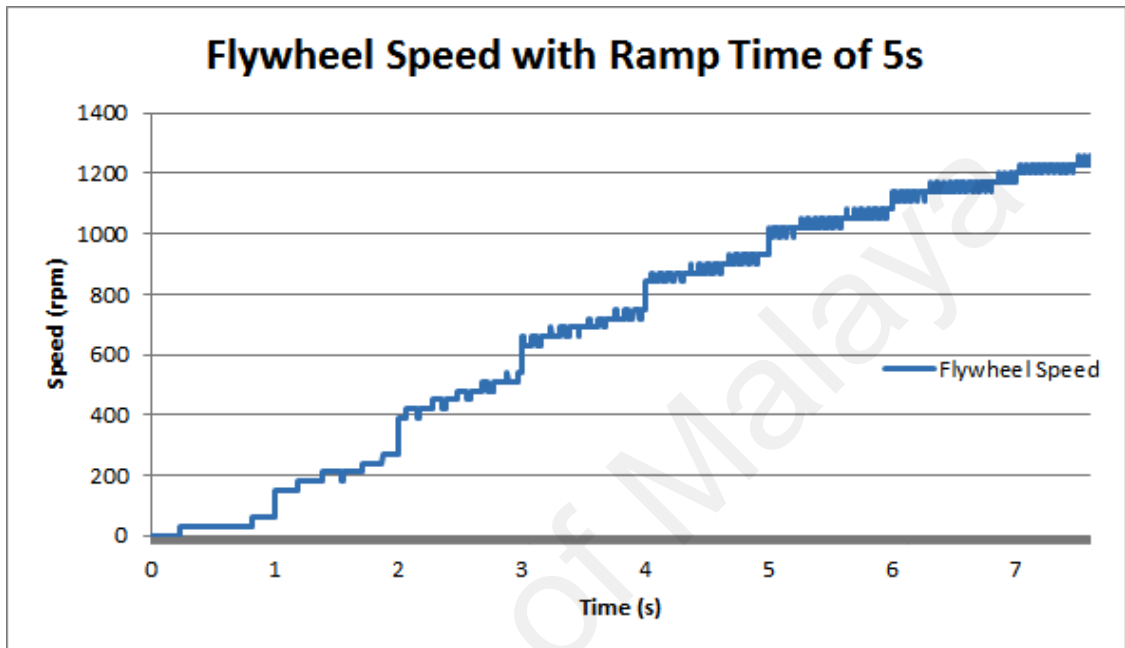


Figure 3.50 Flywheel speed measurement from 0 rpm to 1260 rpm with ramp time of 5s

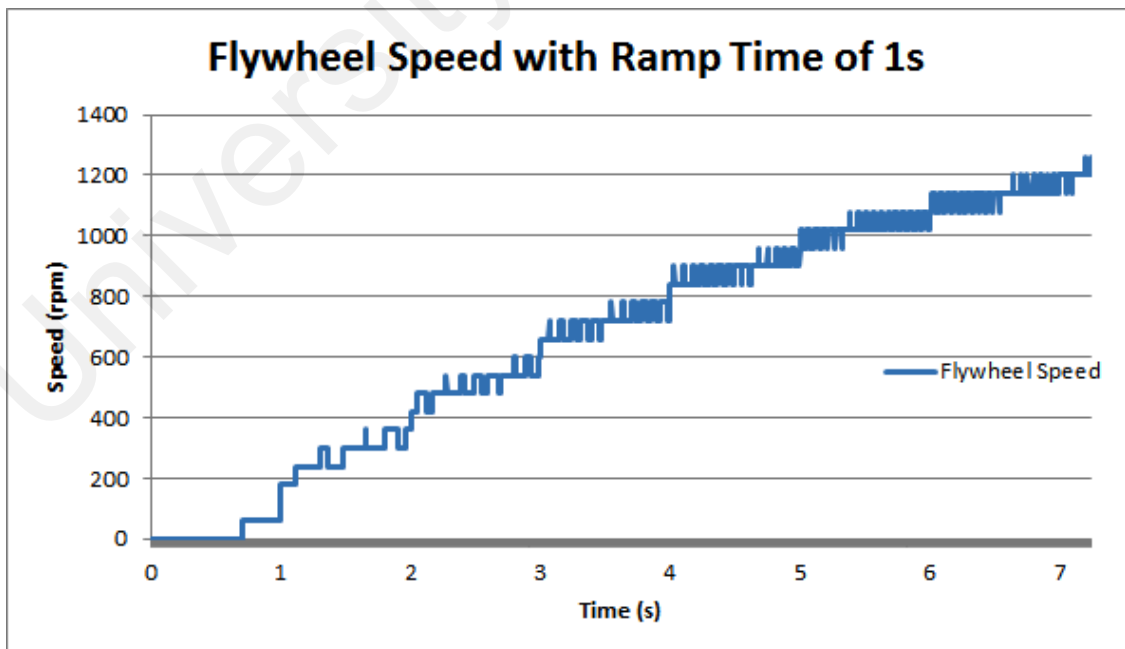


Figure 3.51 Flywheel speed measurement from 0 rpm to 1260 rpm with ramp time of 1s

The speed measurement curves is similar in both cases, in fact, the maximum speed of the flywheel revolution is the same which is 1260 rpm. The time taken to reach the maximum speed for both cases however is not the same. For 5 seconds ramp time, the time taken to reach the maximum speed is 7.608 seconds while for the 1 second ramp time, the time taken is 7.25 seconds.

For this study, the ramp time is set to the approximately 1 second maximum. This ensures that the command value input reaches 100% quickly. Figure 3.52 guided on setting the jumpers to configure a faster ramp time on the amplifier card. For 1s ramp time, jumper on J5 and J6 has to be opened.

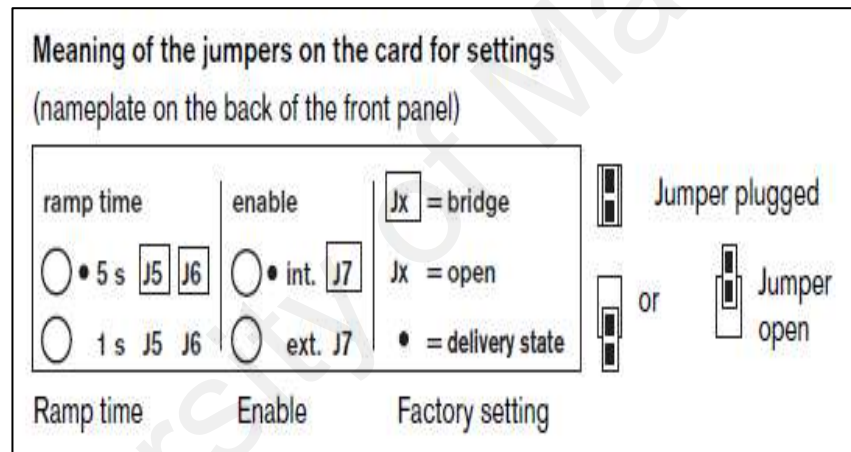


Figure 3.52 Jumpers settings guidelines for the Amplifier Card

3.7.4 Changing swashplate angles

Another test that was done to evaluate the preliminary controller made for the Regenerative Motor-Pump System is changing the swashplate angles. The controller has to be able to change the swashplate angle by sending signals to the amplifier card which will then control the proportional valves of the Axial Piston Unit. The solenoid that is energized will determine the flow of hydraulic fluid from Port A to Port B or vice versa according to the direction of the flywheel shaft (clockwise or counter-clockwise).

To test the effect of different swashplate angles, the Regenerative Motor-Pump System is put on motor mode with different swashplate angles. The swashplate angle is changed to the respective angles before Valve B is opened to allow high pressure hydraulic fluid in the accumulator flow to the APU.

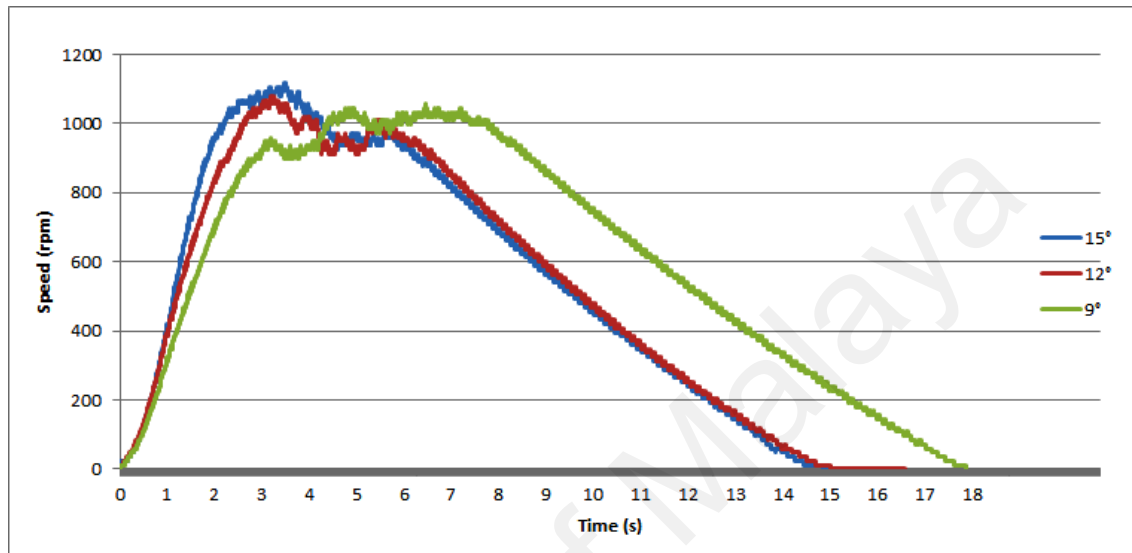


Figure 3.53 Motor Mode Speed Profile using different swashplate angle

Figure 3.53 shows speed profile of the system on motor mode using different swashplate angle. By changing the voltage signal sent to the amplifier card, different swashplate angle can be achieved. Swashplate angle of 15° , 12° and 9° corresponds to 10 V, 8 V and 6 V respectively.

In Figure 3.53, the speed profile with 9° swashplate angle took longer time to halt. The speed profile with the biggest swashplate angle 15° meanwhile has the highest acceleration compared to the other two profiles. The maximum speed attainable for all the three speed profiles of 15° , 12° and 9° are 1116 RPM, 1080 RPM and 1056 RPM respectively.

From these tests, it can be shown that the system is able to change swashplate angles of the APU and that using bigger swashplate angle yields higher revolution speed, but shorter charge sustaining period.

3.8 Conclusion

In this chapter, the design of Regenerative Motor-Pump System has been presented. The system has been described in terms of the base vehicle used and some elaborations have been made on the hydraulic diagrams developed. Detail discussions have been made on the essential components of the Regenerative Motor-Pump System such as the Axial Pump Unit (APU), the accumulators, the power pack, the flywheel, and different valves. A comparison between the Regenerative Motor-Pump System with an actual HHV is made, and different states and processes of the system have been explained by referring to the hydraulic diagram to clearly show the hydraulic flows.

This chapter also presented the instrumentation of the Regenerative Motor-Pump System. To emulate the states and processes, a preliminary controller has been developed by building the data acquisition medium, designing the preliminary controller in Simulink and making the switching circuit as an interface for various devices. Instrumentation of the speed sensor and pressure transducers are presented and discussed, and validation of the preliminary control was done. The best sampling time and ramp time was determined based on the validation. A filter has been applied to the controller to reduce the noise in the pressure transducer reading. The controller has also been tested to operate at different swashplate angles.

The findings in this chapter becomes the foundation of the development of a more robust and flexible controller. The next chapter will discuss on the control development for the Regenerative Motor-Pump System.

4.0 CONTROLLER DEVELOPMENT AND VALIDATION

4.1 Introduction

The development of the controller for the Regenerative Motor-Pumps System was done using Stateflow[®]. In this chapter, Stateflow will be introduced, and common graphical objects associated with Stateflow diagrams will be presented. Common notations used in Stateflow will also be introduced before the actual Stateflow chart for the system is presented. A detail perspective on the Stateflow chart will be given in the elaborate discussions of the states and transition conditions inside the Stateflow charts.

Next, a Graphical User Interface (GUI) for the controller is presented. The GUI is used to ease the operator in controlling the Regenerative Motor-Pump System. Then, two safety measures are discussed and its implementation using Stateflow is presented. One of the safety measures limits the maximum pressure permitted in the accumulator, and the other checks whether a valve is open or closed automatically.

Finally, a validation of the controller is presented in the forms of graph depicting the readings of speed and pressure in the system on different states; before a conclusion summarizes the chapter.

4.2 Stateflow for Control Development

Stateflow[®] is a graphical and interactive design tool that is integrated with MATLAB/Simulink development environment. For the development of controller for the Regenerative Motor –Pump System, Stateflow is used as an approach to the development process. The integration with MATLAB/Simulink allows the developed controller to be build based on the preliminary controller discussed in Chapter 3. The usage of Stateflow allows automation of the system; governance on the current states/modes of the system can be done effectively.

Using Stateflow will introduce a Stateflow chart in the Simulink environment, where the Stateflow chart can be edited in the Stateflow editor accessed by double clicking the Stateflow chart. The Stateflow diagrams are drawn in the Stateflow editor using available objects in the editor. For example, a state is represented as a curved rectangle shape where events and state actions are written in the shape. States are connected to each other by transition arrows. Table 4.1 describes the graphical objects used in Stateflow that are used in the controller development.

Table 4.1 Stateflow graphical objects descriptions

Stateflow Graphical Objects	Object Name	Descriptions
	State	States contains events and state actions. They are used to represent the mode of the system. States that contain other states are called superstates, and those that are inside another state is called as substates.
	Transition	In Stateflow, transitions between states are represented by arrow lines. These transitions may be accompanied by labels that represent transition conditions, condition actions, or transition actions.
	Default Transition	Default transitions specify to the system on which states/junction to enter by default usually used to indicate the initial state of the system.
	Connective Junction	Junctions are used when there is a need to do a transition from one state to two or more states, where the transition occurred based on the same event, but evaluated against different conditions.
	History Junction	History junction is used to indicate the last state that was active to be the next active state.
	Graphical Function	Graphical function is used to code algorithms in Stateflow. The function can be tracked in Stateflow chart in run-time to evaluate its behaviour.
	MATLAB Function	Similar to Graphical Function, but in this case, the algorithms can use the MATLAB/Simulink library to call MATLAB functions which is external to the Stateflow chart.

Other than graphical objects, notations in Stateflow also comprises of text-based notations. There are several Stateflow text-based notations used in this study, for example ‘entry’, or its shorthand ‘en’, is used to indicate the state actions to be done as part of the entering the state. Another example is using different types of brackets in text that accompanies transitions will indicate whether it is an action or a condition. The text-based notations used in this study are summarized in Table 4.2.

Table 4.2 Stateflow text-based notations

Keyword	Shorthand	Meaning
entry	en	Actions that follow this keyword are done as part of entering the state.
during	du	Actions that follow are done as part of the state during action.
exit	ex	Actions that follow this keyword are done as part of leaving the state.
[condition]	-	Conditions guarding transition arrows and are written in square brackets.
{actions}	-	Actions accompanying transitions are written in curly brackets.

To evaluate the conditions, logical binary and unary operations are used in Stateflow. For example, “[A == 1]” is a logical binary operation of comparing a variable A with a constant can be a condition that triggers a transition from one state to another. Two different condition can also be joined using AND and OR operations. Table 4.3 show some of the examples of binary and unary operations that are used in Stateflow.

Table 4.3 Logical binary and unary operations in Stateflow

Example	Description
a && b	AND operations
!a	NOT operations.
a b	OR operations
a == b	Equality comparison
a != b a > b a < b a >= b a <= b	Inequality comparison

Stateflow is used in the development of control for Regenerative Motor-Pump System by indicating several states to be applied as the modes of the system. The Stateflow chart is designed based on the modes of the system, and suitable conditions are planned to be implemented as to guard the transition between the states. Details on application of Stateflow on the control development are discussed in the next section.

4.3 Controller Stateflow Chart

There are 5 states implemented in the Stateflow chart. The 5 states are:

1. Off
2. Neutral
3. Charging
4. Motor Mode
5. Pump Mode

Figure 4.1 shows the overall view of the controller in Simulink diagram. Stateflow in the Simulink diagram is represented by the Chart in the middle. There are 6 inputs from Simulink into the Stateflow chart and there are 5 outputs from the Stateflow chart to the Simulink environment. The development of the Stateflow chart is based on the development of the Preliminary Controller as discussed in Chapter 3.

All the 5 states and the relationship between them can be seen as in Figure 4.2. Generally, the system can change between the states by setting the values of mode_select to numbers assigned to the states. The value of mode_select is often the requirement to change from one state to the other. There are also some other requirements for some of the states. Other than the 5 states, there are also two MATLAB Functions in the Stateflow chart of the controller. They are GainAutoChange and GuiLoader.

Transitions between the states are guarded by conditions that are set based on the device behaviour in different modes as presented in Section 3.3. In the next section, the transitions and the states are discussed as the Stateflow chart is scrutinized for more details.

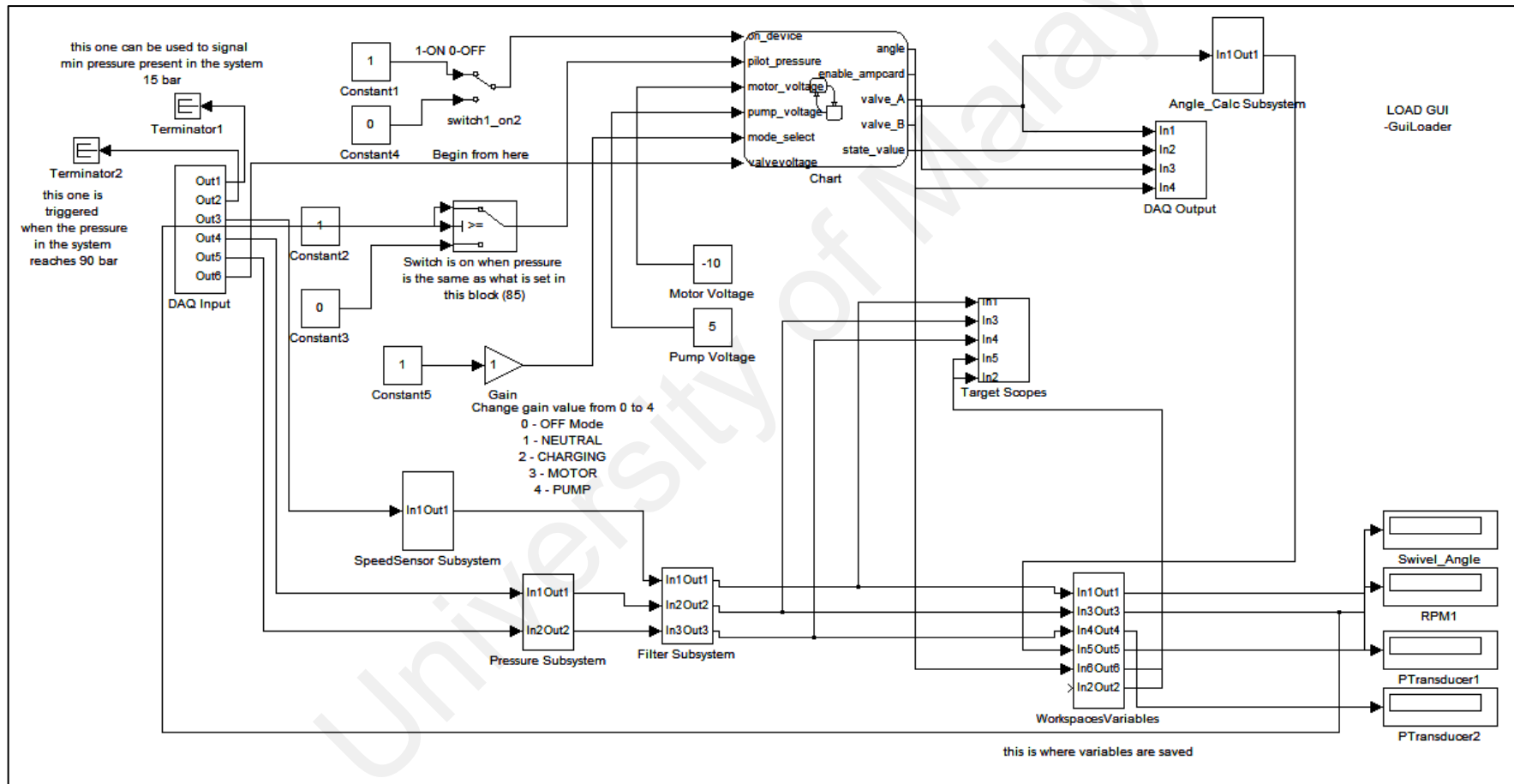


Figure 4.1 Simulink Diagram of the controller

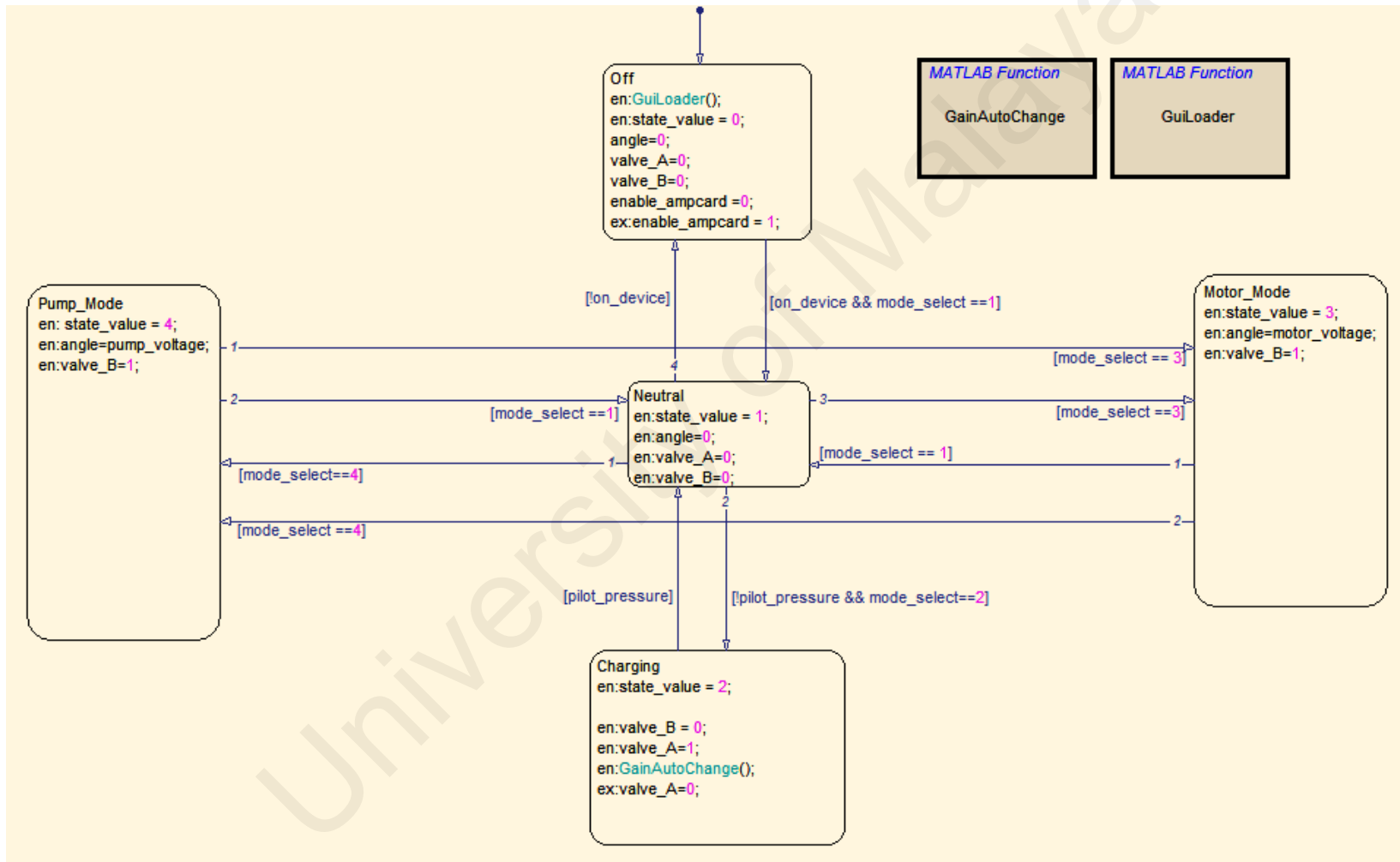
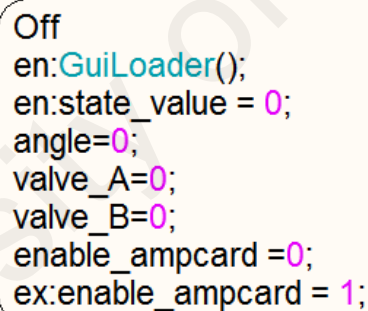


Figure 4.2 STATEFLOW Chart of the controller

4.3.1 OFF State

The OFF state is actually the initiation state for the regenerative motor-pump system. This is the first state that is entered by the system once the controller loads. This state is entered by setting the value of mode_select to zero. By entering this state, input values and output values are initiated, and the Graphical User Interface (GUI) is loaded. The state_value output value is set to zero as an indicator that the system is in this mode. Swashplate angle of the APU is set to 0° in this state, and Valve A and Valve B are both closed. Upon exiting this state, the APU Amplifier Card is enabled by setting the enable_ampcard output value to '1'. Figure 4.3 shows the details of the Off state in the Stateflow chart.

From this state, the system can only enter the Neutral state.



```
Off
en:GuiLoader();
en:state_value = 0;
angle=0;
valve_A=0;
valve_B=0;
enable_ampcard =0;
ex:enable_ampcard = 1;
```

Figure 4.3 Off State of the Stateflow Chart

4.3.2 Neutral State

The Neutral state is the second state in the Stateflow chart. The state is designated with the state_value of '1' and can be entered by the system by setting the value of mode_select to '1'. This will indicate that the system is in Neutral mode. In this state, the swashplate angle is set to zero.

From this state, the system can enter Motor Mode, Pump Mode, Charging and Off states. Entering this state will close Valve A and Valve B. In this state, the Amplifier Card is enabled, thus allowing the swashplate angle to be changed. This is important as the swashplate angle needs to be adjusted when entering Motor Mode or Pump Mode states. Figure 4.4 shows the details of the Neutral state.

```
Neutral
en:state_value = 1;
en:angle=0;
en:valve_A=0;
en:valve_B=0;
```

Figure 4.4 Neutral State of the Stateflow Chart

4.3.3 Charging State

The Charging state is the third state in the Stateflow Chart and is designated with state_value of '2'. This state can be entered by setting the mode_select value to '2'. Entering this state will trigger Valve A to open. The power pack will then pumps hydraulic fluid to the accumulator and increase its internal pressure. The state will also call out to a MATLAB Function GainAutoChange that will change the mode_select value automatically to '1'. The system can enter this state only when pilot_pressure is '0' and can only leave it once pilot_pressure is set to '1'. The value for pilot_pressure is controlled by a Simulink Switch block and the mechanism will be discussed later in Section 4.4.1.

```
Charging
en:state_value = 2;

en:valve_B = 0;
en:valve_A=1;
en:GainAutoChange();
ex:valve_A=0;
```

Figure 4.5 Charging State of the Stateflow Chart

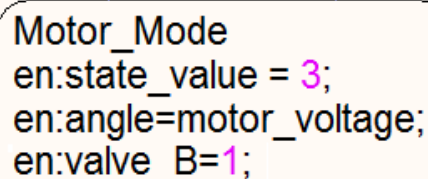
From this state, the system can only enter the Neutral state. By leaving this state, Valve A will be closed and thus, the charging process will be stopped. Figure 4.5 shows the details of the Charging state.

4.3.4 Motor Mode State

The Motor Mode state is the fourth state in the Stateflow chart. It is designated with state_value of '3' and can be entered by the system by setting the mode_select to '3'. The system can enter this state from the Neutral state and the Pump Mode state. Entering this state will allow the system to change the swashplate angle of the APU and allow the hydraulic fluid to flow from the accumulator to the reservoir via the APU.

The swashplate angle is set from motor_voltage value, which is pre-set in the Motor Voltage Simulink block. Entering this block will also trigger Valve B to open, which make it possible for the fluids to start flowing from the accumulator.

Figure 4.6 shows the details of the Motor Mode state. From this state, the system can enter the Neutral state by setting the mode_select to '1' and Pump Mode state by setting the mode_select to '4'.

A rectangular box with rounded corners containing the following text:

```
Motor_Mode
en:state_value = 3;
en:angle=motor_voltage;
en:valve_B=1;
```

Figure 4.6 Motor Mode state of the Stateflow chart

4.3.5 Pump Mode state

The system can enter the Pump Mode state by setting the mode_select value to '4'. The state_value for this state is also '4'. The system can enter this state from the Neutral state and the Motor Mode state. The system will begin recovering energy from

the rotations of the flywheel in this state. The swashplate angle be determined from the pump_voltage value which is pre-set in Pump Voltage Simulink block.

```
Pump_Mode
en: state_value = 4;
en: angle=pump_voltage;
en: valve_B=1;
```

Figure 4.7 Pump Mode state of the Stateflow chart

Entering this state will open Valve B to allow hydraulic fluid from the reservoir to get to the accumulator thus building pressure (state of charge) for the next motor mode. Figure 4.7 shows the details of the Pump Mode state. The system can leave this state for Neutral state or the Motor Mode state.

4.4 Controller Graphical User Interface

A graphical user interface (GUI) has been developed to ease control of the system. Figure 4.3 shows the GUI used to represent the controller. The GUI has been developed in MATLAB's own Graphical User Interface Design Environment (GUIDE). GUIDE is a GUI design tool that facilitates creation of GUI. Furthermore since it is part of MATLAB, it can also be integrated with Simulink and Stateflow. The GUI for the controller is able to process the state requests of the operator and send certain inputs to the Stateflow chart so that it can act accordingly.

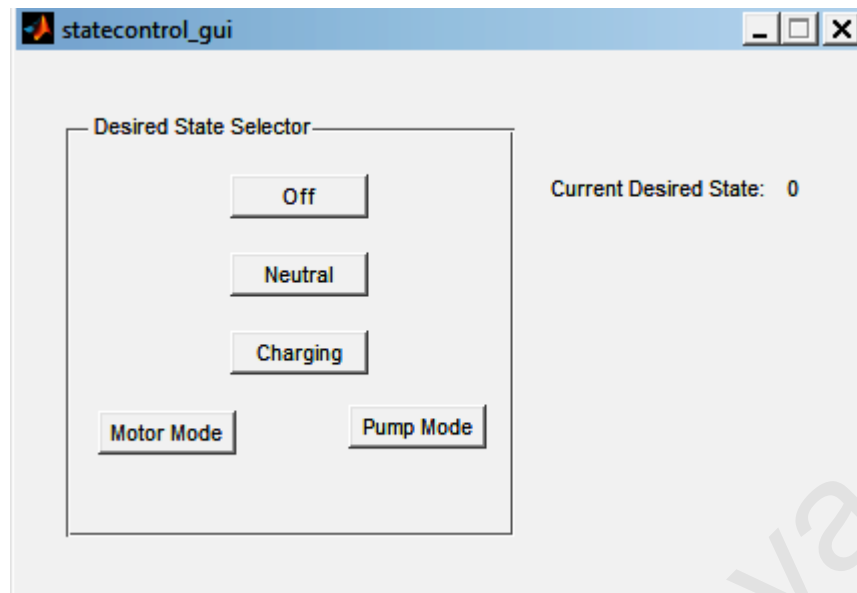


Figure 4.8 GUI for the controller

The GUI in Figure 4.8 consists of several buttons and a label that indicates the current desired state. The buttons are grouped under a frame called as the ‘Desired State Selector’. Clicking on the buttons during run-time will change the indicator label ‘current desired state’ to numbers assigned to each of the states. The numbers are 0, 1, 2, 3, and 4 that corresponds to the ‘Off’, ‘Neutral’, ‘Charging’, ‘Motor Mode’ and ‘Pump Mode’ states respectively. The numbers will also be sent to the Simulink part of the controller, where a Gain block value will be changed. Next, the Gain block will change mode_select input values of the Stateflow chart.

4.5 Safety Features

There are several improvements made from the previous preliminary controller in terms of safety. Since the regenerative motor-pump system deals with high pressure and precision electronics, there are several safety measures taken either physically or programmatically.

4.5.1 Charging mode pressure limiter

In the previous sections, the pressure limiting valve has been introduced as one of the ways to limit the pressures in the regenerative motor-pump system. For the system, one more method has been added to limit pressure in the system by limiting the charged pressure in the accumulator. This is done during the charging state, where pressure inside the accumulator is monitored and compared to a value that was pre-set before operating the system. The pressure inside the accumulator is monitored using one of the pressure transducers. The pressure measurements will be compared to a value set in one Switch block that will be triggered once the value exceeds the pre-set value. In this study, the value is pre-set to 80 bar. Once the accumulator reaches 80 bar, the system will stop charging the accumulator. By doing this, the system can repeatedly be charged at the same pressure level.

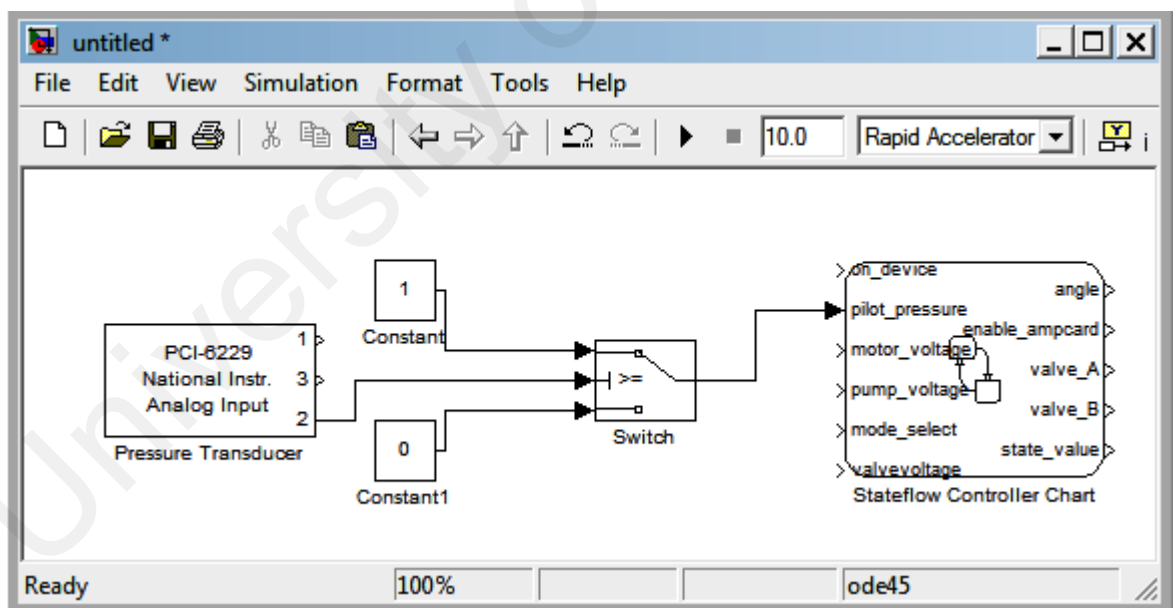


Figure 4.9 Simulink block arrangements for pressure limiter switch

Figure 4.9 shows the arrangements of the Simulink block for this pressure limiter. The accumulator pressure is measured and supplied by the PCI-6229 Analog Input Channel 2 to the Switch block. The Switch block will then compare the value of the second input u_2 , with a threshold value; which is the pre-set pressure.

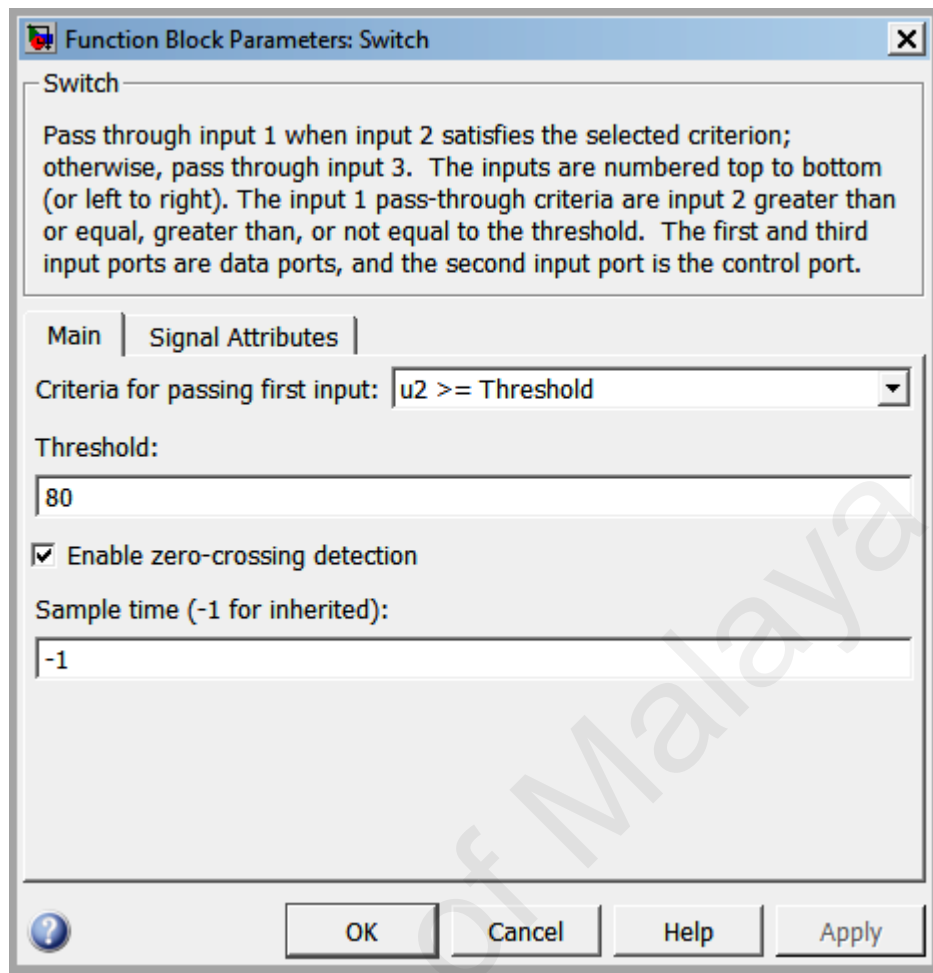


Figure 4.10 Switch block parameters settings

Figure 4.10 shows the parameters settings for the Switch block. The criterion of passing the first input is that the value of u_2 is more than the threshold value. By passing the first value, the constant value of '1' will be passed to the `pilot_pressure` input value in the Stateflow chart, indicating that maximum pressure of 80 bar is reached.

4.5.2 Valve Open check

One the main concerns when operating the regenerative motor-pump system is the high pressure level that can be built in the system. Failure in components such as valve can eventually lead to catastrophic results such as burst and leakage. In controlling the regenerative motor-pump system, immediate pressure change and build up can occur during motor mode and pump mode. For example during pump mode,

rotating flywheel will direct hydraulic fluid from reservoir to charge the accumulator, thus slowing it down (braking) and recover some energy. Failure to open Valve B that connects the reservoir to the accumulator will build pressure near the valve and possibility of bursting adjacent hydraulic linkages and hoses.

In order to avoid these things to happen, the system will need to know that the valves are open before changing the APU swashplate angle that directs the hydraulic fluids. Another improvement of the control is that the system monitors the status of the valves before allowing hydraulic fluids to flow through. Opening Valve B will require a supply of 24V DC. Therefore an input signal from Valve B indicating that it is 'Open' or 'Closed' is obtained by measuring the voltage across the valve. This signal is then sent to the PCI-6229 DAQ card on one of its analog input module, thus increases the channels that needed to be scanned to 3 channels (previously only 2 Pressure Transducer channels). The scan interval is changed to 0.003 s for a sampling time of 0.01 s.

Before allowing the measured voltage to be treated as one of the analog input in the system, the signal needs to be conditioned. As previously mentioned, the PCI-6229 DAQ card can only accept analog input that ranges from -10V to +10V. Valve B voltage supply meanwhile, is 24V DC. The measured voltage is tuned down to 10V by putting the signal through a voltage regulator circuit that will regulate the voltage.

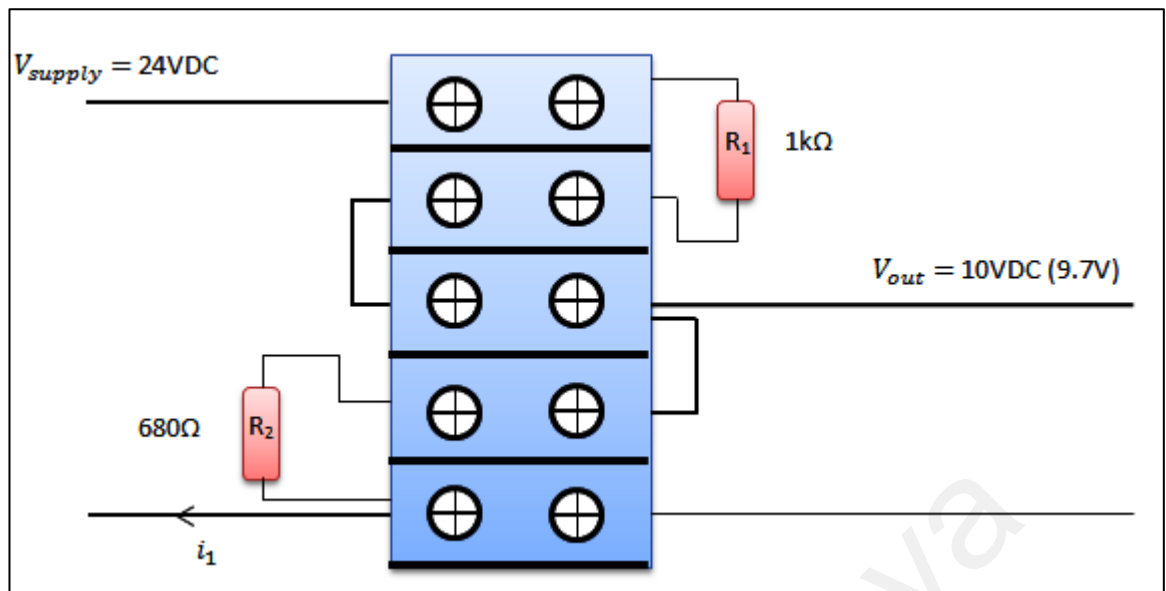


Figure 4.11 Voltage Regulator Circuit for Valve B ON/OFF indicator

Figure 4.11 shows the voltage regulator circuit diagram. The voltage regulator is constructed using two resistors of 1 kilo-ohms and 680 ohms respectively. The input supply and output supply of the voltage regulator is connected to the resistors on a terminal block.

The output voltage can be calculated by:

$$V_{out} = \frac{R_2}{R_1 + R_2} \times V_{supply} \quad (4.1)$$

Where;

V_{out} = Output voltage

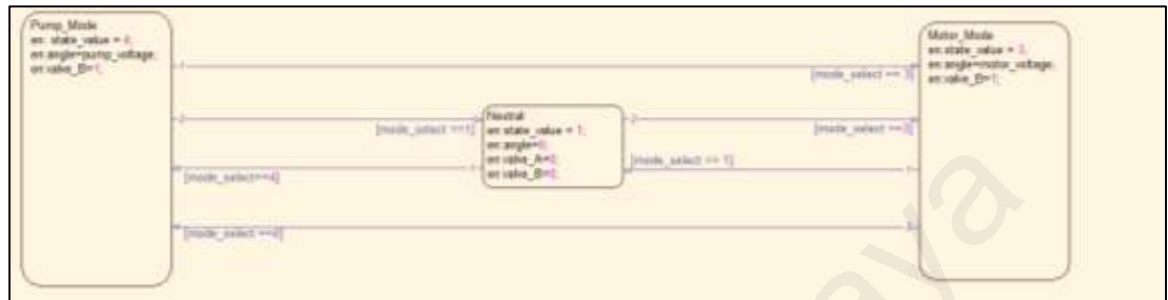
V_{supply} = Supply voltage

R_1 = Resistor, 1 k Ω

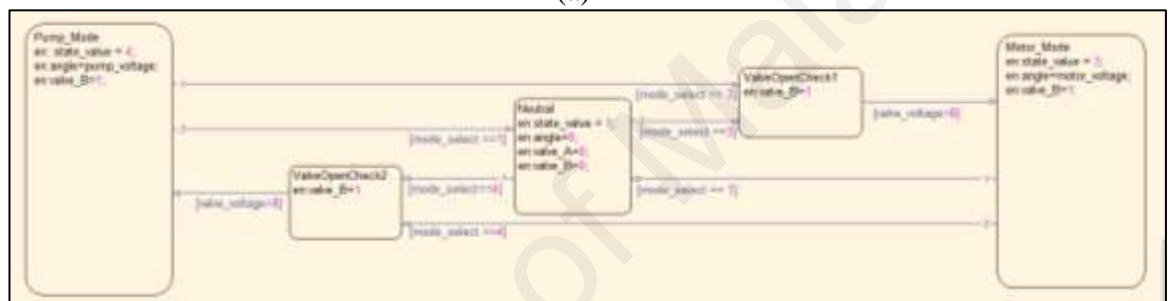
R_2 = Resistor, 680 Ω

Therefore, the voltage supply of 24 V can be regulated to 9.7 V which is compatible with the analog input voltage range.

The system is able to determine whether the valve is open or closed by measuring the voltage across Valve B. To implement this function, two new states are introduced into the Stateflow chart. Figure 4.12 shows the difference in the Stateflow diagram between before and after implementing these measures.



(a)



(b)

Figure 4.12 Valve Open Check States – (a) Before and (b) after implementations

The system will have to enter a new state (ValveOpenCheck1 or ValveOpenCheck2) whenever it wants to enter Pump Mode or Motor Mode. The new states will open Valve B, and only allow entering either state if the `valve_voltage` value is more than 8 V. This ensures that Valve B is open and that the system will only enter Motor Mode or Pump Mode after it made sure of that fact.

4.6 Validations of the Controller

The controller is validated by operating the Regenerative Motor-Pump System in all the different states. The validation is done to make sure that the system can automatically enter any of the states upon request from the operator. Figure 4.13 visually describes the process undergone by the system during evaluation. The evaluation begins from the Off State, then immediately to the Charging State via the Neutral State (A). Charging the accumulator is done until the pre-set value of the pressure is reached (B). The system automatically enters the Neutral State before entering the Motor Mode upon request from the operator (C). Once the pressure in the accumulator is zero, the operator requests for pump mode so that the system starts to recover braking energy from the flywheel revolutions (D).

The pump mode will slow the flywheel down before the operator requests for motor mode once again to make the flywheel revolve (E). In the second motor mode the regenerative motor-pump system also uses energy from the pressure build up in the accumulator. The only difference is the second motor mode uses energy purely from the recovery during the previous pump mode, while the first one uses energy from direct charging of the accumulator. After the pressure in the accumulator drops to zero, the system is returned to Neutral state (F).

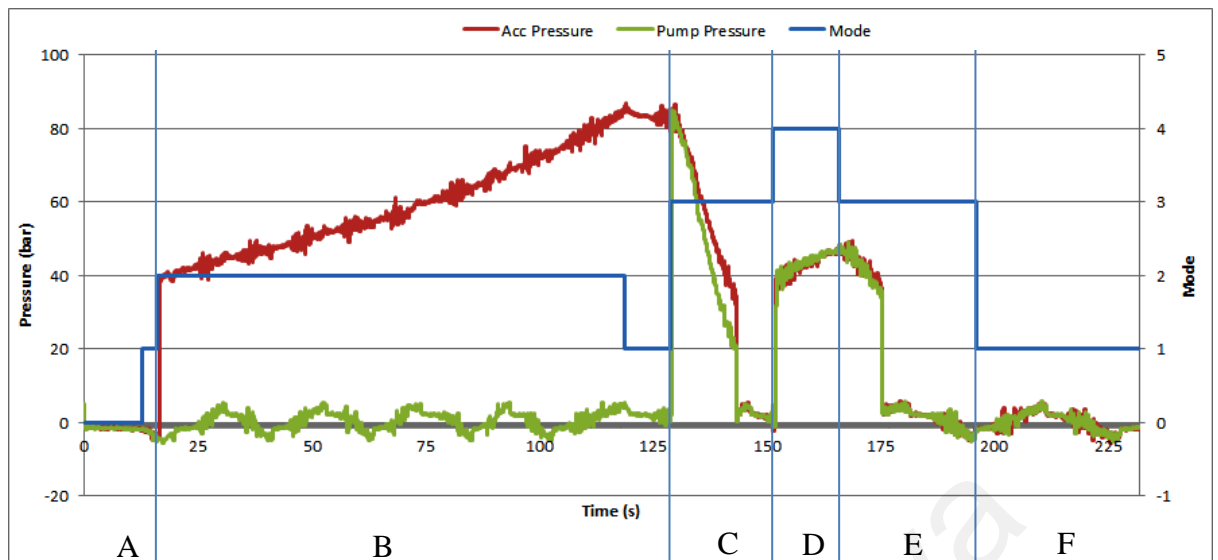


Figure 4.13 Validation of the controller on the 5 states (Pressure)

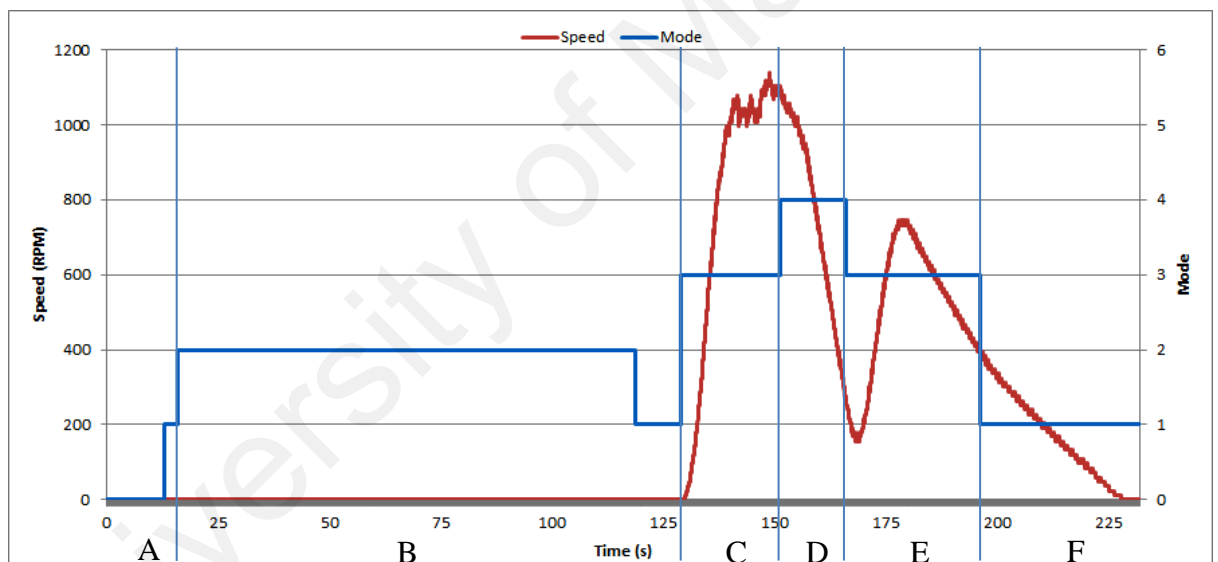


Figure 4.14 Validation of the controller on the 5 states (Speed)

Figure 4.14 describes the processes undergone by the regenerative motor-pump system in terms of flywheel speed. In the figure, part C, D, E and F are the parts that are concerned with flywheel speed. At Part C, the system is in the Motor Mode state, and that is when the flywheel starts rotating. The rotation begins as soon as Valve B is opened and swashplate angle is changed to allow hydraulic pressure to flow from the accumulator to the reservoir.

Part D begins when the system requests for Pump Mode. In part D, the rotational speed of the flywheel starts to slow down. This is because of rotational energy of the flywheel is used to pump hydraulic fluid into the accumulator. Part E begins when the accumulated pressure in the accumulator is released in Motor Mode, where the flywheel starts gaining speed.

From Figure 4.14 it can be noted that the speed attainable in the first motor mode (C) is higher than the second one (E). At C, the maximum speed of the flywheel is 1100 RPM, while at E; the maximum speed is 700RPM.

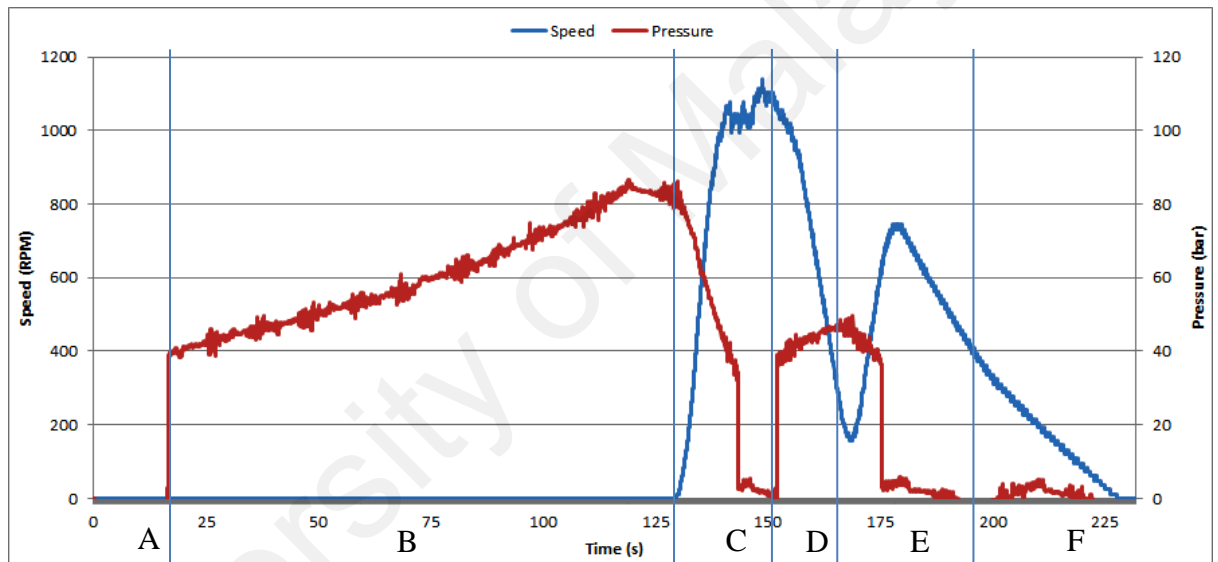


Figure 4.15 Validation of controller – Comparison between Pressure and Speed

Figure 4.15 shows the same evaluation of the controller, but in this case, the comparison between the accumulator pressure and the flywheel speed is made clearer. Since the regenerative motor-pump system operates purely from the pressure inside the accumulator, the comparison can be made directly.

From this study, one can find the relationship between state of charge and vehicle speed of hydraulic hybrid vehicle (HHV) that operates purely on hydraulic motorization. In Figure 4.15, A, B, C, D, and E denotes the same states as previous

diagrams. It can be clearly seen for example in Part C, that when the pressure drops (accumulator discharge), the flywheel speed increases. In Part C, the system can be seen emulating Motor Mode for an actual HHV. In Part D, the system is emulating Motor Mode, where the speed of flywheel starts to drop while at the same time, pressure is building up in the accumulator (accumulator charging).

4.7 Conclusion

A controller for Regenerative Motor-Pump System has been developed based on the development of the earlier Preliminary Controller. The newly developed controller system has successfully emulated processes on real HHV. Several safety features has been integrated into the controller which are (1) Charging Pressure Limiter and (2) Valve Open Check. The next chapter will discuss on the results obtained from the evaluations of the controller.

5.0 SIMULATION AND ANALYSIS

5.1 Introduction

Introducing an auxiliary drivetrain to a conventional vehicle will hybridize the vehicle's source of energy. Installing a Regenerative Motor-Pump System on a conventional vehicle for example will transform the vehicle to a Hydraulic Hybrid Vehicle. One of the most important questions need to be answered in this study is what are the benefits of installing Regenerative Motor-Pump System in a conventional Internal Combustion Engine (ICE) vehicle? This chapter will partly answer the question by simulating HHVs on drive cycles and analyse the results in terms of fuel consumption, energy usage and distance travelled by the simulated HHV.

Before the results on drive cycles can be presented, the chapter will initially discuss the simulation model of the HHV. The HHV is modelled based on ISUZU NKR 71-E commercial truck. The properties of NKR 71-E including its weight and dimension are taken into account to make an accurate model of the truck in Simulink. Then, the simulated NKR 71-E engine model is presented – a validation of the engine model compared to actual dynamometer testing of ISUZU NKR 71-E is shown. The comparison is made to ensure that the engine model is accurate and can be used as a representative of an actual ISUZU NKR 71-E engine.

After a review on the conventional drivetrain of ISUZU NKR 71-E, the chapter will describe the hydraulic drivetrain proposed to be installed on NKR-71E. The ISUZU NKR 71-E is then considered as a HHV and a discussion on the regenerative capability and energy delivery of the Regenerative Motor-Pump System is presented – as the results are used as the basis of the hydraulic drivetrain model. A simple rule is used to represent the Energy Management System (EMS) of the HHV to govern both energy sources.

Finally, both the conventional and hybrid NKR 71-E are simulated on two different types of drive cycle tests. An introduction to the tests is presented, before the results of the simulation of the two different vehicles are shown. The results are then analysed by comparing both vehicles simulation results side by side. A summary of the chapter and the results are given to complete the chapter.

5.2 HHV Conventional Driveline Model

This section will discuss on the conventional driveline of the HHV. The conventional driveline is modelled in the simulation based on ISUZU NKR 71-E truck. Specifications of the NKR 71-E has been given in Table 3.1. The weight and dimensions of NKR 71-E were taken into consideration to develop the conventional driveline model.

5.2.1 Simulink model for NKR 71-E Conventional Driveline

A Simulink model for ISUZU NKR-71 E is developed for the use of simulation testing. Figure 5.1 depicts the Simulink model of the vehicle. The Simulink model uses a PID controller to control the speed of the vehicle based on the demand curve in the signal builder. Error comparison between the demand and the current speed will yield throttle values that is then evaluated in the Driveline Subsystem. Positive throttle values will be translated as acceleration, while negative throttle values are translated as braking events.

Several results can be obtained from the Simulink model which are (1) power measurements from the ICE, (2) required and actual vehicle speed, (3) rotational speed of different shafts in the driveline, (4) work done (Energy used) and (5) distance travelled throughout the simulation.

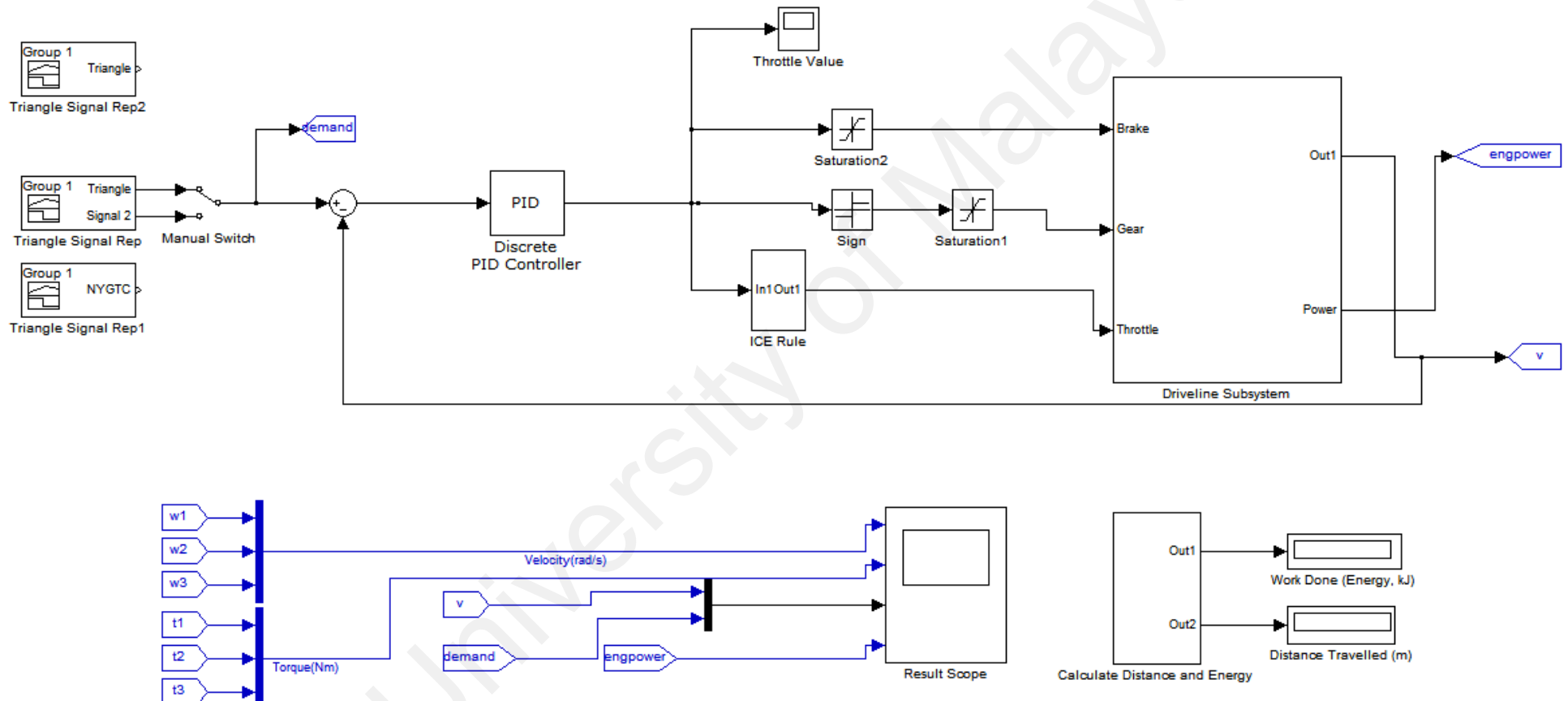


Figure 5.1 Simulink model of ISUZU NKR 71-E

The same Simulink model is used for both ISUZU NKR 71-E and its hybrid version. The only difference between the two is in the addition of a hydraulic drivetrain in the HHV ISUZU NKR 71-E. The Simulink model uses mostly blocks from SimDriveline library which is one of the components in Simscape library. Figure 5.2 shows the Simulink blocks arrangements for the ICE and the vehicle dynamics which is a closer look into the Driveline Subsystem.

There are some essential blocks from the SimDriveline library used in developing the conventional driveline model. They are:

- (1) Generic Engine
- (2) Vehicle body
- (3) Tire
- (4) Simple Gear
- (5) Inertia
- (6) Differential

The parameters used for each of the blocks are default values, unless otherwise stated. The parameters are an approximation of the values of an actual NKR 71-E vehicle behaviour. The details of the parameters and the functions of the blocks will be discussed next. Additionally, an introduction to calculations of fuel consumption will be discussed right after that.

5.2.1(a) Generic Engine

In SimDriveline, modelling an engine is achieved with available Generic Engine block. The Generic Engine block can be used to model the ISUZU NKR 71 E engine from the data saved in WinPEP 7. Figure 5.4 shows the Data Export Preview from the WinPEP 7 interface. The engine data are able to be saved in .txt format.

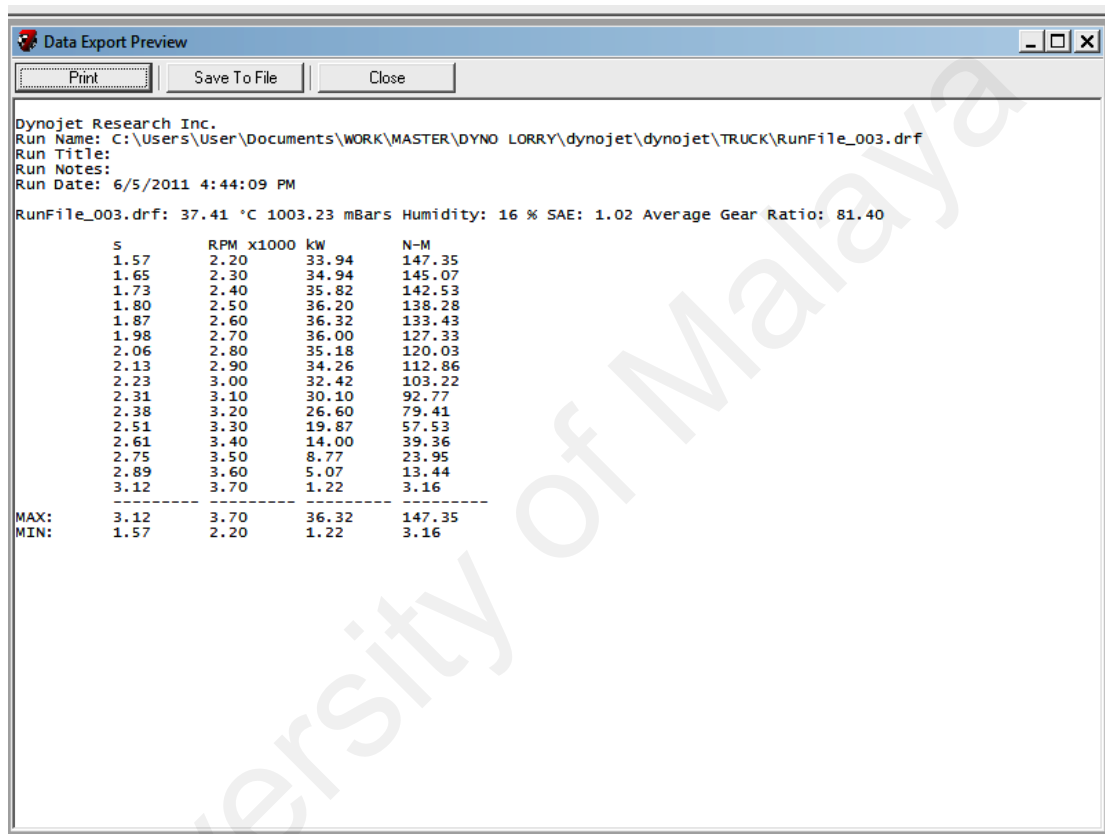


Figure 5.3 WinPEP 7 GUI - Data Export Preview

In the Generic Engine block, we can manually input the engine data into the parameters of the block. In this way, we can simulate the actual truck engine in Simulink environment. In the Generic Engine block, there are three options that can be selected to model an engine. They are (1) Normalized 3rd order polynomial matched to peak power, (2) Tabulated torque data and (3) Tabulated power data. Figure 5.4 shows the Generic Engine block interface in the SimDriveline library.

For this study, the second option which is tabulated torque data is selected. For this model parameterization, we need to manually input the RPM and its corresponding torque value (N-m) into the block. The first speed value entered into the block is considered as the stall speed, while the last speed value is considered as the maximum speed. The torque value will be blended to zero once the speed is below the stall speed. Meanwhile, if the speed exceeds the maximum speed, the simulation will stop with an error.

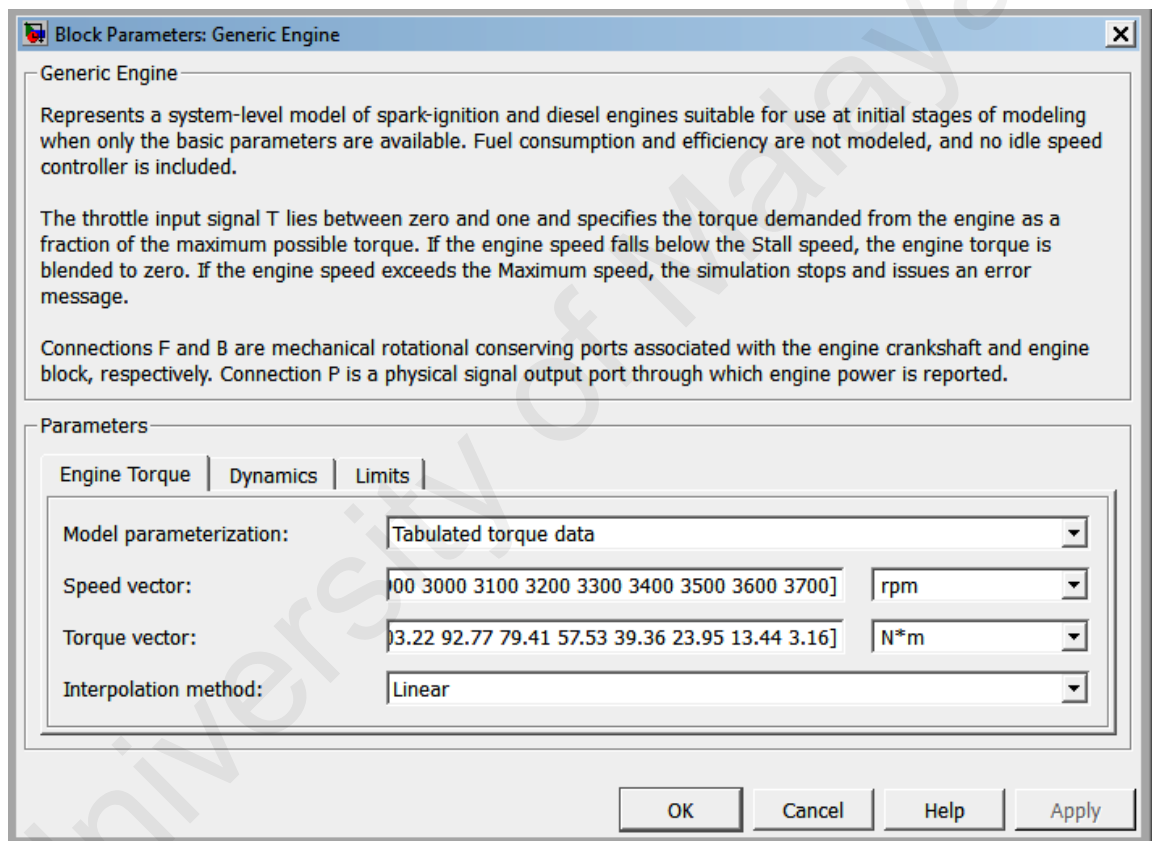


Figure 5.4 Simulink Block – Generic Engine interface

Parameters for the engine model in the Generic Engine block are summarized in the Table 5.1. The Generic Engine block has 3 different tabs which are engine torque, dynamics and limits. The different tabs include different parameters as summarized in Table 5.1. Speed vector and torque vector in the Engine Torque tab is represented inside a matrix with the each elements in the speed vector corresponds to the elements

in the torque vector. In this study, the interpolation method is selected to be Linear.

Other interpolation methods available to be chosen from are Cubic and Spline.

Table 5.1 Generic Engine block parameters settings

Categories	Parameter	Parameter Value(s)
Engine Torque	Model parameterization	Tabulated Torque Data
	Speed vector (rpm)	[500 600 700 800 900 1000 1100 1200 1300 1400 1500 1600 1700 1800 1900 2000 2100 2200 2300 2400 2500 2600 2700 2800 2900 3000 3100 3200 3300 3400 3500 3600 3700]
	Torque vector (N.m)	[147.35 147.35 147.35 147.35 147.35 147.35 147.35 147.35 147.35 147.35 147.35 147.35 147.35 145.07 142.53 138.28 133.43 127.33 120.03 112.86 103.22 92.77 79.41 57.53 39.36 23.95 13.44 3.16]
	Interpolation method	Linear
Dynamics	Inertia (kg.m ²)	1
	Initial velocity (rpm)	800
	Engine time constant (s)	0.2
	Initial normalized throttle	0
Limits	Speed threshold (rpm)	100

A more detail look on the ISUZU NKR 71-E engine model will be presented in Section 5.2.2. The section will discuss further on the validation of the engine model in accordance to actual dynamometer testing data for NKR 71-E.

5.2.1(b) Vehicle Body

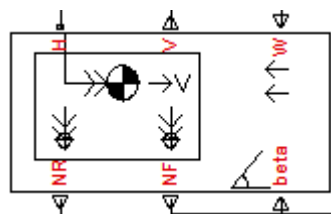


Figure 5.5 Vehicle body block in Simulink

Figure 5.5 shows the Vehicle Body block. In the Vehicle Body block, there are six ports. Port H is for the mechanical translation of the vehicle. This port is connected to the tires. Port V outputs the velocity of the vehicle whereas NR and NF outputs the normal forces for rear and front wheels and is also connected to the tires. Port W and port beta are headwind forces input and road inclination input respectively, and they are not used in the current study. Basically, this block is responsible for representing motion of two axle vehicles.

Table 5.2 Vehicle Body block parameters

Parameters	Value(s)
Mass	2180 kg
Number of wheels per axle	2
Horizontal distance from CG to front axle	1.530 m
Horizontal distance from CG to rear axle	3.060 m
CG Height above ground	0.7 m
Frontal area	6 m ²
Drag coefficient	0.65
Initial velocity	0 m.s ⁻¹

The vehicle body block is responsible to consider several factors when representing a two-axle vehicle. The factors are among others: (1) aerodynamic drag, (2) vehicle mass, (3) distribution of load on the axles, (4) the vehicle response on acceleration and road profile. The block parameters have to be adjusted to reflect the vehicle being simulated. Table 5.2 summarizes the parameters input in the vehicle body block.

5.2.1(c) Tire



Figure 5.6 Tire block in Simulink

Figure 5.6 illustrated the tire block used in the modelling of the truck. The blocks have 4 ports and they are represented by N, A, S and H. Port N connects to the port NR

of the Vehicle Body block which will input the normal forces acting on the tire from the axle. Port A is connected to the differential, where the mechanical rotation is connected. Port S outputs slip information for the tires whereas port H is for mechanical translational motion of the vehicle and connects to port H of the Vehicle Body block.

Table 5.3 summarizes the parameters that are able to be manipulated and configured to use the tire block as a representation of the truck's tire. The tire can be parameterize using (1) Peak longitudinal force and corresponding slip, (2) Constant magic formula coefficient or (3) Load-dependent magic formula coefficient. For this study, the tire is parameterized using the peak longitudinal force and corresponding slip.

Table 5.3 Tire block parameters

Categories	Parameter	Parameter value(s)
Tire Force	Parameterize by	Peak longitudinal force and corresponding slip
	Rated vertical load	3000 N
	Peak longitudinal force at rated load	3500 N
	Slip at peak force at rated load (percent)	
Dimensions	Rolling Radius	0.4 m
Dynamics	Compliance	No compliance – Suitable for HIL simulation
	Inertia	No inertia
Slip calculation	Velocity threshold	0.1 m/s

5.2.1(d) Simple Gear

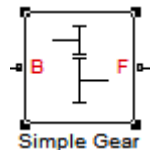


Figure 5.7 Simple Gear block in Simulink

Figure 5.7 shows the Simple Gear block used in the modelling of the HHV truck. The block has two ports and they are base (B) and follower (F). The block allows

viscous losses and frictional losses in the system to be modelled. The present study considers to model the first gear of the HHV, therefore a simple gear block such as this one is sufficient.

5.2.1(e) Inertia

Two inertia blocks are included in the simulation. The two inertia blocks are there to represent the inertia of the connecting shafts. One of the inertia blocks is placed before the torque converter, while the other is placed after it, as illustrated in Figure 5.2. One of the inertia blocks are set to have an initial velocity of 800 RPM to represent the idle speed of the engine, with the other one sets to be stationary.

5.2.1(f) Differential

Differential connects the engine to the wheels. The three connection ports namely D, S1 and S2 represents connections to the driveshaft and two output shafts respectively. This is shown in Figure 5.8. The differential is fixed as a planetary bevel gear train. An additional bevel gear transmission between the driveshaft and the carrier is also placed in the differential. In this study, the meshing losses and viscous losses of the differential is not modelled. Table 5.6 summarizes the parameters of the Differential Simulink block.

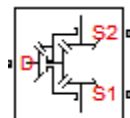


Figure 5.8 Differential block in Simulink

Table 5.4 Differential block parameters

Categories	Parameter	Parameter value(s)
Main	Crown wheel located	To the right of center-line
	Carrier (C) to driveshaft (D) teeth ratio (NC/ND)	4
Meshing losses	Friction model	No meshing losses – suitable for HIL simulation
Viscous losses	Sun-carrier and driveshaft-casing viscous friction coefficients N.m/(rad/s)	[0 0]

5.2.1(g) Fuel Calculations

A simple fuel calculation has been integrated into the engine model Simulink simulation. A formula to calculate the fuel consumption that is used in this study is based on the works of Ilkilic et al. (Ilkilic et al., 2011). The Brake Specific Fuel Consumption (BSFC) is assumed to be a constant value of 200 g/kWh. Fuel consumption is given by:

$$Fuel\ Consumption = \frac{BSFC \cdot P_e}{3600 \cdot v_t} \quad (5.1)$$

Where;

P_e = Engine power, W

v_t = Velocity of the truck, m/s

$BSFC$ = Brake Specific Fuel Consumption

The fuel consumption is given in g/km unit. To get the amount of fuel used along the course of simulation, the distance travelled by the simulated truck should be known. The fuel is assumed to be 0.83 kg/L diesel. Therefore, the fuel volume that is consumed in litres is given by:

$$\text{Fuel Volume} = \frac{\text{Fuel Consumption} \times D_t}{\rho_f} \quad (5.2)$$

Where;

D_t = Distance travelled by the truck

ρ_f = Density of the fuel

5.2.2 ISUZU NKR 71-E Engine Model

A short discussion on how to actually model NKR 71-E Engine in Simulink has been presented in Section 5.2.1(a). The modelling of the engine is done by utilising one SimDriveline block which is called as “Generic Engine”. The block is able to exploit tabulated data from actual dynamometer testing on NKR 71-E. In this study, the engine is modelled using actual dynamometer testing data fed into the block.

The results from the dynamometer testing have been collected using Dynojet Research Software called as Dynojet WinPEP 7. WinPEP 7 enables viewing of data collected from the dynamometer testing. Other than that, the software also allows generation of graphs and data export, making it easier to analyse the results from the dynamometer test. The dynamometer testing was conducted on the truck ISUZU NKR 71-E without any other load, making the weight of the vehicle to be 2180 kg. The dynamometer testing was done to characterize all 4 gears available in the ISUZU NKR 71-E.

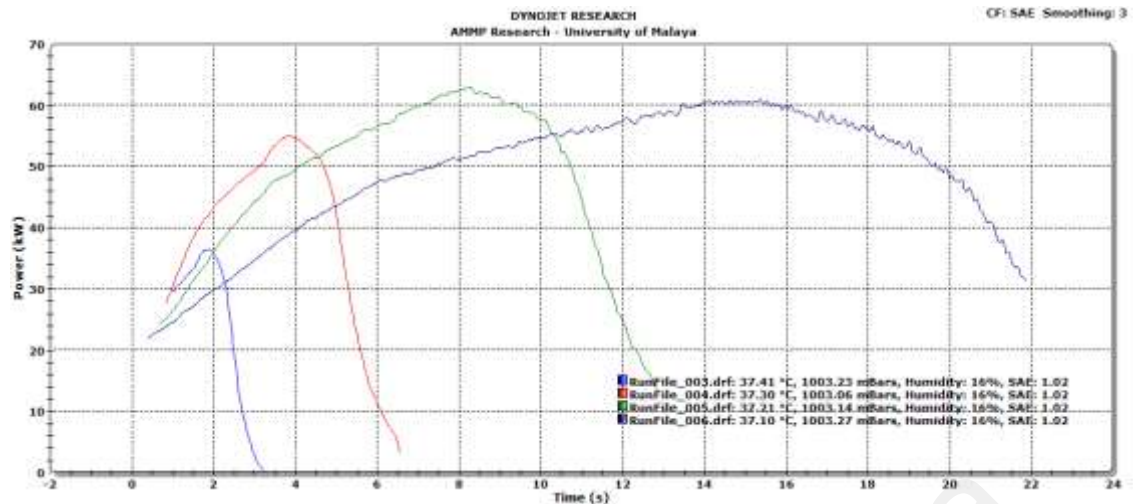


Figure 5.9 Engine Data for ISUZU NKR 71 E: Power versus Time (Gear 1 - 4)



Figure 5.10 Engine Data for ISUZU NKR 71 E: Power versus Speed (Gear 1 – 4)

Figure 5.9 shows the Engine Data of the truck ISUZU NKR 71-E for all four gears. The graph shows a plot of engine power (Power) versus time. In the graph, Gear 1 is represented by the blue curves labelled as RunFile_003. Gear 2, Gear 3 and Gear 4 are all represented by curves labelled as RunFile_004, RunFile_005 and RunFile_006 respectively. Power peaked at 36.34kW for Gear 1, the smallest compared to the other 3 gears.

Meanwhile, Figure 5.10 represents the graph of Power versus vehicle speed for all the four gears. In this graph, the maximum reachable vehicle speed can be determined for all the gears. Gear 1 has the maximum speed of 42 km/hr, where the

other three gears have faster speed. Towards the maximum speed, the power required from the engine is reduced greatly for all the four gears.

The simulated engine of ISUZU NKR 71-E was developed using generic engine from SimDriveline in Simulink. In order to validate the engine model, the simulated vehicle is tested with a full throttle input, and the power measurement obtained from the simulation is compared to the power curve obtained from the dynamometer testing. This validation is important to check whether the engine model is reliable and able to emulate ISUZU NKR 71-E truck.

Figure 5.11 shows the curves obtained from the power measurements in the simulation for Gear 1, Gear 2, Gear 3 and Gear 4. The curves can be compared to the curves obtained from the dynamometer testing in Figure 5.9. Generally, both exhibited similar characteristics. This demonstrates that the ISUZU NKR 71-E engine is successfully modelled for the simulation.

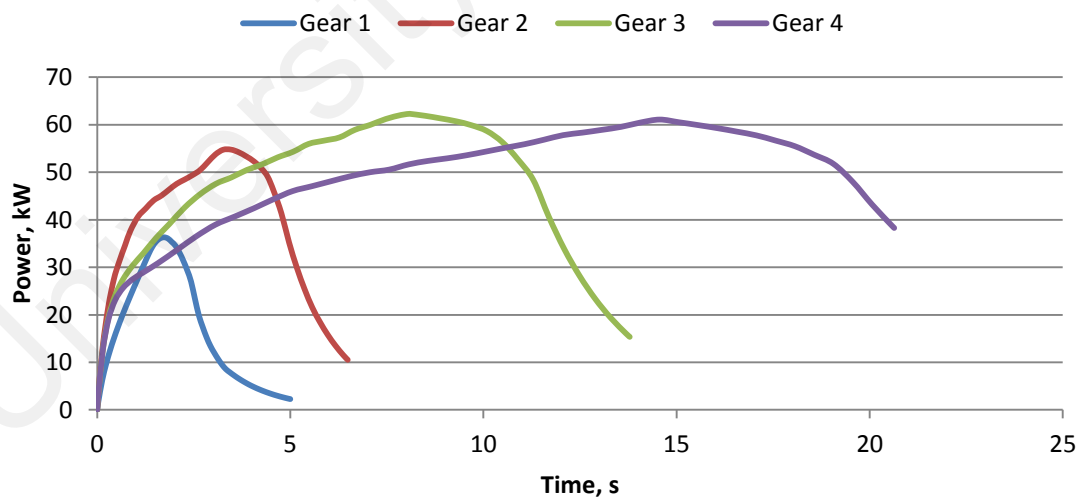


Figure 5.11 Simulated Engine Data for ISUZU NKR 71-E (Gear 1 – 4)

Table 5.5 Engine Characteristics of NKR 71-E

Gears	Maximum Power	Maximum Attainable Speed
1	36.34 kW	42.58 km/h
2	55.02 kW	76.37 km/h
3	62.85 kW	120.37 km/h
4	60.79 kW	161.20 km/h

Table 5.5 summarises the difference between the four gears based on the maximum power and the maximum vehicle speed attainable. Gear 3 has the highest measure of maximum power while Gear 4 has the highest maximum attainable speed. However, since we want to see whether the Regenerative Motor-Pump System is able to use recovered braking energy to initially move the vehicle, only the Gear 1 data are relevant to be used as a comparison to the data points harvested from the Regenerative Motor-Pump System.

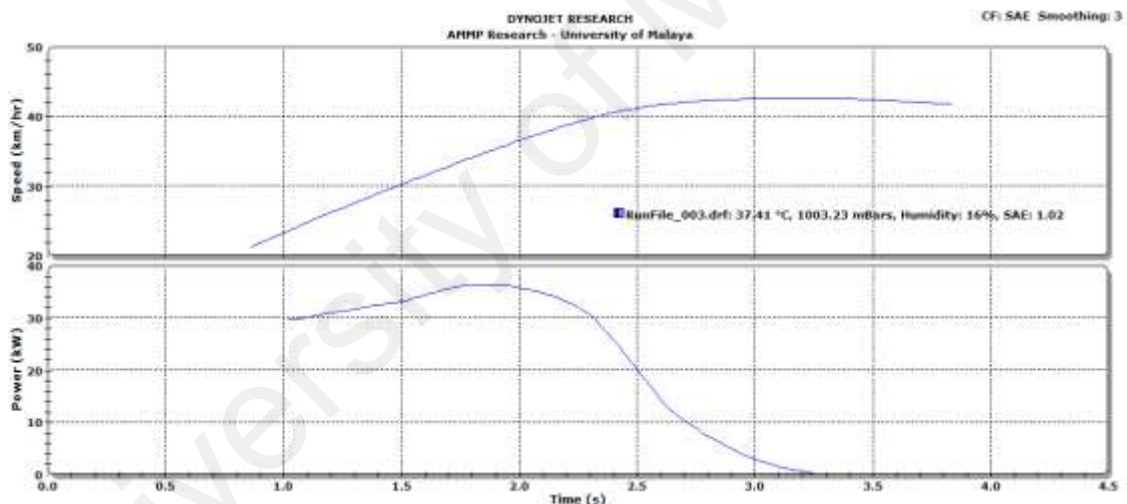


Figure 5.12 Engine Data for Gear 1 – Speed (km/h) and Power (kW) versus Time

Figure 5.12 shows a graph of Speed and Power versus time for Gear 1. This figure shows that the engine took about 3 seconds to reach the maximum speed of 42.5 km/h. The engine reached the peak power of 35.82 kW around 2 seconds after which the power starts to decline. These describe the characteristics of the engine – the power required to bring a truck from stationary to motion is usually the highest. This is why a higher power density auxiliary power supply is desirable. Having a good hybrid system

that can provide the power in the initial acceleration of the vehicle can eventually lead to great savings in fuel consumption.

In order to find out the fuel savings achievable by installing a Regenerative Motor-Pump System on the drivetrain of a truck, there is a need to simulate the ICE in the base vehicle. The simulated Engine results will then be compared to the experimental results obtained from tests done with the Regenerative Motor-Pump System

5.3 HHV Hydraulic Driveline Model

To actually develop the hydraulic driveline for the HHV simulation, experimental data obtained from the testing with Regenerative Motor-Pump System is used as its foundation. Two different factors of the Regenerative Motor-Pump System will be used as the basis of the hydraulic driveline model. The factors considered are (1) Energy Recovery and (2) Energy Delivery of the Regenerative Motor Pump System. This subsection will look into the two factors before a discussion on modelling the hydraulic driveline is presented.

5.3.1 Energy Recovery and Energy Delivery

In order to model the hydraulic drivetrain accurately, the study focuses on its energy recovery and energy delivery. The hydraulic drivetrain should be modelled based on the Regenerative Motor-Pump System experimental results. For this matter, the study refers to the second motor mode – referring to Figure 4.15 where the energy used in the motor mode is actually recovered energy from the previous pump mode. It can be seen that the pressure attained from charging is higher than the recovered pressure in pump mode. This different initial pressure for the two motor modes results to different flywheel speed. In that matter, this study can state the amount of energy recovered and will look on the details on the significance of this amount of energy.

The energy recovered will be used as the basis to determine the speed of the vehicle, to put into perspective the possibilities of the energy recovered to actually move the HHV. The approximation of the speed is made possible using equations and theory as discussed in Section 3.24. The flywheel will be a substitute of the vehicle's mass, and the speed of the vehicle depends on the rotational speed of the flywheel.

Table 5.6 Energy and velocity data comparison between Motor Mode I and Motor Mode II

	Motor Mode I (Figure 4.14- Part C)	Motor Mode II (Figure 4.14 - Part E)
Maximum Flywheel Speed	1080 rpm	744 rpm
Angular Kinetic Energy	18.89 kJ	8.94 kJ
Velocity of the truck	14.97 km/h	10.31 km/h
Velocity of the HHV (additional weight)	13.89 km/h	9.57 km/h

Table 5.6 shows the data from both motor modes compared side by side. For the velocity of the truck, it is assumed that the angular kinetic energy calculated from the maximum speed of the flywheel rotations equals to the kinetic energy attainable by the HHV. This results to the approximate value for the truck velocity. Equation 3.4 from Section 3.2.4 is used to calculate the approximate velocity value of the HHV.

From Table 5.6, it can be concluded that the regenerative motor-pump system is able to recover energy enough to actually move the HHV to 10.32 km/h. In Motor Mode I, the original angular kinetic energy was 18.89 kJ, whereas in Motor Mode II, the angular kinetic energy attained from the recovered pressure in the accumulator is 8.94 kJ. From this observation, it can be established that the Regenerative Motor Pump System is able to recover up to 40% of the braking energy. This shows that the HHV is able to supply additional energy for the vehicle without the usage of fuel and may save 8.96kJ of energy.

5.3.2 Hydraulic Driveline Simulink Model

Figure 5.13 describes the driveline of the HHV ISUZU NKR 71-E. The driveline subsystem is developed based on examples from a MATLAB demo that feature multiple drivetrains vehicle that uses ICE and an Electric Motor (sdl_parallel_hybrid). In this study, the hydraulic drivetrain is connected to the ICE by a simple gear. The ICE block as shown in Figure 5.13 contains the conventional driveline previously presented in Figure 5.2.

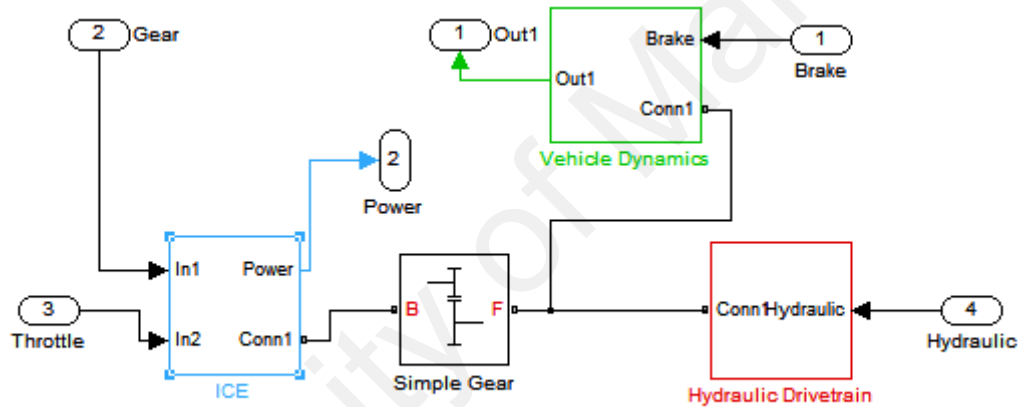


Figure 5.13 Driveline Subsystem for HHV

The hydraulic drivetrain is made using simple torque supply that is activated using a simple rule. The rule is a representation of an Energy Management System (EMS) of the HHV. The EMS is an essential part of the HHV as it governs the utilization of either the ICE or the hydraulic energy supply. For the simulated HHV in the study, two assumptions are used as the rules for the hydraulic drivetrain.

(1) The hydraulic drivetrain is used to supply torque on the HHV until the vehicle moves to 10km/h. This is based on the energy delivery and recovery of Regenerative Motor-Pump System discussed in the previous section.

(2) The energy recovered on each braking events in the accumulator is always enough for subsequent acceleration events.

The EMS is translated into Simulink blocks and used along with the Simulink model of the hydraulic drivetrain. This in turn becomes the proposed hydraulic drivetrain to be installed on ISUZU NKR 71-E.

5.4 Simulation Results of the developed HHV Model

Due to many limitations in the Regenerative Motor-Pump System, simulation tests has been set up to further study on the benefits of HHV as compared to conventional vehicle. The simulation is done based on (1) the experimental results on the Regenerative Motor-Pump System and (2) dynamometer testing on the ISUZU NKR 71-E truck. The model has been developed and discussed in the previous two sections. The simulation results in this topic will be divided into four subtopics that cover different types of simulation tests done on the simulated ISUZU NKR 71-E truck.

The first subtopic will discuss on the results of simulation of two trucks of different weights. The difference in weight is what differentiates the ISUZU NKR 71-E truck with its HHV alternative. Discussions on the effects of the additional weight of the Regenerative Motor-Pump System to the loading on the truck engine are presented in the second subtopic. The additional weight that is contributed by the Regenerative Motor-Pump System is significant; therefore further study on its effects can determine whether the energy supplied by the auxiliary drivetrain can compensate the additional weight of the Regenerative Motor-Pump System.

The second subtopic begins by elaborating further on the results obtained from the simulated ISUZU NKR 71-E. The results from the simulation will be used as a basis of comparison with experimental results from Regenerative Motor-Pump System. ISUZU NKR 71-E is simulated to accelerate from stationary to 10 km/h to be compared

with the results discussed in Section 5.2 that indicated the Regenerative Motor-Pump System is able to supply energy to move the vehicle to 10 km/h. The experimental results are taken from the second Motor Mode of the results discussed in Section 5.2.

The third subtopic exhibits results of the vehicle simulation on a cycle test. For this study, a Stop-Go cycle test was developed and used to evaluate the benefit of HHV as compared to conventional vehicle. For this simulation, an additional hydraulic drivetrain is also modelled based on the assumption that the hydraulic drivetrain is only able to supply energy to accelerate to 10 km/h before the ICE take over. This simulation will give insights on the benefits of HHV on longer trips.

5.4.1 Comparison between Conventional truck and HHV truck

Two different simulations have been carried out using the engine model in Figure 5.6. One of the simulations is trying to simulate a conventional truck moving from stationary to 10 km/h. Another simulation is the same truck, but with extra loading of the Regenerative Motor-Pump System. The extra loading involves additional weight of 350 kg (M Z Norhirni, 2012). The two simulations were carried out so that a comparison can be made and the effect of the additional weight can be measured.

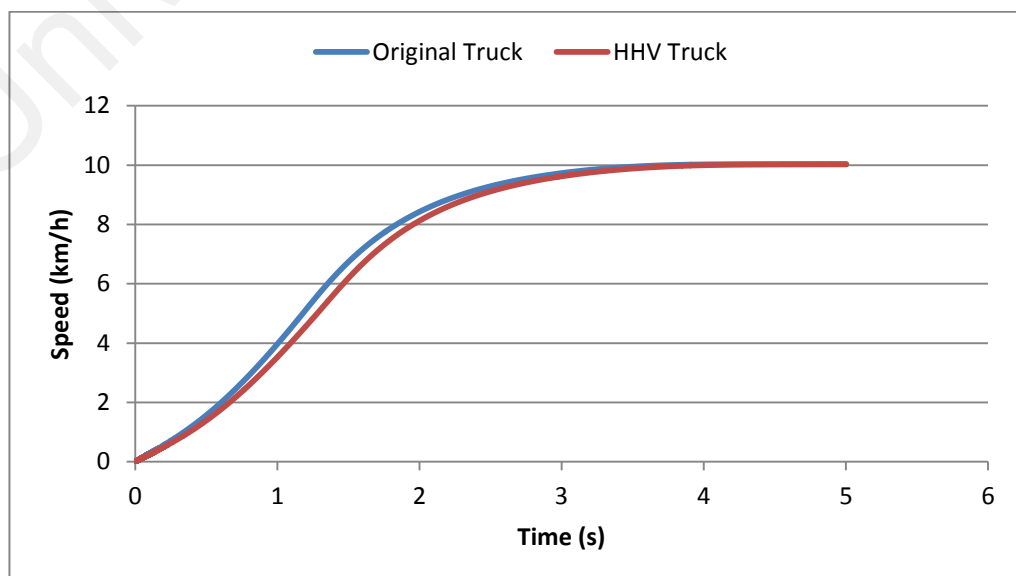


Figure 5.14 Speed comparison between Original truck and HHV truck

Figure 5.14 shows speed comparison between the original truck and the one with additional weight due to the installation of the Regenerative Motor-Pump System. Both vehicles are simulated to achieve the speed of 10 km/h, and it took both vehicles around 4 seconds to achieve the required speed. However, there are differences between the two as demonstrated by the non-overlapping curves of the two vehicles. The original truck is accelerates to the speed of 10 km/h faster than the HHV truck, albeit small differences.

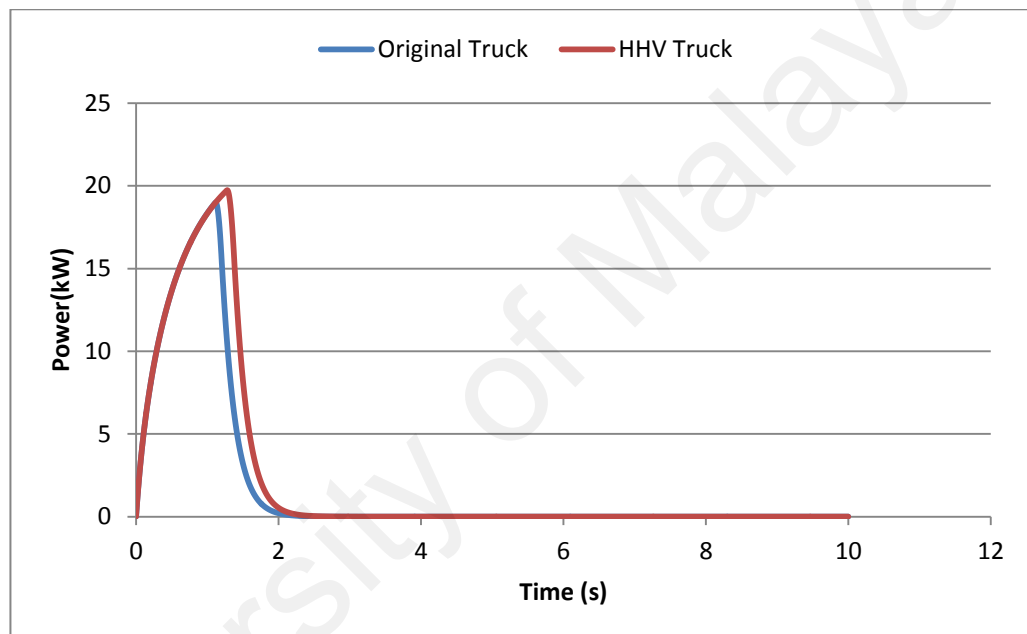


Figure 5.15 Power comparison between Original truck and HHV truck

Figure 5.15 shows a two graph curves of power versus time for the 10 seconds simulation. Initially the two curves overlapped between each other. The overlapping continues until the engine reaches the required power to move the vehicle to 10 km/h. The peak power of the simulation is reached firstly by the Original truck, then only the HHV truck. After the peak, both vehicles have declines in power, resulting to two distinct curves that separate the Original truck and the HHV truck. Figure 5.15 shows that the heavier truck requires more power to begin moving at the same speed.

Meanwhile, Figure 5.16 demonstrates the difference between engine speeds of the two simulated trucks. Similar to the power curves of Figure 5.15, both engine speed curves are initially overlapped, until a peak speed is reached. The original truck reaches the peak engine speed before the HHV truck. This can be seen in the two curves stop overlapping and begin to show two different curves. Higher engine power usually means higher engine rotational speed, even when satisfying the same vehicular speed demand.

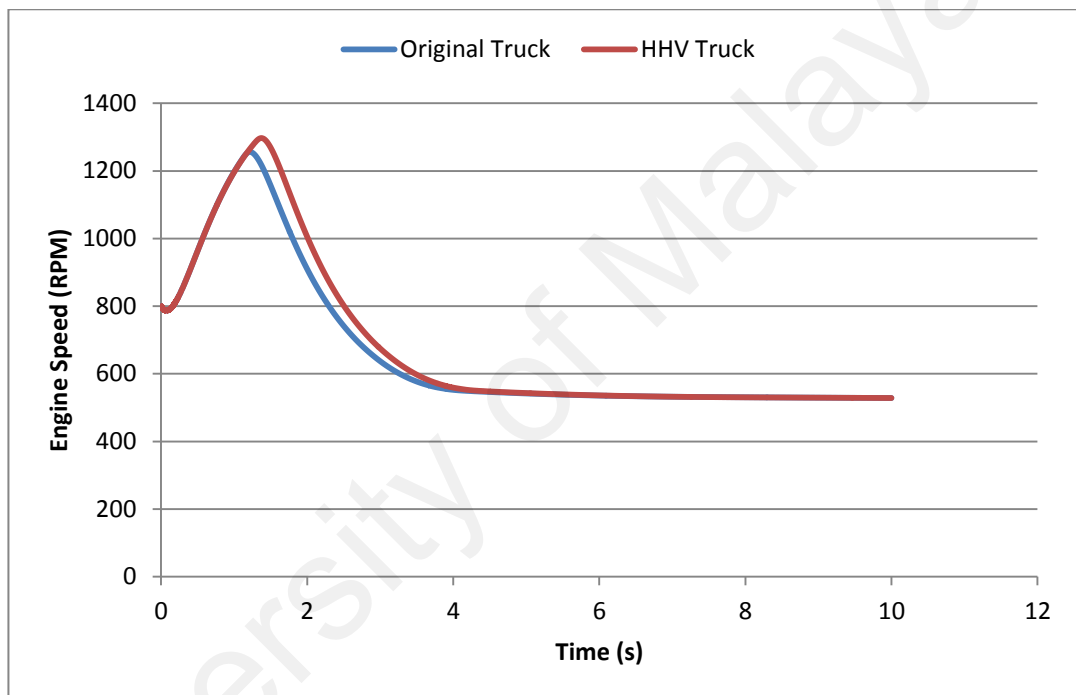


Figure 5.16 Engine Speed Comparison between Original truck and HHV truck

Table 5.7 summarizes the results of the two simulations. The study has found that the original truck uses 19.03 kJ of energy as compared to 22.46 kJ of energy by the HHV truck. This means that the original truck uses 15% less energy than the HHV truck. The HHV truck requires more energy as it is 14% heavier than the original truck. The results also demonstrated that it will require energy around 9.52 J to move one additional kilogram to the speed of 10 km/h.

Table 5.7 Summary of Comparison between conventional and hybrid NKR 71-E truck

Simulation	Conventional NKR71-E	Hybrid NKR 71-E
Weight (kg)	2180	2530
Weight of Regenerative Motor-Pump System (kg)	0	350
Peak Power (kW)	19.004	19.744
Peak Engine Speed (RPM)	1256	1297
Energy Required to move from stationary to 10 km/h (kJ)	19.03	22.46

Comparing the two results managed to reveal the effects of adding a Regenerative Motor-Pump System to the vehicle chosen earlier. The truck engine uses more energy as soon as additional weight is added to the truck. The Regenerative Motor-Pump System constitutes 14% of the Hybrid NKR 71-E weight, which is a high percentage. Installing the same system on a smaller vehicle will yield even a higher percentage. There is a need to know whether installing the Regenerative Motor-Pump System can compensate the additional weightage in terms of energy recovery and/or energy delivery of the system.

5.4.2 Comparison between ICE drivetrain and Hydraulic drivetrain

To compare between the two different drivetrains, results for the hydraulic drivetrain is taken from the experimental results of Regenerative Motor-Pump System. Calculations that convert the experimental data to the actual truck speed and energy used has been discussed in Section 3.2.4. The comparison is then made based on the energy conversion of angular kinetic energy to translational kinetic energy that will later yield vehicular velocity. The ICE drivetrain results is the simulation results of HHV truck engine as discussed in the previous subtopic. In this subtopic, the results are presented in further detail.

The truck is simulated to move from stationary to 10 km/h. This is done so that a comparison between a simulated HHV and experimental data gathered from the Regenerative Motor-Pump System can be made. In this case, the modelled truck is assumed to be having the same weight as the HHV. This enables the study to assume that the HHV is moving using ICE as the main drivetrain.

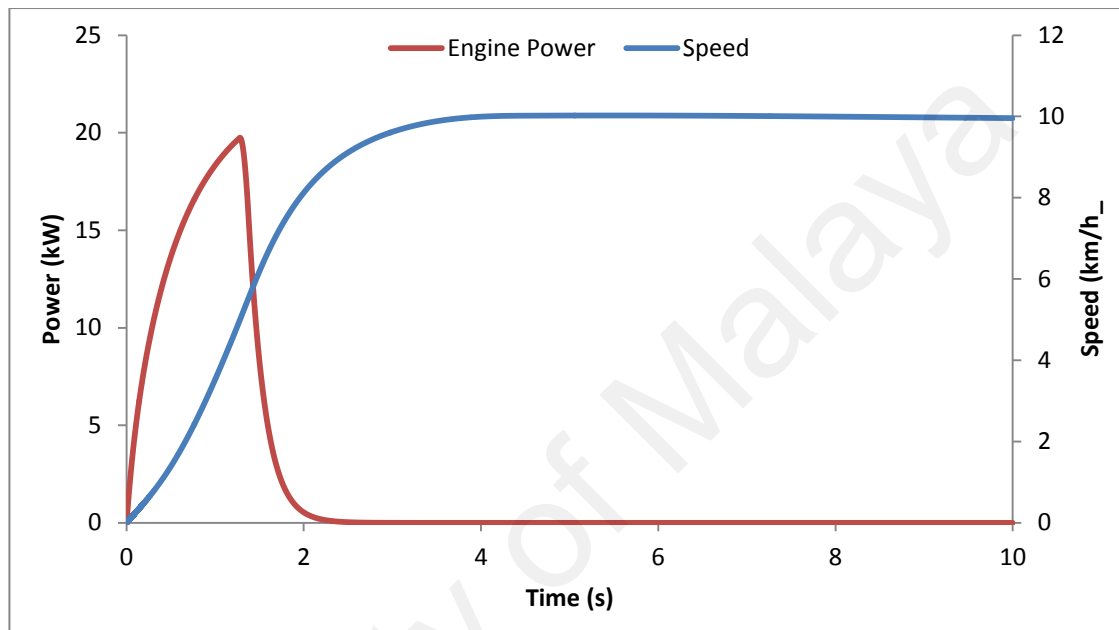


Figure 5.17 Engine Power and Speed data from the Simulated HHV

In Figure 5.17, the engine power peaks at 19.74 kW at around 1 second before starting to decline. The speed of the simulated HHV gains its final velocity of 10 km/h around 4 seconds. The engine certainly requires more energy in the initial phase to start the HHV moving from stationary position. The engine uses less power when the vehicle starts moving at the desired speed.

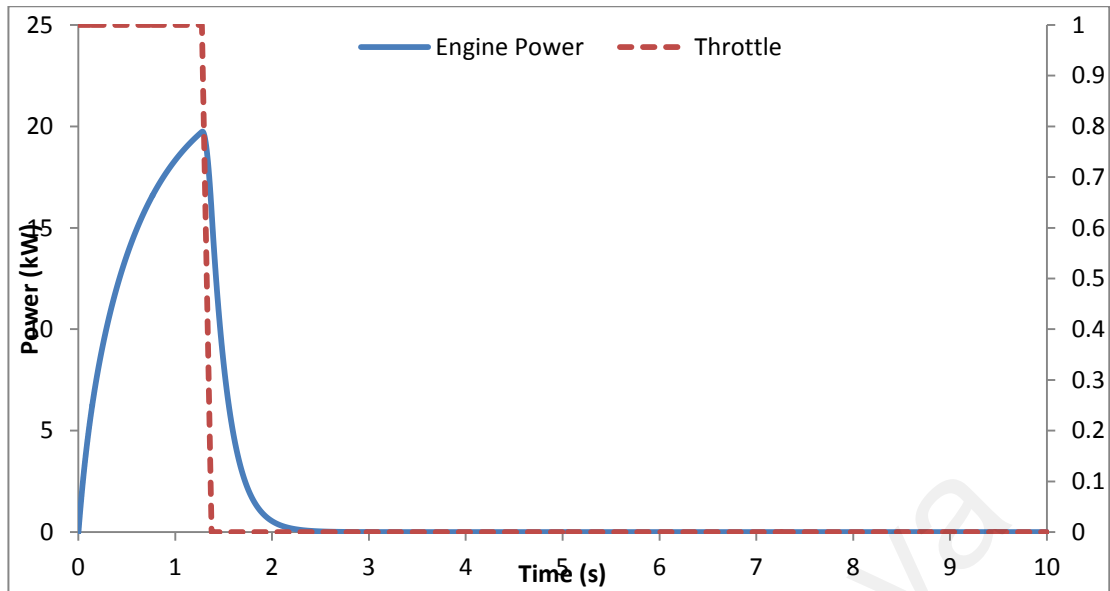


Figure 5.18 Engine Power and Throttle data of the Simulated HHV

Figure 5.18 shows the relation between the engine power and the throttle control that gets the truck moving. In the beginning, the vehicle is kept at full throttle in order to achieve the desired speed. This operates the engine and raises its power level. After a while, when the vehicle is near to its desired speed level, the throttle value declines to 0. The throttle level shows how the PID controller associated with this simulation operates. This is also similar to the engine speed. The maximum RPM of the engine speed is 1297 RPM. This is illustrated in Figure 5.19.

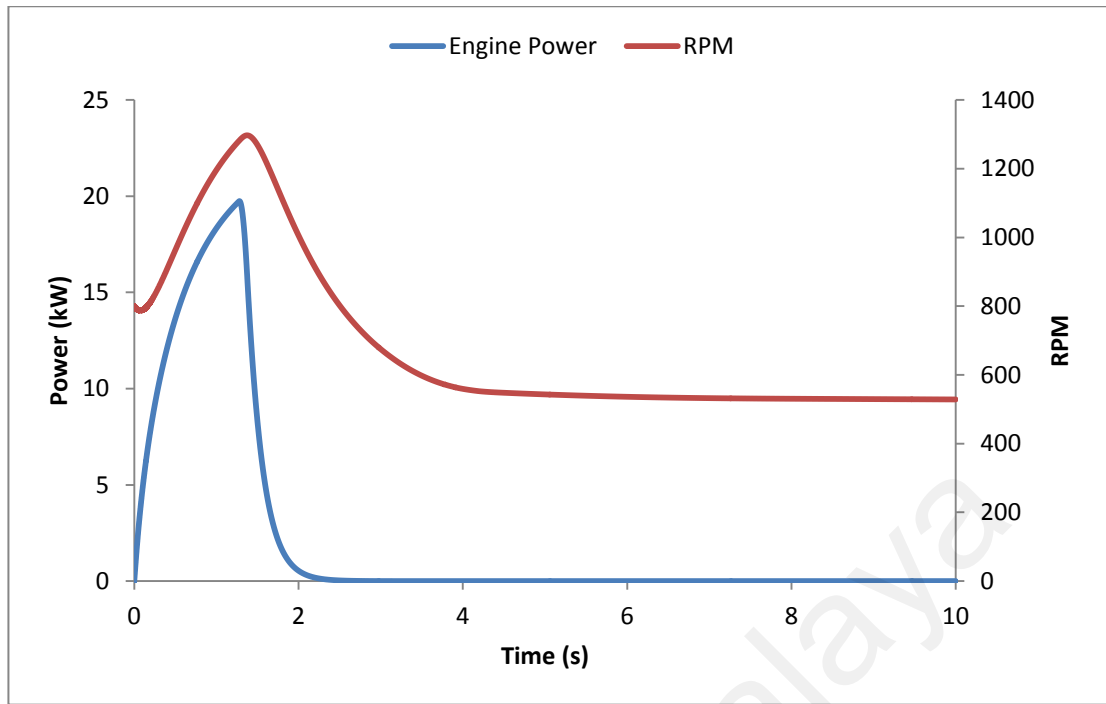


Figure 5.19 Power and RPM data of the Simulated HHV

Table 5.8 Comparison between ICE and Hydraulic Drivetrain of the HHV

HHV Drivetrain	Hydraulic Drivetrain	Internal Combustion Engine
Data Sources	Experimental - Motor Mode II (Figure 5.3 – Part E)	Simulation - Simulated HHV in MATLAB/Simulink
Energy sources	Hydraulic Accumulator discharge	Energy conversion from fuel in ICE
Energy required to move HHV to 10 km/h	8.94 kJ	22.46 kJ
Fuel used (L)	0	12.155

Table 5.8 summarizes a comparison between the ICE and hydraulic drivetrain of the HHV. From the table, it is shown that the hydraulic drivetrain uses lesser energy to move the HHV from stationary to 10 km/h. Around only 40% of the energy required to move the vehicle using the ICE is used by the hydraulic drivetrain to move the vehicle at the desired speed. This shows that the hydraulic accumulator has indeed greater power density and is able to convert energy from high pressure to translational motion more effective than the ICE with combustion. Furthermore, the same speed is attained at the cost of zero consumption of fossil fuel.

5.4.3 Simulations on Drive Cycles

From the regenerative capabilities and energy delivery capacities discussed in previous sections, test was designed to further demonstrate the capability of Regenerative Motor-Pump System. The massive nature of the system and the fact that the system needs to recover energy from braking in order to utilise it in the subsequent acceleration, a drive cycle with a lot of stop and go sequence will be the best choice to demonstrate the system's capabilities.

Previous literatures discussed on using the hydraulic drivetrain previously untapped power on garbage trucks and buses, because they usually travel in a stop-go route, having to stop by for garbage or bus stops. They also travel in densely populated area, mostly in urban areas where their services are more typical. Garbage trucks and buses are generally larger than conventional passenger vehicle, and will most likely be able to compensate the extra weight carried owing to the system by regenerative braking. Among the drive cycles used to evaluate garbage trucks are:

- (1) New York Garbage Truck Cycle (NYGTC)
- (2) West Virginia University Refuse Truck Cycle (WVU)
- (3) Orange County Refuse Truck Cycle (ORCTC)
- (4) U.S Environmental Protection Agency/Hybrid Truck Users Forum (EPA/HTUF)
- (5) National Renewable Energy Laboratory Automated Side Loader Cycle (NREL ASL Cycle)

For this study, two drive cycles will be used in the simulation. One drive cycle was developed based on the works of Wagner, who developed a hybrid drive cycle to exhibit the benefits of auxiliary drivetrain and efficient driving. The drive cycle was developed with by collaboration between New West Technologies and Bosch-Rexroth

(Wagner, 2011). The drive cycle that was developed by Wagner is shown in Figure 5.20 and is called as Hybrid 1 Cycle. In this study, the drive cycle that is a derivation of Hybrid 1 Cycle is used and is called as Stop-Go Cycle. Another drive cycle used in the simulation for this study is New York Garbage Truck Cycle (NYGTC) as shown in Figure 5.21.

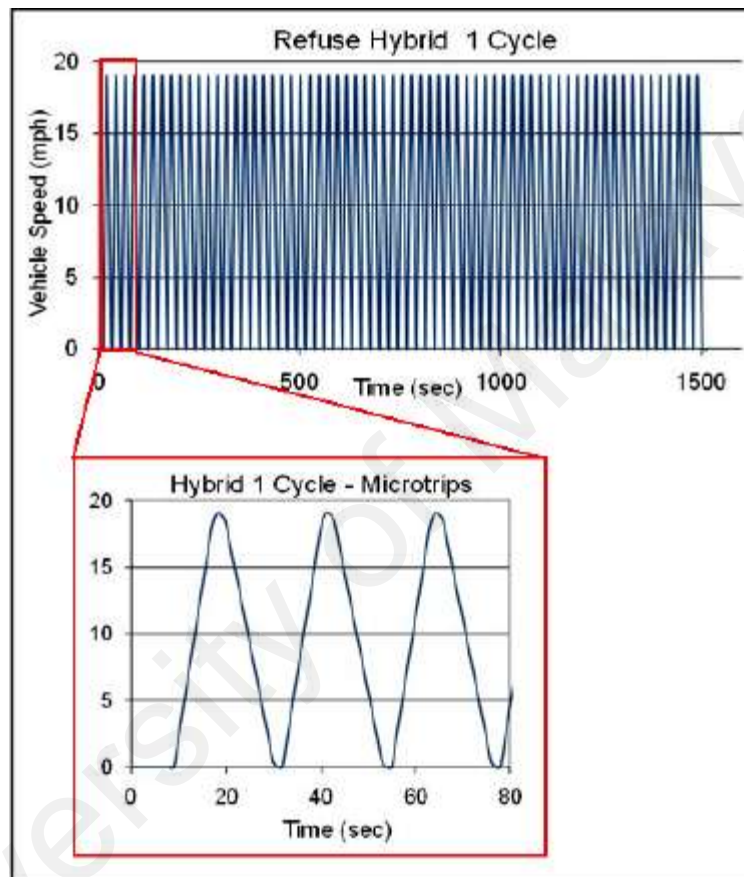


Figure 5.20 Hybrid 1 Drive Cycle by New West and Bosch Rexroth

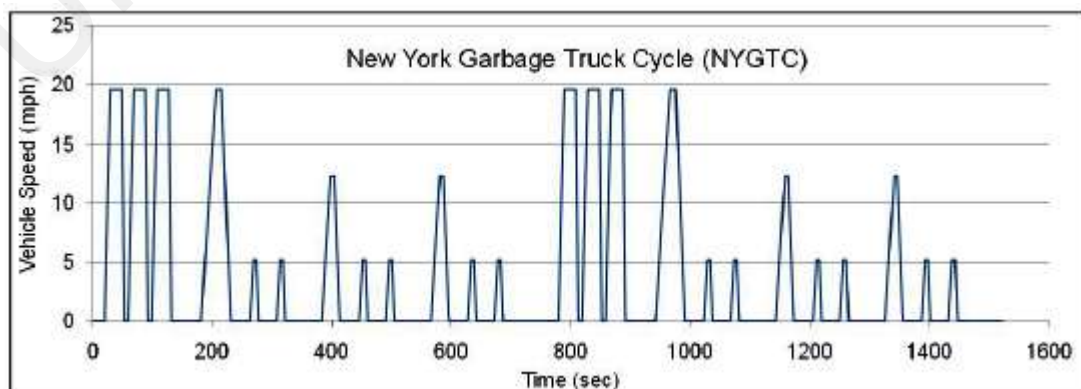


Figure 5.21 New York Garbage Truck Cycle (NYGTC)

Figure 5.22 shows the developed Stop-Go Drive Cycle. The drive cycle lasts 200 seconds, with peak speed of 20 km/hr. The drive cycle can be used to evaluate a hybrid system based on the frequency of stops in the drive cycle that translates to braking energy recovery opportunity.

In this study, the drive cycle is developed in a signal builder. The signal is plotted in the signal builder and delivered to the system based on the sample time that is set in the Simscape solver configuration block. In Figure 5.22, the Stop-Go Drive Cycle is shown in a Signal builder, while Figure 5.23 contains the New York Garbage Truck Cycle (NYGTC).

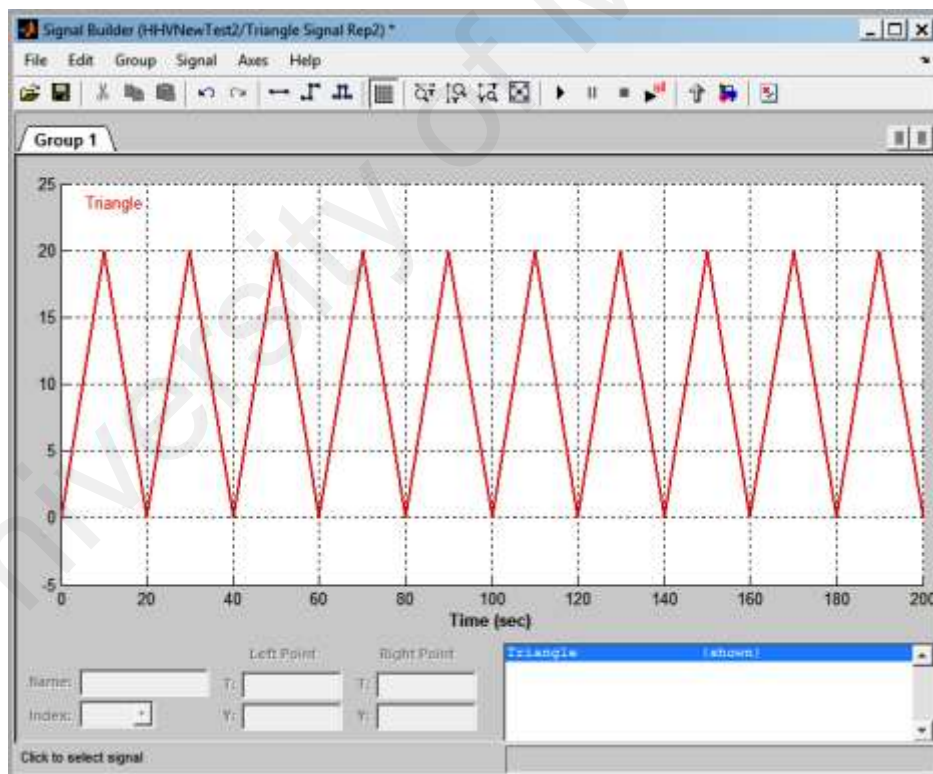


Figure 5.22 Stop-Go Drive Cycle based on Hybrid 1 drive cycle

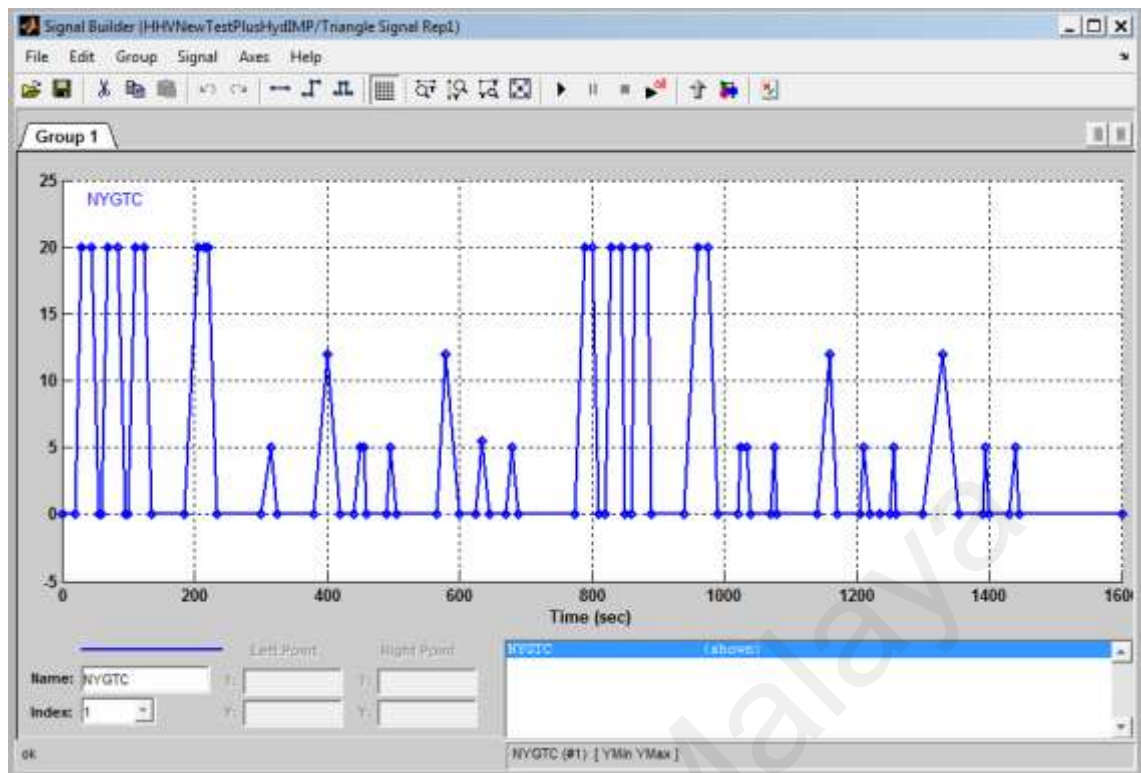


Figure 5.23 New York Garbage Truck Cycle (NYGTC) on Signal Builder

From previous sections, the study has made evident that the hydraulic drivetrain managed to capture around 40% of the braking energy. It is also proved experimentally that the energy delivered from the 40% recovered braking energy can be used to accelerate the truck to 10 km/hr. Using the drive cycle test, a comparison between two conventional and hybrid ISUZU NKR 71-E is made. Similar parameters has been applied to the two models as defined in the previous sections except that for HHV, an auxiliary drivetrain has been added to the original simulation model, which uses a simple Energy Management System (EMS) to govern two energy sources. Since both drive cycles has a peak speed of 20 km/hr., the hydraulic drivetrain will supply the initial torque before switching to the ICE.

5.4.3 (a) Stop-Go Drive Cycle Simulation Results

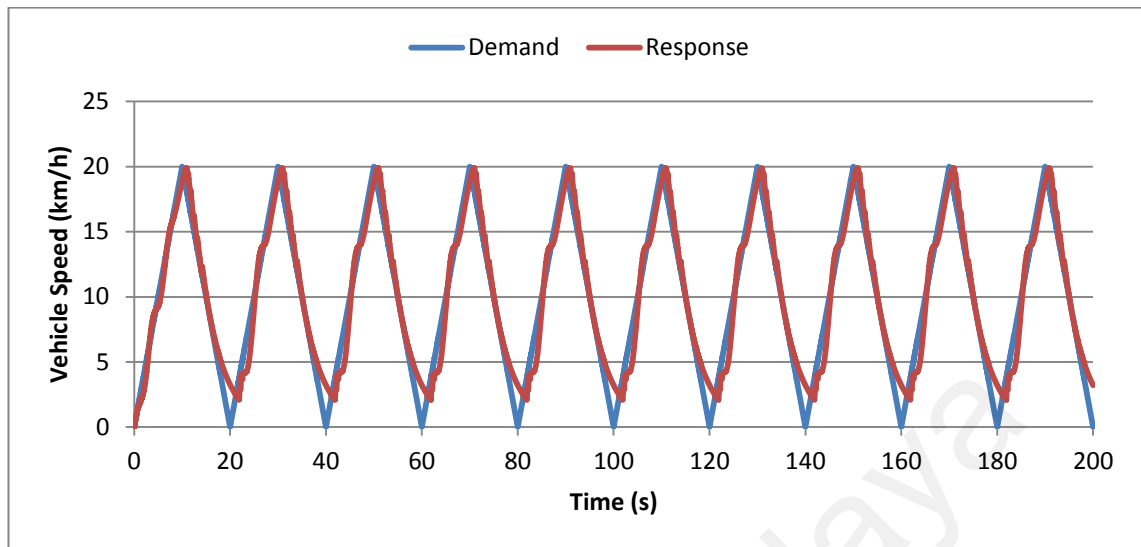


Figure 5.24 Speed of NKR 71-E on Stop-Go Drive Cycle

Figure 5.24 shows the speed response of the simulated truck on the Stop-Go Drive Cycle. The simulation model receives the speed demand from the signal builder that is connected to a PID controller that generates throttle values based on the error from the vehicle speed feedback. The throttle values are in positive values and negative values. Positive throttle values will be sent to the engine model where it will generate torque to move the vehicle. At the same time, a gear clutch will connect the engine directly to the vehicle model to put it into motion. Negative throttle values will activate a brake clutch that decelerates the vehicle. The combination of acceleration and braking ensures that the vehicle achieve the speed requested.

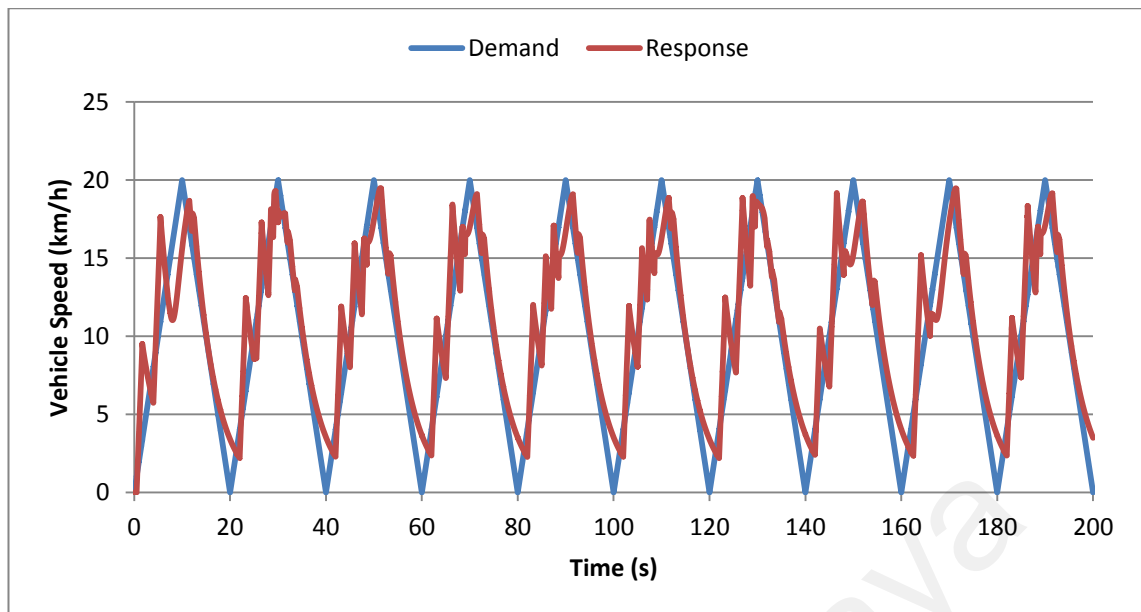


Figure 5.25 Speed of Hybrid NKR 71-E on Stop-Go Drive Cycle

Figure 5.25 meanwhile, shows the speed response of a HHV on the same drive cycle. The same rule applies on the HHV where the signal builder will send a signal that will be translated to positive and negative throttle values. In addition, the HHV has an extra rule that made the vehicle satisfy the speed demand up to 10 km/hr. using hydraulic drivetrain. Speed beyond 10 km/hr. will be met using the ICE. This additional rule, however results to the jagged response curve. This translates to drivability problem commonly associated to the introduction of an additional drivetrain (Zhang, Yin, & Zhang, 2010).

In Figure 5.26, a comparison between the engine power in Conventional Truck and HHV Truck is presented. The Engine Power values are based on the trucks undergoing the Stop-Go Drive Cycle. The graph is plotted from zero seconds to 50 seconds to clearly show the curves for both simulation models. The graph shows that the Conventional Engine Power curves have bigger area under the curves. This translates to higher energy required from the truck engine to satisfy the speed demands. In the initial sections, the HHV also requires higher energy from the ICE to satisfy the demand

signals. This is because, in the beginning, the ICE is in its idle speed, and would need to spin at higher RPM to achieve the vehicle speed requested.

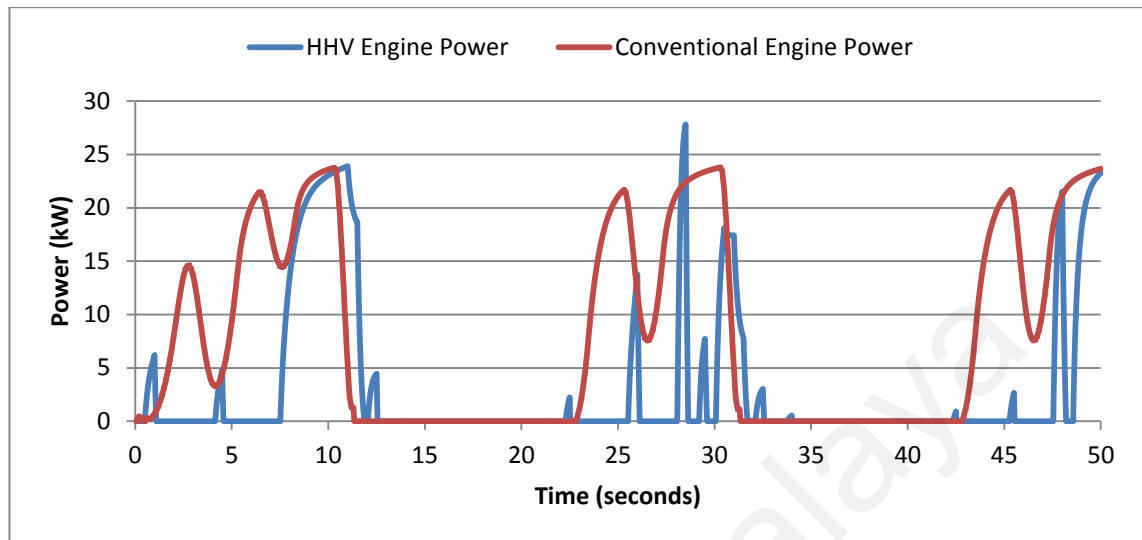


Figure 5.26 ICE Power comparison in conventional and hybrid NKR 71-E on Stop-Go Cycle

The simulated model of the two truck types managed to show the capability of adding a hydraulic drivetrain on a conventional truck. Table 5.9 summarizes other information from the two simulated models. The HHV truck uses lesser energy than the conventional truck by benefiting from the energy supplied by its hydraulic drivetrain. The average power of the ICE for the hybrid truck is also lesser than its conventional counterpart along the 200 seconds drive cycle. However, the HHV truck travelled an extra 123 metres on the drive cycle.

Table 5.9 Summary of Comparison between HHV ISUZU NKR 71-E Truck and Conventional ISUZU NKR 71-E truck on Stop-Go Drive Cycle

Truck Types	HHV Truck	Conventional Truck
Drivetrain	Hybrid Hydraulic - ICE	ICE
Energy used in Stop-Go Drive Cycle (kJ)	922.4	1376
Average Power (kW)	2.492	3.453
Energy used per distance travelled (kJ/m)	0.429	0.680

5.4.3 (b) New York Garbage Truck Cycle (NYGTC)

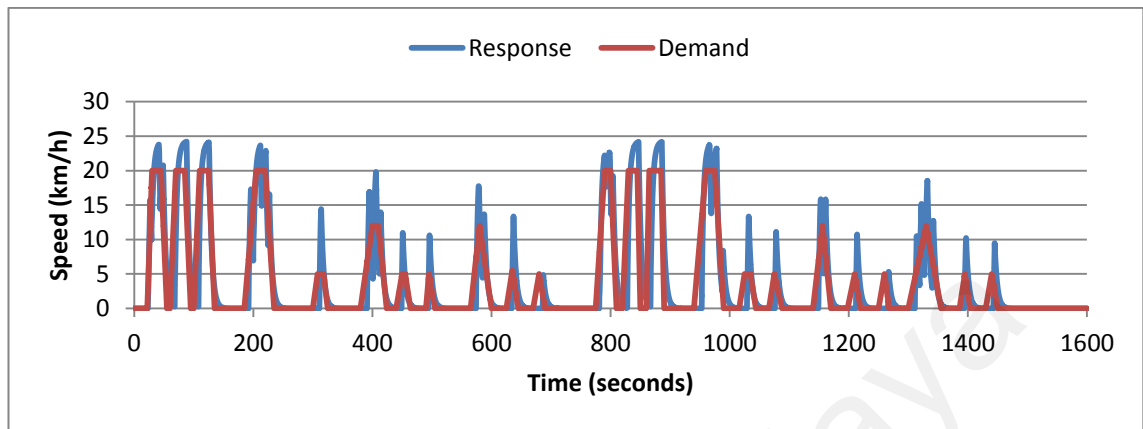


Figure 5.27 Speed of NKR 71-E on NYGTC

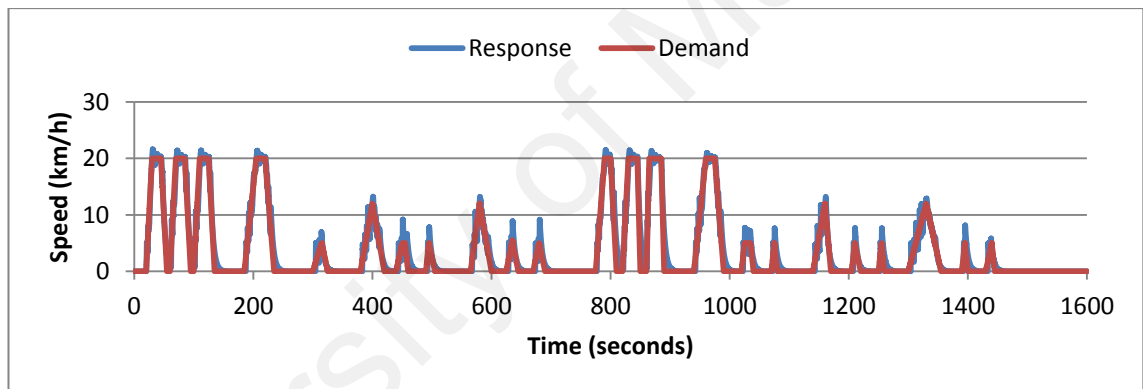


Figure 5.28 Speed of Hybrid NKR 71-E on NYGTC

Figure 5.27 and 5.28 shows the speed response of the conventional and hybrid ISUZU NKR 71-E respectively. The speed response were based on the demand curves of the NYGTC. The simulation was done in similar fashion to the Stop-Go Cycle drive cycle test, except for the different demand curves.

In Figure 5.29, a comparison between the engine power for both conventional and hybrid NKR 71-E is presented. The Engine Power values are based on the trucks undergoing the NYGTC. Similarly to Figure 5.26, the graph on Figure 5.39 is also plotted from 0 to 50 seconds to clearly show the difference in the 1600 seconds-long

cycle. The graph shows that the Conventional Engine Power curves have bigger area under the curves. This translates to higher energy required from the truck engine to satisfy the speed demands. This is similar to what has been observed in the earlier discussions on Stop-Go Cycle.

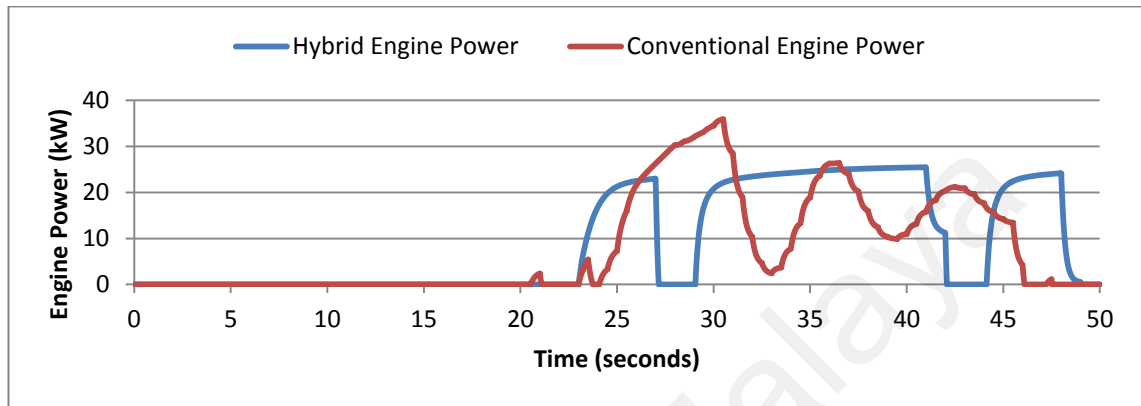


Figure 5.29 ICE Power Comparison in conventional and hybrid NKR 71-E on NYGTC

Table 5.10 Summary of Comparison between HHV ISUZU NKR 71-E Truck and Conventional ISUZU NKR 71-E truck on NYGTC

Truck Types	HHV Truck	Conventional Truck
Drivetrain	Hybrid Hydraulic - ICE	ICE
Energy used in NYGTC(kJ)	3393	4823
Average Power (kW)	3.501	2.635
Energy used per distance travelled (kJ/m)	0.559	0.814

The results of simulation of ISUZU NKR 71-E on NYGTC managed to show similar results as the results of the simulation on Stop-Go Cycle except in the average power of the ICE. Table 5.10 summarizes some other results from the simulation on NYGTC. From the results, we can observe that the Hybrid NKR 71-E uses less energy during the course of the NYGTC, and managed to travel further based on the demand curve of the cycle. These results show the direct benefit of installing Regenerative Motor-Pump System on a conventional ISUZU NKR 71-E in terms of energy.

5.5 Conclusion

In this chapter, the regenerative capability and energy delivery of Regenerative Motor-Pump System has been demonstrated with the aid of simulation. The system successfully exhibited pump modes and motor modes, two of important states in an actual HHV. Comparison between two different motor modes in an experiment shows that the Regenerative Motor-Pump System is able to recover 40% of the braking energy. It was also shown that the recovered energy is able to move the HHV to speed around 10 km/hr. A simulation of a truck based on a dynamometer testing of ISUZU NKR 71 E has also been developed to as a basis for comparison between a conventional truck and a HHV truck. It is found that an extra 18% of energy is required from the ICE to move an extra weight of 350 kg – approximate of the added system weight.

A simulation of conventional truck and HHV truck on a simple drive cycle is also developed and analysed. The results show that the HHV managed to save up to 33% energy on the 200 seconds drive cycle. The other drive cycle test, NYGTC shows that the Hybrid NKR 71-E consumes 29.6% less energy than the conventional NKR 71-E. However, some drivability problems are predicted from the introduction of hydraulic drivetrain into the conventional truck driveline based on the speed response graph of the HHV on the Stop-Go Drive Cycle.

6.0 CONCLUSIONS

6.1 Conclusions

This study presents the instrumentation and simulation of Regenerative Motor-Pump System for the applications of hydraulic hybrid vehicle. The Regenerative Motor-Pump System is developed and tested using a preliminary controller to emulate real processes that will take place on a hybrid hydraulic vehicle. A controller is then developed as an upgrade to the preliminary controller. Development of the controller and the Regenerative Motor-Pump System is based on actual ISUZU NKR 71-E truck. Two important properties of the Regenerative Motor-Pump System which are (1) energy recovery and (2) energy delivery are then evaluated. The study can be concluded as follows:

- (1) Instrumentation and control of Regenerative Motor-Pump System has been successfully developed. The Regenerative Motor-Pump System is able to emulate processes of a hydraulic drivetrain of a Hydraulic Hybrid Vehicle. This is shown from the capability of the system to recover energy in pump modes and deliver the captured energy in motor modes.
- (2) A controller has been developed to control the Regenerative Motor-Pump System. The controller allows the processes to be controlled automatically instead of manually determined by the operator. Safety features are also implemented in the controller such as (1) Charging Pressure Limiter and (2) Valve Open Check.
- (3) The Regenerative Motor-Pump System is able to recover up to 40% of the braking energy and stored in the hydraulic accumulator. This is shown in experimental data from comparing between the initial energy

and the energy delivered after the recovered energy has been released (motor mode).

- (4) A simulation model of the ICE drivetrain and the hydraulic drivetrain of the HHV has been developed. The simulation is used as a comparison between hydraulic drivetrain and conventional drivetrain to reveal the Regenerative Motor Pump System capability to deliver energy to the vehicle.
- (5) The Regenerative Motor-Pump System is able to deliver energy to move a truck from stationary to the speed of 10 km/h effectively using 60% less energy than the Internal Combustion Engine.
- (6) Implementation of the Regenerative Motor Pump System s on the HHV truck shows that it can save up to 33% of energy as compared to a conventional truck on Stop-Go cycle developed for the study and up to 29.6% on New York Garbage Truck Cycle (NYGTC)

This study was done as a foundation to implementation of Regenerative Motor-Pump System on ISUZU NKR 71-E truck. It is hoped that the present study can be extended to include more tests and simulations to provide better perspective of how Regenerative Motor-Pump System operates. Extensive tests using drive cycles can be considered to discover better strategies towards developing the Energy Management System (EMS) for the HHV.

RESEARCH OUTPUT

Journal Paper

- (1) M. Z. Norhirni, M. Hamdi, S. Nurmaya Musa, L.H. Saw, N.A. Mardi, **N. Hilman**, Design and Modelling of Swash Plate in Axial Piston Pump (2011), Journal of Dynamic Systems, Measurement and Control, November 2011, Volume 133, Issue6, 064505 (ISI).

Conference

- (1) **N. Hilman**, L.H. Saw, M.Fadzil , M.Hamdi, M.Z. Norhirni, 2010, Design and Evaluation of Regenerative Braking, International Conference on Sustainable Mobility 2010, Kuala Lumpur, 1-3 December 2010.
- (2) **N. Hilman**, L.H. Saw, M.Hamdi and M.Z. Norhirni 2010. *Performance Evaluation of Parallel Hydraulic Hybrid Vehicle using EPA US06 Aggressive Drive Cycle Simulation*. Proceedings of the 5th AOTULE International Postgraduate Student Conference on Engineering, Bandung, Indonesia, 1-2 November 2010.
- (3) M. Z. Norhirni, L.H. Saw and **N. Hilman**, Simulation of crash analysis of parallel HHV based on High Precision Nonlinear FEA, International Conference on Sustainable Mobility 2010.
- (4) M. Z. Norhirni, L.H. Saw and **N. Hilman**, Design and Development of Hydraulic Axial Piston Unit, International Conference on Sustainable Mobility 2010.

Awards

(1) Bronze Medal - Malaysian Technology Expo 2011

Hydraulic Regenerative Braking System (HRBS) for Small Commercial Vehicle

Name of PI: Professor Dr. Mohd Hamdi Abd Shukor

Name of Team Members: Dr. Nor Azizi b. Mardi

Mohd Fadzil Jamaludin

Norhirni Binti Md Zahir

Mohamad Hilman Bin Nordin

Bernard Saw Lip Huat

University of Malaysia

REFERENCES

- Ahn, J. K., Jung, K. H., Kim, D. H., Jin, H. B., Kim, H. S., & Hwang, S. H. (2009). Analysis of a Regenerative Braking System for Hybrid Electric Vehicles Using an Electro-Mechanical Brake. *International Journal of Automotive Technology*, 10(2), 229-234.
- Andersson, B. A., & Jacobsson, S. (2000). Monitoring and assessing technology choice: the case of solar cells. *Energy Policy*, 28(14), 1037-1049.
- Bernard, J., Delprat, S., Buchi, F. N., & Guerra, T. M. (2009). Fuel-Cell Hybrid Powertrain: Toward Minimization of Hydrogen Consumption. *Ieee Transactions on Vehicular Technology*, 58(7), 3168-3176.
- Bossche, P. V. d. (2006a). Structure of a combined hybrid vehicle. In Hybridcombined.png (Ed.). Wikimedia Commons: Creative Commons Attribution.
- Bossche, P. V. d. (2006b). Structure of a parallel hybrid vehicle. In Hybridpar.png (Ed.). Wikimedia Commons: Creative Commons Attribution.
- Bossche, P. V. d. (2006c). Structure of a series hybrid electric vehicle with peak power unit. In Hybridpeak.png (Ed.). Wikimedia Commons: Creative Commons Attribution.
- Carson, I., & Vaitheeswaran, V. V. (2007). *Zoom : the global race to fuel the car of the future* (1st ed.). New York: Twelve.
- Caux, S., Hankache, W., Fadel, M., & Hissel, D. (2010). On-line fuzzy energy management for hybrid fuel cell systems. *International Journal of Hydrogen Energy*, 35(5), 2134-2143.
- Chasse, A., & Sciarretta, A. (2011). Supervisory control of hybrid powertrains: An experimental benchmark of offline optimization and online energy management. *Control Engineering Practice*, 19(11), 1253-1265.
- Chavez-Rodriguez, M. F., & Nebra, S. A. (2010). Assessing GHG Emissions, Ecological Footprint, and Water Linkage for Different Fuels. *Environmental Science & Technology*, 44(24), 9252-9257.
- Clarke, P., Muneer, T., & Cullinane, K. (2010). Cutting vehicle emissions with regenerative braking. *Transportation Research Part D-Transport and Environment*, 15(3), 160-167.
- Dosthosseini, R., Kouzani, A. Z., & Sheikholeslam, F. (2011). Direct method for optimal power management in hybrid electric vehicles. *International Journal of Automotive Technology*, 12(6), 943-960.
- Erdinc, O., Vural, B., & Uzunoglu, M. (2009). A wavelet-fuzzy logic based energy management strategy for a fuel cell/battery/ultra-capacitor hybrid vehicular power system. *Journal of Power Sources*, 194(1), 369-380.

- Ferreira, A. A., Pomilio, J. A., Spiazzi, G., & Silva, L. D. (2008). Energy management fuzzy logic supervisory for electric vehicle power supplies system. *Ieee Transactions on Power Electronics*, 23(1), 107-115.
- Fontaras, G., Pistikopoulos, P., & Samaras, Z. (2008). Experimental evaluation of hybrid vehicle fuel economy and pollutant emissions over real-world simulation driving cycles. *Atmospheric Environment*, 42(18), 4023-4035.
- Geng, B., Mills, J. K., & Sun, D. (2011). Energy Management Control of Microturbine-Powered Plug-In Hybrid Electric Vehicles Using the Telemetry Equivalent Consumption Minimization Strategy. *Ieee Transactions on Vehicular Technology*, 60(9), 4238-4248.
- Geng, B., Mills, J. K., & Sun, D. (2012). Two-Stage Energy Management Control of Fuel Cell Plug-In Hybrid Electric Vehicles Considering Fuel Cell Longevity. *Ieee Transactions on Vehicular Technology*, 61(2), 498-508.
- Gokalp, B., Buyukkaya, E., & Soyhan, H. S. (2011). Performance and emissions of a diesel tractor engine fueled with marine diesel and soybean methyl ester. *Biomass & Bioenergy*, 35(8), 3575-3583.
- Hebbal, O. D., Reddy, K. V., & Rajagopal, K. (2006). Performance characteristics of a diesel engine with deccan hemp oil. *Fuel*, 85(14-15), 2187-2194.
- Hilman, N., Saw, L. H., Fadzil, M., Hamdi, M., & Norhirni, M. Z. (2010). *Design and Evaluation of Regenerative Braking on Conventional Passenger Vehicle*. Paper presented at the International Conference on Sustainable Mobility 2010, Kuala Lumpur, Malaysia.
- Hui, S., Ji-hai, J., & Xin, W. (2009). Torque control strategy for a parallel hydraulic hybrid vehicle. *Journal of Terramechanics*, 46(6), 259-265.
- Hui, S., Lifu, Y., & Junqing, J. (2010). Hydraulic/electric synergy system (HESS) design for heavy hybrid vehicles. *Energy*, 35(12), 5328-5335.
- Hui, S., Lifu, Y., Junqing, J., & Yanling, L. (2011). Control strategy of hydraulic/electric synergy system in heavy hybrid vehicles. *Energy Conversion and Management*, 52(1), 668-674.
- Ilkilic, C., Aydin, S., Behcet, R., & Aydin, H. (2011). Biodiesel from safflower oil and its application in a diesel engine. *Fuel Processing Technology*, 92(3), 356-362.
- Jin, K., Ruan, X. B., Yang, M. X., & Xu, M. (2009). A Hybrid Fuel Cell Power System. *Ieee Transactions on Industrial Electronics*, 56(4), 1212-1222.
- Johannesson, L., Pettersson, S., & Egardt, B. (2009). Predictive energy management of a 4QT series-parallel hybrid electric bus. *Control Engineering Practice*, 17(12), 1440-1453.

- Kannan, G. R., Karvembu, R., & Anand, R. (2011). Effect of metal based additive on performance emission and combustion characteristics of diesel engine fuelled with biodiesel. *Applied Energy*, 88(11), 3694-3703.
- Karden, E., Ploumen, S., Fricke, B., Miller, T., & Snyder, K. (2007). Energy storage devices for future hybrid electric vehicles. *Journal of Power Sources*, 168(1), 2-11.
- Kerr, R. A. (1998). The Next Oil Crisis Looms Large--and Perhaps Close. *Science*, 281(5380), 1128-1131.
- Kessels, J. T. B. A., Koot, M. W. T., van den Bosch, P. P. J., & Kok, D. B. (2008). Online Energy Management for Hybrid Electric Vehicles. *Ieee Transactions on Vehicular Technology*, 57(6), 3428-3440.
- Kim, N., Cha, S., & Peng, H. (2011). Optimal Control of Hybrid Electric Vehicles Based on Pontryagin's Minimum Principle. *Ieee Transactions on Control Systems Technology*, 19(5), 1279-1287.
- Kisacikoglu, M., Uzunoglu, M., & Alam, M. (2009). Load sharing using fuzzy logic control in a fuel cell/ultracapacitor hybrid vehicle. *International Journal of Hydrogen Energy*, 34(3), 1497-1507.
- Lin, B. F., Huang, J. H., & Huang, D. Y. (2008). Effects of Biodiesel from Palm Kernel Oil on the Engine Performance, Exhaust Emissions, and Combustion Characteristics of a Direct Injection Diesel Engine. *Energy & Fuels*, 22(6), 4229-4234.
- Lukic, S. M., Cao, J., Bansal, R. C., Rodriguez, F., & Emadi, A. (2008). Energy storage systems for automotive applications. *Ieee Transactions on Industrial Electronics*, 55(6), 2258-2267.
- Moreno, J., Ortuzar, M. E., & Dixon, J. W. (2006). Energy-management system for a hybrid electric vehicle, using ultracapacitors and neural networks. *Ieee Transactions on Industrial Electronics*, 53(2), 614-623.
- Mulcahy, T. M., Hull, J. R., Uherka, K. L., Niemann, R. C., Abboud, R. G., Juna, J. P., & Lockwood, J. A. (1999). Flywheel energy storage advances using HTS bearings. *Ieee Transactions on Applied Superconductivity*, 9(2), 297-300.
- Nikiforuk, A. (2010). *Tar Sands: Dirty Oil and the Future of a Continent, Revised and Updated Edition*: Douglas & McIntyre
- Norhirni, M. Z. (2012). *Development of a Test Rig for Hydraulic Regenerative Braking System (HRBS)*. M.Eng.Sc, University of Malaya, Kuala Lumpur.
- Norhirni, M. Z., Hamdi, M., Nurmaya Musa, S., Saw, L. H., Mardi, N. A., & Hilman, N. (2011). Load and Stress Analysis for the Swash Plate of an Axial Piston Pump/Motor. *Journal of Dynamic Systems, Measurement, and Control*, 133(6), 064505.1-064505.10.

- Nzisabira, J., Louvigny, Y., & Duysinx, P. (2009). Comparison of Ultra Capacitors, Hydraulic Accumulators and Batteries Technologies to Optimize Hybrid Vehicle Ecoefficiency. *2009 International Conference on Power Engineering, Energy and Electrical Drives*, 342-347.
- Saeks, R., Cox, C. J., Neidhoefer, J., Mays, P. R., & Murray, J. J. (2002). Adaptive control of a hybrid electric vehicle. *Ieee Transactions on Intelligent Transportation Systems*, 3(4), 213-234.
- Satoh, H. (2011). Fukushima and the Future of Nuclear Energy in Japan: The Need for a Robust Social Contract. *Elcano Newsletter*, 79.
- Sayin, C. (2011). An Experimental Investigation on the Effect of Injection Pressure on the Exhaust Emissions of a Diesel Engine Fueled with Methanol-diesel Blends. *Energy Sources Part a-Recovery Utilization and Environmental Effects*, 33(23), 2206-2217.
- Seki, H., Ishihara, K., & Tadakuma, S. (2009). Novel Regenerative Braking Control of Electric Power-Assisted Wheelchair for Safety Downhill Road Driving. *Ieee Transactions on Industrial Electronics*, 56(5), 1393-1400.
- Sezer, V., Gokasan, M., & Bogosyan, S. (2011). A Novel ECMS and Combined Cost Map Approach for High-Efficiency Series Hybrid Electric Vehicles. *Ieee Transactions on Vehicular Technology*, 60(8), 3557-3570.
- Silva, C., Ross, M., & Farias, T. (2009). Analysis and simulation of "low-cost" strategies to reduce fuel consumption and emissions in conventional gasoline light-duty vehicles. *Energy Conversion and Management*, 50(2), 215-222.
- Sinoquet, D., Rousseau, G., & Milhau, Y. (2011). Design optimization and optimal control for hybrid vehicles. *Optimization and Engineering*, 12(1-2), 199-213.
- Sundstrom, O., Soltic, P., & Guzzella, L. (2010). A Transmission-Actuated Energy-Management Strategy. *Ieee Transactions on Vehicular Technology*, 59(1), 84-92.
- Taghavipour, A., Alasty, A., & Saadat, M. (2009). Nonlinear Power Balance Control of a SPA Hydraulic Hybrid Truck. *2009 Ieee/Asme International Conference on Advanced Intelligent Mechatronics, Vols 1-3*, 805-810.
- Thounthong, P., Raël, S., & Davat, B. (2009). Energy management of fuel cell/battery/supercapacitor hybrid power source for vehicle applications. *Journal of Power Sources*, 193(1), 376-385.
- Wagner, J. (2011). Multi-Fleet Demonstration of Hydraulic Regenerative Braking Technology in Refuse Truck Application. Albany, New York: New West Technologies, LLC.
- Won, J. S., Langari, R., & Ehsani, M. (2005). An energy management and charge sustaining strategy for a parallel hybrid vehicle with CVT. *Ieee Transactions on Control Systems Technology*, 13(2), 313-320.

- Wu, B., Lin, C. C., Filipi, Z., Peng, H., & Assanis, D. (2004). Optimal power management for a hydraulic hybrid delivery truck. *Vehicle System Dynamics*, 42(1-2), 23-40.
- Xu, L. F., Li, J. Q., Hua, J. F., Li, X. J., & Ouyang, M. G. (2009a). Adaptive supervisory control strategy of a fuel cell/battery-powered city bus. *Journal of Power Sources*, 194(1), 360-368.
- Xu, L. F., Li, J. Q., Hua, J. F., Li, X. J., & Ouyang, M. G. (2009b). Optimal vehicle control strategy of a fuel cell/battery hybrid city bus. *International Journal of Hydrogen Energy*, 34(17), 7323-7333.
- Yusaf, T. F., Yousif, B. F., & Elawad, M. M. (2011). Crude palm oil fuel for diesel-engines: Experimental and ANN simulation approaches. *Energy*, 36(8), 4871-4878.
- Zhang, C., Vahidi, A., Pisu, P., Li, X. P., & Tennant, K. (2010). Role of Terrain Preview in Energy Management of Hybrid Electric Vehicles. *Ieee Transactions on Vehicular Technology*, 59(3), 1139-1147.
- Zhang, J. L., Yin, C. L., & Zhang, J. W. (2010). Improvement of Drivability and Fuel Economy with a Hybrid Antiskid Braking System in Hybrid Electric Vehicle. *International Journal of Automotive Technology*, 11(2), 205-213.
- Zhang, J. M., Song, B. Y., Cui, S. M., & Ren, D. B. (2009). Fuzzy Logic Approach to Regenerative Braking System. *2009 International Conference on Intelligent Human-Machine Systems and Cybernetics, Vol 1, Proceedings*, 451-454.
- Zou, G., & Chau, K. W. (2006). Short- and long-run effects between oil consumption and economic growth in China. *Energy Policy*, 34(18), 3644-3655.